MICRO-TECHNOLOGIES TO CONSTRAIN NEURONAL NETWORKS

by

Ashwin Vishwanathan

MS, West Virginia University, 2007

BE, Osmania University, 2004

Submitted to the Graduate Faculty of

the Swanson School of Engineering in partial fulfillment

of the requirements for the degree of

Ph. D. in Bioengineering

University of Pittsburgh

2011

UNIVERSITY OF PITTSBURGH

SWANSON SCHOOL OF ENGINEERING

This dissertation was presented

by

Ashwin Vishwanathan

It was defended on

November 10, 2010

and approved by

Dr. Henry Zeringue, Assistant Professor, Department of Bioengineering

Dr. Lance Davidson, Assistant Professor, Department of Bioengineering

Dr. Xinyan Tracy Cui, Associate Professor, Department of Bioengineering

Dr. Sung Kwon Cho, Associate Professor, Department of Mechanical Engineering and Material Science

Dissertation Director: Dr. Henry Zeringue, Assistant Professor, Department of Bioengineering

MICRO-TECHNOLOGIES TO CONSTRAIN NEURONAL NETWORKS

Ashwin Vishwanathan, PhD

University of Pittsburgh, 2011

Micro-technologies broadly encompass a range of technologies that deal with the development of tools on the order of a few microns. These tools have made steady inroads into traditional biology and have helped probe the functioning of cells on the order of tens of microns. The objective of this work was to use engineering techniques to ask specific questions in neuroscience.

Using two different techniques, namely microcontact printing and microfluidics we successfully restricted the spread of networks of neurons to defined geometries. In the former case, we chose to restrict networks to 'ring' shaped geometries, in order to study emergent reverberating properties in the resulting network. Ring shaped neuronal networks displayed reverberatory activity upon brief stimulation. This reverberatory activity was enhanced when network inhibition was abolished pharmacologically. Finally the effect of varying geometric parameters on this form of network activity was assessed. Here we found that small changes in the geometry did not have any significant effect on the reverberatory activity.

In the second case, we restricted networks of neurons inside microfluidic devices. These microfluidic devices were capable of maintaining two populations of neurons in a fluidically

isolated manner. The two populations communicated via microgrooves that allowed axons to reach across either population. We integrated an electrophysiological framework onto the microfluidic device such that one of the two populations could be electrically stimulated. We show, using calcium imaging it was possible to stimulate neurons inside these devices.

In conclusion, we have demonstrated the use of micro-technologies to constrain neuronal networks to specific geometries. We show here the emergence of reverberation in 'ring' shaped networks. Finally, we also created a novel microfluidic platform to culture neurons for extended periods of time.

Keywords: Micro-technology, Microcontact printing, Microfluidics, Neuronal networks, Reverberation, Electrophysiology, Calcium imaging.

TABLE OF CONTENTS

LIST OF TABLES

LIST OF FIGURES

ACKNOWLEDGEMENTS

Dedicated to *C. V. N. Swami*

I would like to acknowledge my advisor Henry Zeringue for giving me the opportunity to purse research in a independent manner. He has been very encouraging and supportive of all ideas that I kept constantly presenting. I would like to thank my committee members for all the discussions and helpful suggestions. I would specially like to thank Dr. Lance Davidson for numerous discussions, countless suggestions and insights through the course of my research. Dr. Davidson has been much like a friend in terms of conversations on a varied number of topics, research apart. I would also like to thank Drs. Tracy Cui and Sung Kwon Cho for helpful suggestions.

I am indebted to Dr. Guoqiang Bi for discussions regarding reverberations, ring cultures and the use of equipment at his lab. Dr. Mee H Choi for enjoyable discussions and help with cultures and Dr. Rick Gerkin for help getting started on the ephys rig. I would like to thank Rich, Shawn and Lacey for the wonderful lab environment and all the good times.

Rakshita for being my life-support, colleague and critic throughout my stay at graduate school, this would not have been possible without you. To my parents for having been the best teachers of science. Lastly, I would like to thank my friends and colleagues (Murali, Anand, Parikshit, Deepti, Sagar, Sid) for inputs along the way. Chris Withers for initial work on ring networks, Jason Castro for help with imaging, Sachin Velankar for the plasma machine and Conrad Hong for cultures. The support and awesome intellectual environment provided by the CNBC.

1.0 GENERAL INTRODUCTION

1.1 OUTLINE

In this chapter I shall introduce all the important concepts that have been dealt with and implemented in some form or the other for this study. Each section will introduce the topics and talk about its application in this study. The introduction I provide in this chapter should be applicable to all the following chapters.

1.2 BACKGROUND

The human brain consists of approximately 10^{11} neurons, that are connected to each other forming one giant network that is capable of intelligence, emotion, abstract thought, etc. Neurons are the fundamental units of the nervous system and are highly specialized to receive and transmit cellular signals. The basic morphology of the neuron contains the soma or the cell body, the axon which transmits signals, and dendrites which receive signals. There are two main ways by which neurons transmit signals, (i) via chemical transmission and (ii) via electrical synapses . *Synapses* are the specialized regions of neurons that receive and transmit signals either electrically or chemically. In a chemical synapse there is no contact

between the two cells, instead they are separated by a small region called the *synaptic cleft* through which neurotransmitters are released (Figure 1a). Electrical synapses are formed between regions of neurons that are in contact with each other via specialized pores called *gap junctions*(Figure 1b) Electrical synapses have the ability to provide almost instantaneous signal transmission, whereas chemical synapses transmit signals with a small time delay.

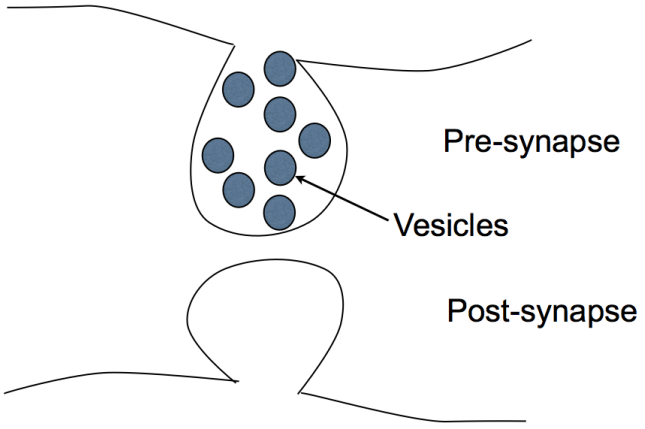

(a)

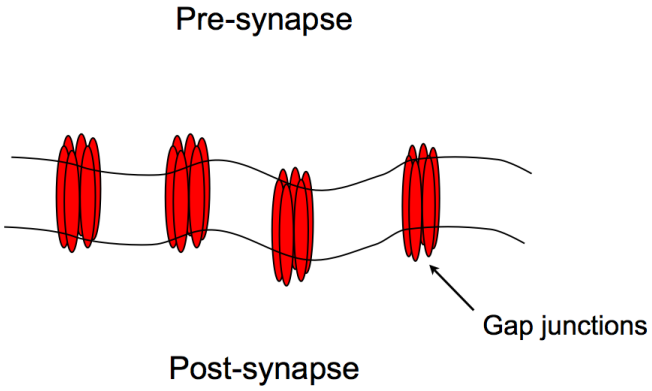

(b)

Figure 1: Synaptic transmission

(a). Schematic representing chemical synaptic transmission via synapses. Upon a signal arrival, Ca^{2+} ions enter the presynapse triggering a release of neurotransmitter, causing the signal to propagate. (b). Schematic of gap junction, an example of electrical synapses. Each gap junction (red) facilitates the transfer of ions from the pre-synapse to the post-synapse.

The study of neurons in networks has important consequences since all resulting behavior is a consequence of networks of neurons. The ability to culture neurons *in vitro* allowed researchers to begin questioning the role of activity in networks of neurons. *In vitro* neuronal networks are tools that allow researchers to study aspects of neuronal communication between groups of neurons. *In vitro* neuronal networks offer researchers the possibility of understanding network behavior from networks of varying sizes that can be probed by existing molecular biological tools. Culturing of neurons into networks also serve as sensors, network of neurons as biosensor that report changes by change in activity patterns can be used to detected critical events [1]. Most studies of neuronal networks culture random networks formed by plating neurons over conducive surfaces like glass. Neurons in these networks are free to connect with any number of neurons forming any number of synapses giving rise to complex network properties such as spontaneous bursting activity. To exploit all features of neuronal networks, parameters governing network behavior must be controlled. Some of the parameters that are known to control *in vitro* network behavior are cell type, cell density, cell plasticity and cell interaction [2].

The crux of this dissertation is dedicated to develop techniques to constrain neuronal networks to specific geometries in order to elucidate certain properties of network behavior and to remove confounding effects of random networks. Most of the work to constrain neuronal networks thus far has been performed to improve electrical signals from neurons plated on Multi Electrode Arrays (MEAs). It has been shown that patterning of neuronal networks can modulate and enhance activity of networks [2, 3]. Constraining networks in this manner has been performed to ensure higher-degree of contact of neurons to substrate bound electrodes.

Our interest in constraining neuronal networks is two fold. The first is to investigate a network phenomenon know as reverberation, that occurs in small neuronal networks (~ 100 neurons). The second is to create a platform that allows for a means of controlling direction of network formation (with a defined input and output). Currently, it is possible to limit the connectivity of neurons to their neighbors only in computational models. The only physical limitation that can be applied is to control the regions over which the network is formed. Here we use two different techniques to constrain neural networks in order to study two distinct aspects of network behavior with the intention of setting a framework that can be used by researchers in the future. These two techniques are (i) microcontact printing (ii) physical constraining of neuronal networks .

1.3 SOFT LITHOGRAPHY

Soft lithography is the collective term used to describe the techniques of microcontact printing (μCP) [4], replica molding [5], micro-transfer molding (μTM) [6], micromolding in capillaries (MIMIC) [7] and solvent-assisted micromolding (SAMIM)[8]. This term has been popularized by Whitesides and colleagues since, " *in each case an elastomeric stamp or mold is the key element that transfers the pattern to the substrate and, more broadly, because each uses flexible organic molecules and materials rather than the rigid inorganic materials now commonly used in the fabrication of microelectronic systems* " [9]. Microfabrication is the term used to describe the process of constructing micron sized structures. Microfabrication technology was developed for the semicondutor industry where it is used to make integrated circuit boards, micro processors etc. Photo-lithography is one of the most versa-

tile techniques in microfabrication [9]. Photo-lithography has been used extensively in fields other than microelectronics. Xia and Whitesides [9] (figure 2) identified the future of photo-lithography in 1998 as one that will span a range of fields. Today in 2010, in retrospect photo-lithography has truly spanned this range and made the field truly interdisciplinary. Xia et. al [9] have described some of the advantages and disadvantages of soft lithography. Some of the advantages include low cost, ease of manufacturing, good control over surface chemistry and optical clarity. On the flip side these elastomer are susceptible to deformation and degradation and features $< 1\mu$m are difficult to achieve. In this study we use two of the above soft lithographic techniques, namely microcontact printing (μCP) and replica molding to create all elastomeric structures.

Microfabrication is the term used to describe the process of constructing micron sized structures. Microfabrication technology was developed for the semiconductor industry where it was used to make integrated circuit boards , micro-processors, etc. Photolithography is one of the most versatile techniques in microfabrication. Photolithography has been used extensively in fields other that microelectronics. Xia and Whitesides [9] identified the future of photolithography in 1998 as one that will span a range of fields. Today, in retrospect, photolithography has spanned that range and made the field truly interdisciplinary.

The microfabrication process begins by making the desired pattern using a computer aided design (CAD) software and printing it on a high resolution transparency. This transparency is referred to as a 'mask' hereon. The mask facilitates the travel of light over specific areas and blocks light from traveling over other areas. In order to render the desired patten solid, a photoresist is coated over a silicon wafer, the wafer acts as a substrate that allows the adhesion of the photoresist in a covalent manner. To achieve a planar coating of the

photoresist over the silicon wafer, the photoresist is spin coated over the silicon wafer on a spinner. The wafer now is exposed to Ultra Violet (UV) light to fix the resist permanently over the wafer. At this point, the mask is sandwiched between the wafer and the UV light source in order to render the desired pattern that is on the mask. Thus areas of resist that have been exposed to UV light cross-react and bind to the surface and areas that were not can be washed out. The wash out of unexposed areas is carried out in a developer that removes regions of resist that have not cross-reacted. The resulting wafer is termed a 'master' since it forms a template that can be used repeatedly.

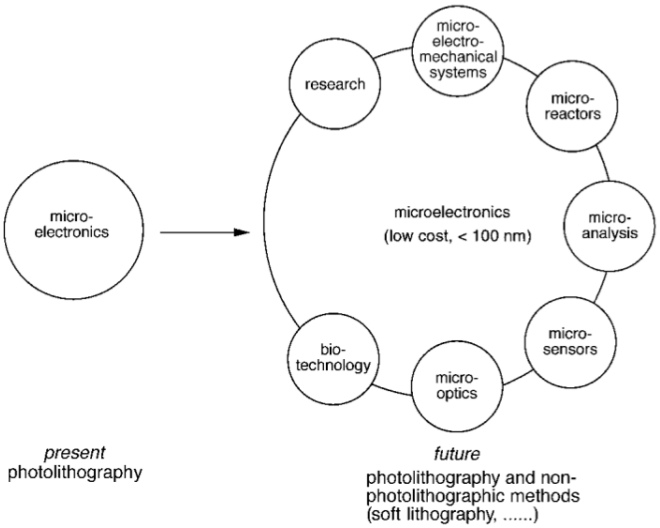

(a)

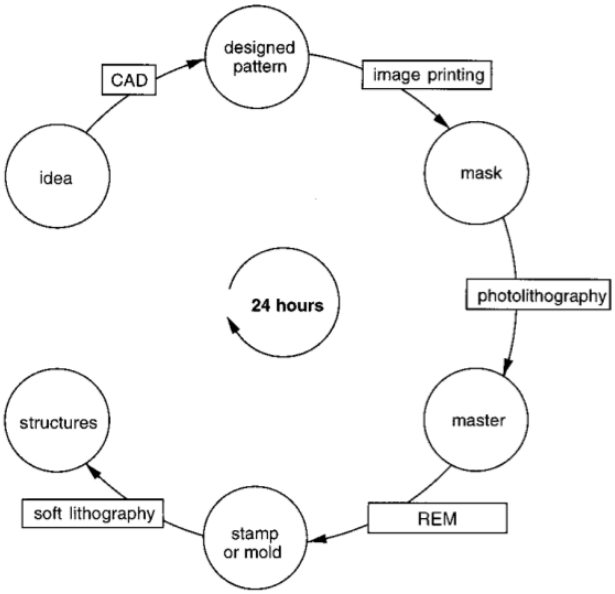

(b)

Figure 2: Future applications of photo-lithography

(a) The future of photo-lithography as identified by Xia and Whitesides [9] in 1998 (b) The rapid prototyping process of soft lithography [9]

Techniques such as these have spawned a complete field dealing with science at the micro-scale. Mammalian cells are on the order of microns or tens of microns. *In vitro* cell culture methods used to grow such cells have been in place for over half a century and have lead to numerous discoveries regarding the inner workings of cells. Despite all these progresses, one cant help but ask the question, " how does removing a cell from it native environment affect its workings?". There is thus a need to develop newer methods that can bridge the gap between current *in vitro* platforms and *in vivo* systems. Microtechnology (collective for all soft lithography technologies) has the potential to develop new platforms to help bridge this divide. Such technologies offer the possibility of maintaining mammalian cells in environments similar to that *in vivo*. It is now possible to assay cells at scales similar to the size of the cell. Cells can be constrained over patterns, grown in microenvironments, exposed to dynamic gradients in a precise spatiotemporal manner as seen *in vivo*.

Neurons offer researchers a seperate dimension of accessibility by means of their electrical nature. Microtechnologies offer the ability to interface with neural cells by means of electrical inputs. MEAs (a product of the semiconductor industry) are arrays of silicon electrodes the size of neurons, over which neural cells are grown. The electrodes can both receive as well as provide electrical impulses to the neurons. MEA technology has revealed the complex dynamics of networks of neurons. MEAs have also been shown to be useful as sensors to sense release of neurotransmitter from neurons [1]. Finally, MEAs are being used to deliver 'agents' in a controlled manner to a network of neurons by releasing such agents in an electrochemical manner [10]. A new line of MEAs are being developed that have pointed electrodes to make them compatible with neural tissue as compared to dissociated cultures [11]. Such MEAs are being used to study networks of neurons and their role in learning and

memory. Thus, it is easy to see in a short time, microtechnologies have proven extremely useful to researchers and have revealed new properties of complex systems. Indeed two reviews published recently highlight the role of microtechnologies and their applications to neuroscience [12, 13] and the importance of effective collaborations between fabricators and neurobiologists.

1.4 MICROFLUIDICS

Microfluidics can be described as the flow of fluids at a micron scale. In general microfluidic devices have a few generic geometric components, some form or method to load the fluids in question, some form of manipulation of these fluids (e.g. mixing), geometric features to read an output. Microfluidics as a field can trace its beginnings to molecular analysis, defense applications, molecular biology and microelectronics [14]. Beebe et. al. [15] have identified Reynolds number (Re), laminar flow, diffusion, fluidic resistance, surface area to volume ratio and surface tension as the fundamental physics involved in microfluidics devices. Design of a microfluidic device for biological applications must consider the above physics and their resulting phenomena in order to achieve desired results. Microfluidic devices offer the ability to recreate *in vivo* like environments *in vitro*. Such devices, owing to the unique physics at micro scales, offer exceptional control of input parameters over conventional *in vitro* platforms. Here we shall review some of the important physics and their application to microfluidic devices.

1.4.1 Laminar flow

The ratio of Inertial forces to viscous forces of a fluid is summarized by the non-dimensional Reynolds number (Re) At a micron scale, the viscous forces of a fluid overcome its inertial forces, this is represented by the equation;

$$Re = \frac{\rho V L}{\mu} \tag{1.1}$$

Here Re is the Reynolds number, ρ is the density of the fluid, L is the linear dimension, V is the velocity of the fluid and μ is the Viscosity of the fluid.

Typically at a macro scale when $Re < 2000$ there is laminar fluid flow defined by the lack of disruption in layers of fluid (i.e. the velocity of any random particle in the fluidic stream does not fluctuate with time). In laminar flow conditions different fluids do not mix with each other, instead they flow parallel to each other with limited diffusion in a plane normal to the direction of fluid flow. In contrast, when $Re > 4000$ the flow is turbulent, resulting in mixing of the fluidic layers. However at a micro scale the linear dimension is in the micron range, this dramatically reduces the Re of the fluid, limiting it to regimes of laminar flow only, thus preventing mixing of various fluid layers. For biologist this presents a unique degree of control of the fluid flowing in scales equivalent to the size of single cells. One of the very first demonstrations of the laminar flow to cell culture was elegantly demonstrated by Takayama et. al [16] where they patterned cell substrates, cell types and cell culture media using laminar flows, highlighting the simple yet highly reproducible nature of experiments possible using microfluidic devices.

1.4.2 Diffusion

Diffusion is the phenomena by which a concentration of particles, will by means of Brownian motion, move out in a manner such that the final concentration of these particles reaches an average in a given volume. Mathematically diffusion can be modeled by

$$d^2 = 2Dt \tag{1.2}$$

Here d is the distance traveled by a particle in time t with a diffusion coefficient of D.

Diffusion at microscales happens much faster than at macroscales since distances vary as square power of diffusion. Thus, it take shorter time for species to diffuse across microchannels as compared to macrochannels. This phenomena allows for creating complex gradients of active species inside microfluidic devices [17]. Apart from the fact that static gradients of active species can be patterned over substrates [17, 18, 19], it is also possible to expose cells to dynamic gradients [20]. However, neuroscience faces one big challenge with respect to dynamic gradients. Axons and other neurites do not take well to shear-stress. Most microfluidic devices used to create dynamic gradients operate at fluid velocity ranges that causes significant shear-stress to neurites. Recently, Wang et. al. developed a microfluidic device that addresses this specific issue [20]. They exploited a feature of fluid flow called 'lid driven flow' that reduced the shear-stress on the neurites yet allowed them to be exposed to a dynamic gradient. Similarly traditional platforms such as bioreactors exert tremendous mechanical forces on the cells being grown. These reactors need constant stirring in order to facilitate distribution of nutrient media to cells. The constant movement and stirring creates mechanical forces that are not experienced by cells otherwise. Microfluidic device do not

require constant stirring like bioreactors, mechanical forces such as shear stress effects on cells in devices can be overcome by carefully designing the device [21].

Thus Microfluidic devices offer the ability to recreate *in vivo* like environments *in vitro*. Such devices, owing to the unique physics at micro scales, offer exceptional control of input parameters over conventional *in vitro* platforms. Neuroscience has largely been plagued by problems associated with *in vitro* platforms and their limitations. The advent of microfluidics has allowed researchers the possibility of superior control and reliability over experiments involving the interactions of neurons and their environments. Microfluidics is still a nascent technology with the potential to revolutionize research and point-of-care diagnostics that has a strong background in classic physics [14] making it an ideal candidate for portable biomedical devices.

1.5 MICROCONTACT PRINTING (μCP)

The study of neurons in culture requires control of attachment of neurons over substrates [22]. Typically neurons in culture are plated on glass surfaces that are treated with polymers of basic amino acids like poly-D-lysine or proteins like laminin [23]. In order to achieve greater degree of control over neuronal attachment, control over the regions of protein deposition is desirable. During development neurons constantly migrate in response to external cues. The neurons are constantly sending their axons out and probing the extracellular space in search of cues. These external cues are typically presented in the form of gradients of guidance molecules. Most of the guidance molecules known today have been discovered in invertebrates like the fruit fly, where the model system allows for detailed knock-out type

experiments required to reveal their roles. In higher order model systems however, it is much more difficult to answer such questions. Most experiments performed *in vitro* involve modifying the substrate used to culture neurons. Axonal guidance in particular requires the creating of some kind of diffusible gradient and monitoring the response of the axons to these gradients. Much of the initial work involving the turning of growth cones to diffusible gradients of guidance molecules involved repeated injections of the active molecule to create the gradients [24, 25]. This method, though effective does not produce precise gradients, it is equally difficult to study membrane or matrix-bound proteins using such a technique [26].

Microcontact printing (μCP) is the process of printing micron sized geometrical features of a biomolecular protein ink over substrates. This method allows for the precise control over the region of protein deposition on a substrate. It typically involves using photolithographic techniques to make precise featured stamps that can then be used to stamp proteins over the substrate. The first study that attempted to pattern neurons was conducted by Kleinfeld and colleagues [27], they attempted to pattern neurons in order to recreate order among dissociated cells. μCP has since been used extensively by researchers to study neuronal networks *In vitro* by culturing neurons over electrodes plated on glass substrates. Patterning of networks to obtain high-resolution neural networks was pioneered by Branch and colleagues in order to improve electrical signals from these neurons [28]. This technique has similarly been extended to low-density cultures, where neuronal networks were patterned over MEAs and recorded from [29, 30].

μCP has also been used to study potential synaptogenic molecules [31]. Agrin a molecule know to cause postsynaptic differentiation at neuromuscular junctions was patterned in a grid shaped geometry. It was observed that neuromuscular junctions co-localized over these grids

of agrin. This methods was then extended to test other potential synaptogenic molecules to assay for their synaptogenic properties [31]. μCP has been one the the most successful methods to have translated from a bioengineering realm into traditional biology. The field has seen widespread acceptance and has also been constantly evolving. New improvements to the field of μCP like electromagnetic patterning, electrochemical transfer and the transfer of patterned metals [32] are pushing the boundaries of the field further.

The development of the brain and for that matter most early developmental process depend largely on the creation of spatial and temporal gradients. In order to recreate these processes *in vitro* it is of importance to create such gradients. μCP allows for the creation of very precise static gradients that have proved very useful to researchers in detailing molecules associated with axonal guidance. The combination of μCP and microfluidics bring closer the possibility of creating both static and dynamic gradients. Recent work by the Folch group demonstrates this very elegantly. Here they used μCP to pattern muscle cells inside a microfluidic device followed by delivery of a synaptogenic molecule by means of a dynamic gradient to study the formation of neuromuscular junction synapses [33]. Although neuronal cells were not used in this study, it still brings the possibility of using such techniques to nerve cells ever so close.

1.6 PHYSICAL CONSTRAINING OF NEURONAL NETWORKS

Neurons grown *in vitro* by definition grow in a random manner into a random network. Networks grown in such a manner give rise to certain phenomena that are not observed otherwise. Constraining dissociated neuronal networks can have effects on the properties of

the network. It has been observed that networks of different sizes self-organize and adjust their activities over certain periods of time [34, 35]. Another feature of cultured neurons is the emergence of spontaneous activity [36, 37]. In general constraining neurons into smaller networks tends to maintain essential properties of the network whilst reducing the complexity of the overall network. Networks of randomly growing neurons have also been constrained to achieve growth of neurites in a specific manner. Initial work involving the effect of growth factors on axonal guidance required restricting the cells bodies from their neurites. This method can be viewed more as a high throughput method to study axonal guidance when compared to following axons in a randomly growing culture.

Robert Campenot first developed a method to confine neural cultures to specific 'compartments' using physical barriers. He demonstrated the role of nerve growth factor (NGF) on spinal ganglion cells [38]. These Campenot chamber - named after Robert Campenot, contain three small chambers on a single piece of machined Teflon. This piece of Teflon is aligned on top of a glass coverslip that has small grooves etched (or scratched) in it. Using vacuum grease, the device is assembled and filled with media. The neurons are placed in the middle compartment and allowed to grow, extending their processes through the grooves into the opposing chambers. The chambers have since been used to study roles of signaling pathways involved in axonal guidance [39], neuronal competition [40], retrograde trafficking and translation [41].

More recently a microfluidic device was developed to study axon injury models, wherein the neurons were separated from their distal processes. This device consists of two opposing chambers that are separated by a series of microgrooves [42]. These microgrooves are extremely small and are on par with the size of a couple of neurites. These microgrooves

owing to their small size have high fluidic resistance. Fluidic resistance can denoted by the equation

$$\Delta P = RQ_m \tag{1.3}$$

where ΔP is the pressure difference along the channel and Q_m is the mass flux and R is the resistance [43].

This can be imagined as analogous to resistance in electrical circuits where the pressure corresponds to the voltage and the flux corresponds to the current. However it must be noted that this analogy is valid in low Re schemes only. These microgrooves allows for the fluidic isolation of the two chambers for up to 14 hours [44]. This microfluidic device now allow researchers the possibility of studying isolated axonal populations, transport along axons and dendrites, protein translation at sites distant from the soma etc.

1.7 CALCIUM IMAGING

Calcium (Ca^{+2}) is an important secondary messenger molecule in neurons, for this reason the amount of calcium present inside a cell is typically buffered immediately and stored in intracellular stores [45]. Steady calcium flux is central to many cell types including neurons, cardiac cells and skeletal muscle cells. Calcium is also implicated in secondary messenger pathways that involve aspects of synaptic plasticity[46, 47, 48]. During sustained depolarization of nerve cells, calcium enters a cell via voltage gated calcium channels as well as N-methyl-D-aspartate (NMDA)-type glutamate receptors, it is this entry of calcium through NMDA-receptors that triggers a cascade of events that either leads to synaptic strengthening or its weakening depending on the levels of postsynaptic calcium [49].

Our current knowledge of the role of calcium in nerve cells can largely be attributed to the successful use of calcium indicators. Much of the initial work on using Calcium as an indicator was performed by Roger Tsien's group using genetic calcium indicators [50, 51]. There have been since many forms of calcium indicators, broadly they can be classified into two types (i) Genetic indicators (GI) and (ii) Chemical indicators (CI). CIs have many advantages over GIs, they exhibit a greater dynamic range (change in ratio or intensity), they are easier to load, they are available in a wide range of calcium affinities and display faster kinetics[52, 53]. GIs on the other hand typically have to be expressed in cells requiring gene transfer but the are more stably expressed and less susceptible to compartmentalization unlike CIs [52, 53]. CIs are typically available in three forms: salts, dextran conjugates and acetoxymethyl (AM) esters. Salts are hydrophilic and are membrane impermeable, thus require invasive methods to load the dye. Once loaded these dyes are quickly compartmentalized and are typically used within the first 30 min of loading [53]. Dextrans were specifically engineered to prevent compartmentalization and are highly water soluble, thus requiring invasive loading methods as well. The newest form of calcium indicator is the AM esters that are relatively hydrophobic and can be taken up by cell membranes simply by adding to the extracellular medium. Once inside the membrane, the AM groups are cleaved by esterases thus resulting in relatively large concentrations of dye intra-cellularly [53].

Typically cells, once loaded/expressing the indicator are monitored at varying time stages using a microscope. Cells that fire or receive a signal display a rapid increase in intracellular calcium followed by buffering of this calcium albeit with at varying degrees. Calcium indicators reveal a similar signal, in that there is a rapid rise in the signal followed by a slower time scale decay of the signal. Monitoring calcium in the manner offers researchers

advantages over different scales of network. One can follow single cells and their processes like dendrites and spines, or one can follow groups of neurons. This method of studying networks of neurons was pioneered by Rafael Yuste and Winfred Denk's groups. Early on they popularized the two-photon method of imaging thick cortical tissue prone to light scattering and concluded the existence of calcium channels in individual spine and their ability to distinguish between input to the cell and outputs from the cell [54]. Later work by the group looked at methods to follow postsynaptic neurons in a network of neurons, such that one 'trigger' neuron set off other 'follower' neurons and other higher lever cortical dynamics in networks [55], using calcium signal. More recently, this method of inferring activity is steadily moving from *in vitro* slide cultures to *in vivo* whole animal studies. Transgenic animals expressing genetic calcium indicators in specific neurons have been used to correlate activity in neurons to behavior [56]. These methods now permit researchers to follow groups of cells over a period of months and report long-term changes in activity patters, morphology etc. Thus, it is easy to see that calcium imaging has revolutionized the field of neuroscience, offering the ability to image at different scales of networks (few neurons to many neurons) and ultimately correlating activity to behavior.

1.8 ELECTROPHYSIOLOGY

Neurons, unlike most cells are constantly processing information via electrical signals. In addition to the secondary signaling methods employed by most other cells, neurons possess the ability to generate action potentials. An action potential is an all-or-none event much like a binary signal, indicating yes or no. These action potentials are caused by a carefully

orchestrated series of events involving the precise opening and closing of channels controlling the flow of ions that causes the membrane potential of the cell to make a sudden deflection. It has been theorized that information is encoded largely in the rate of these action potentials. Much of the initial work in understanding the action potential came from Hodgkin and Huxley around the middle of the century. The next significant leap forward was the 'patch-clamping' technique developed by Erwin Neher and Bert Sakmann [57].

The patch-clamp technique involves inserting a very fine glass capillary tube into the cell in such a manner as to gain access to the inside of the cell without rupturing the cell membrane. Typically the internal solution of the pipette contains a buffer that mimics the inside of the cells. The other end of the pipette contains a silver electrode that can be used to record as well as stimulate the cell. In this manner, one can induce spikes in the cell as well as read-out signals received by the cell that is being patched. This methods has give researchers unparalleled advantages over other techniques and has helped reveal many details of the workings of nerve cells. However, patch clamping is limited to the number of cells that can be patched. One pipette can patch onto one cell only and this requires dedicated hardware. Simultaneously patching from multiple cells can be performed with a hand full of cells only. If we need to understand working of networks, we need to have the ability to record from multiple cells simultaneously.

Here again the microelectronics industry has made it possible to make tiny electrodes that can be inserted into neural tissue. These electrodes are fabricated on tiny pieces of silicon that can be inserted via surgery into neural tissue. These probes are comprised of multiple electrodes scattered across the surface of the silicon. This method now permits researchers to record as well as stimulate multiple neurons simultaneously. Such electrodes

are being actively used to record from freely behaving animals and in some cases have also been implanted in human subjects. Less invasive techniques like EEG also allow for the monitoring of electrical activity from the brain.

There are now multiple methods of conducting electrophysiological experiments in nerve cells. Researchers can choose between any of these techniques based on their needs. Typically studies involving single cells with high temporal resolution and high signal to noise ratio use the patch clamping technique. Studies involving small networks of neurons tend to use MEAs and finally studies that involve recording from freely behaving animals tend to used *in vivo* electrodes.

2.0 CONSTRAINING USING MICROCONTACT PRINTING (μCP)

2.1 INTRODUCTION

Microcontact printing of fine micron sized features was developed by the Whitesides group [4]. It involves the deposition of amine based proteins over substrates that were chemically modified to promote their adhesion over selected regions. This method is still extensively used even today without much change in the chemistry. This method, though precise can prove to be detrimental to neurons since it exposes the neurons to chemicals attached to the substrates. A modification to this method was developed by Chang et. al [2, 58], where a photoresist is deposited over a glass substrate in a pattern opposite to the desired pattern. The surface is then bathed in the biomolecular ink, which adheres to both the glass substrate as well as the photoresist. Finally the photoresist is removed, leaving the protein over the glass substrate in a selective pattern. This technique was used extensively by Banker and colleagues to develop numerous growth cone assays for cortical an hippocampal neurons [59].

μCP has also been used extensively to pattern neuronal networks over MEAs. The Wheeler group has used μCP successfully to print poly-L-lysine (PLL) over electrodes in order to study the electrical behavior of the resulting network. They concluded that patterning, indeed had the ability to modulate activity in neuronal networks [3]. Micropatterned

substrates influence the neurite outgrowth length, rate and orientation of the cultured neurons [60]. Various patterns like square grids[61], circular spots [3, 62], triangular grid[30] etc. have been demonstrated to improve extracellular recording from neural networks.

Here we demonstrate the use of μCP to pattern neurons into circular 'ring' shaped networks. The purpose of this is to create a recurrent geometry such that the neurons are connected in a recurrent manner.

2.2 MATERIALS AND METHODS

2.2.1 Microfabrication

The process used to make the stamps involves making a pattern that is created by using a single layer of photoresist. The specific protocol involves cleaning and dehydrating mechanical grade Si wafer (University wafers, MA) at 150°C, followed by spinning photoresist SU8-3025 (Microchem, Il) over the Si wafers at 400 rpm for 25 sec followed by 1500 rpm for 45 sec to form a layer $\sim 60\mu$m in thickness. The coated wafer is then soft baked at 95°C for 15 min or until the resist has set. The wafer is then exposed to UV light for 20 sec followed immediately by hard baking at 95°C for 10 min or until the features are clearly embossed on the surface. The wafer is then developed in SU8 developer until all features are clearly visible. The masters are then hard baked for 30 more minutes at 150°C to improve mechanical stability of the features. In order to remove traces of developer and remaining un-crosslinked resist, the masters are washed throughly in 5% TritonX-100 for 20 min followed by multiple washes in distilled water before pouring any elastomer over the master.

Ring shaped stamps were created using poly-dimethylsiloxane (PDMS). In order to keep all stamps and structured clean, the stamps were immersed in Deionized (DI) water at all times. Before printing the protein, the stamps were air dried inside a laminar flow hood. In order to load the protein over the stamps, the surface of the PDMS stamps were made hydrophilic by oxygen plasma treating the stamps. The stamps were immediately transferred to a laminar flow hood, protein was then loaded over the stamps with the aid of a paint brush. The stamp was immediately placed in contact with a glass coverslip to transfer the protein. For all imaging studies we used Poly-L-Lysine (PLL) conjugated to FITC diluted to $1\mu g/\mu L$ in order to visualize the stamped regions. In subsequent studies we used PLL diluted in borate buffer.

2.2.2 Cell culture

Preliminary studies were done using primary visual cortical neurons harvested from embryonic day 17-18 mice. Briefly, the lower 1/3 of the cortex are removed and treated with trypsin and DNAase for 10 min at 37° followed by gentle washing in HBSS. The cortices are then titurated mechanically using three grades of fire polished glass pipettes in culture medium until all the chunks were broken. The dissociated cells were plated in microfluidic devices at native concentration (usually between $2-3$ million cells/ml. Approximately 10μL of cell suspended media was loaded into each of the fluidic reservoirs and the cells were allowed to flow into the device and adhere onto the glass surface. The culture medium consisted of Neurobasal medium (GIBCO, Invitrogen, Carlsbad, CA) supplemented with 2% B-27 (GIBCO, Invitrogen, Carlsbad, CA), 0.25% Glutamax (GIBCO) and 50 units/ml of penicillin/streptomycin (Sigma, St. Louis, MO).

Primary hippocampal neurons was then harvested from embryonic day 18-19 rats. Hippocampi were removed from rats and treated with trypsin for 15 min at 37° followed by gentle washing in HBSS. The hippocampi were then titurated mechanically using a fire polished pipette in culture medium until all the chunks were broken down. The dissociated cells were plated on 12mm diameter glass coverslips that were previously cleaned and auto-calved. The culture medium consisted DMEM (GIBCO, Invitrogen, Carlsbad, CA) supplemented with 10% heat-inactivated bovine calf serum (HyClone), 10% Ham's F-12 with glutamine (Bio-Whittaker), 50 units/ml penicillin/streptomycin (Sigma, St. Louis, MO), and 1X B-27 supplement (GIBCO, Invitrogen, Carlsbad, CA). Twenty-four hours after plating, one-third of the culture medium was replaced with the same medium supplemented with 20 mM KCl. Cytosine arabinoside (AraC) (Sigma, St. Louis, MO) was added to the culture dish (final concentration, 5 μM) around 7-10 days in vitro (div) to prevent overgrowth of glial cells.

2.2.3 Immunostaining

For immunocytochemistry the cells were fixed in 4% Paraformaldehyde (Sigma, St. Louis, MO) and Sucrose prepared freshly for 10 min followed by three washes in phosphate buffered saline (PBS). The cells were then permeabilized in 0.3% TritonX-100 for 5 min followed by three washed in PBS. The cells were then incubated for 1 hr in 5% BSA in PBS, used as a blocking agent. Primary and secondary antibodies were diluted in 1% BSA in PBS at 1:500 for Tau1 (Millipore, Billerica, MA), 1:1000 for MAP2 (Sigma, St. Louis, MO) and 1:1000 for Synapsin1 (Chemicon, Billerica, MA), incubated with the cells for 1 hrs. This was followed by three washes in PBS. Following primary, secondary antibody , Alexa-555 (Invitrogen, Carlsbad, CA) or Alexa - 488 (Invitrogen, Carlsbad, CA) was incubated with the cells for

1 hr followed by three washes. After the second wash, nuclear stain Hoechst (Invitrogen, Carlsbad, CA) diluted in PBS at 1:10000 was incubated with the cells for 5 min, followed by the third and final wash. The coverslips were then briefly dunked in DI water to remove any traces of salt and placed over a bead of FluormontG (Southerbiotech, Birmingham, AL) used as a mounting agent.

2.2.4 Imaging

All imaging was perform on an inverted epi-fluorscence imaging microscope (Leica). Images were collected individually at each of the filter ranges and merged using ImageJ (Wayne Rasbald, NIH). Some of the rings used in the first generation stamps were too big to be imaged at the least magnification of the microscope (100X). For such rings, images of different regions of the ring were acquired and stitched using the 'stitch' plugin on Fiji (ImageJ image processor).

2.3 RESULTS

2.3.1 Microcontact printing of ring shapes

The first technique that was used to constrain neuronal networks is microcontact printing. μCP uses a stamp to print a biomolecular ink over a chosen substrate. In order to print the pattern, a positive relief of the pattern was made in PDMS, this relief pattern is called the microstamp. The microstamps were classified into two groups (Table 1), group 1 had a fixed outer radius of 300μm and group 2 had an outer radius of 200μm. The outer radius of the

Table 1: Dimensions of microstamps

Group	Outer radius μm	Inner radius μm	Track Width μm	Track Length μm
1	300	250	50	1727
		225	75	1648.5
		200	100	1570
		150	150	1413
		100	200	1256
2	200	190	10	1224.6
		175	25	1177.5
		150	50	1099
		100	100	942
		75	125	785

'loop' structures were chosen such that each loop was completely visible within a single field of view (FOV) under the microscope. Initial versions of the stamps were much bigger and multiple images had to be acquired and stitched in order to visualize the complete 'loop'. The 'loop' geometries were made using AutoCAD inside a grid like structure. The grid like structure serves two purposes, one is to separate the individual 'loops' to improve visibility of each individual structure and the second is to relive the stresses developed during removal of elastomeric stamp (Figure 3, 4). The grid structure is also created in the positive relief stamp and gets stamped onto the surface of the substrate. This facilitates the growth of cells over the grid structure that help sustain the cell population on the 'loop' structures by releasing trophic factors that help in conditioning the media.

Neuronal networks activity strongly depends on the number of neurons present and the connectivity of these neurons to each other. We chose to address these parameters by choosing two analogous parameters, 'track length' and 'track width' (Table 1) . The track length is defined as the circumference of a circle that passes through the center of any given loop. The track width is defined as the thickness of the loop, which is the difference of the radius of the outer circle from the inner circle in any given loop. Control over these two parameters of the stamps allows for control over the neuronal network to be formed. The track length gives us a measure of length to be traversed by a signal to return to its origin; longer the track length, longer is the time taken. Similarly, track width gives a measure of number of neurons in a network, thus larger track width equals more neurons and vice versa. Thus signal propagation time gives us a measure of the connectivity of the network.

2.3.2 Stamp characterization

The stamps were created using soft-lithography techniques described in the previous section, PDMS elastomer in a 1:10 ratio was poured over the stamps and baked at 95 for 120 min and allowed to cool. Following the cooling of the stamps, they were cut out using a sharp scalpel and immediately immersed in DI water for storage.

In order to obtain a homogeneous transfer of the protein from the surface of the stamp to the glass substrate it is imperative that the stamps created were planar in nature. The stamps were measured under an alpha-stepper (profilometer) to measure small changes in height. Each ring provides two numbers each time the stepper steps over the edge of the ring. These number, depending on the approach of the tip were classified as the left or right heights of the rings (Figure 5a). Comparison of the heights of the ring structures reveals

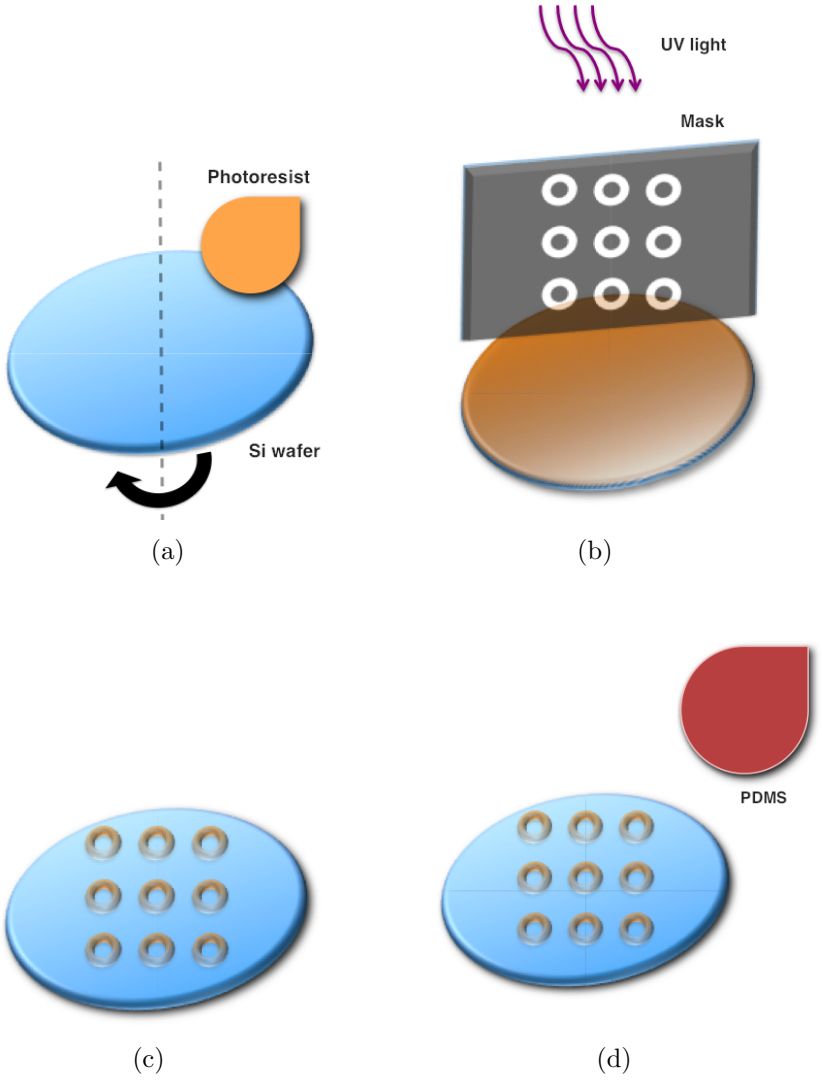

Figure 3: Microstamping process: from creation to stamping-part a

(a) Photoresist is spin coated over the silicon wafer (b) Silicon wafer is exposed to UV light in presence of a mask (c) The resulting wafer is developed to remove all unexposed regions of photoresist (d) Polymer is poured over the master to create the elastomer stamp.

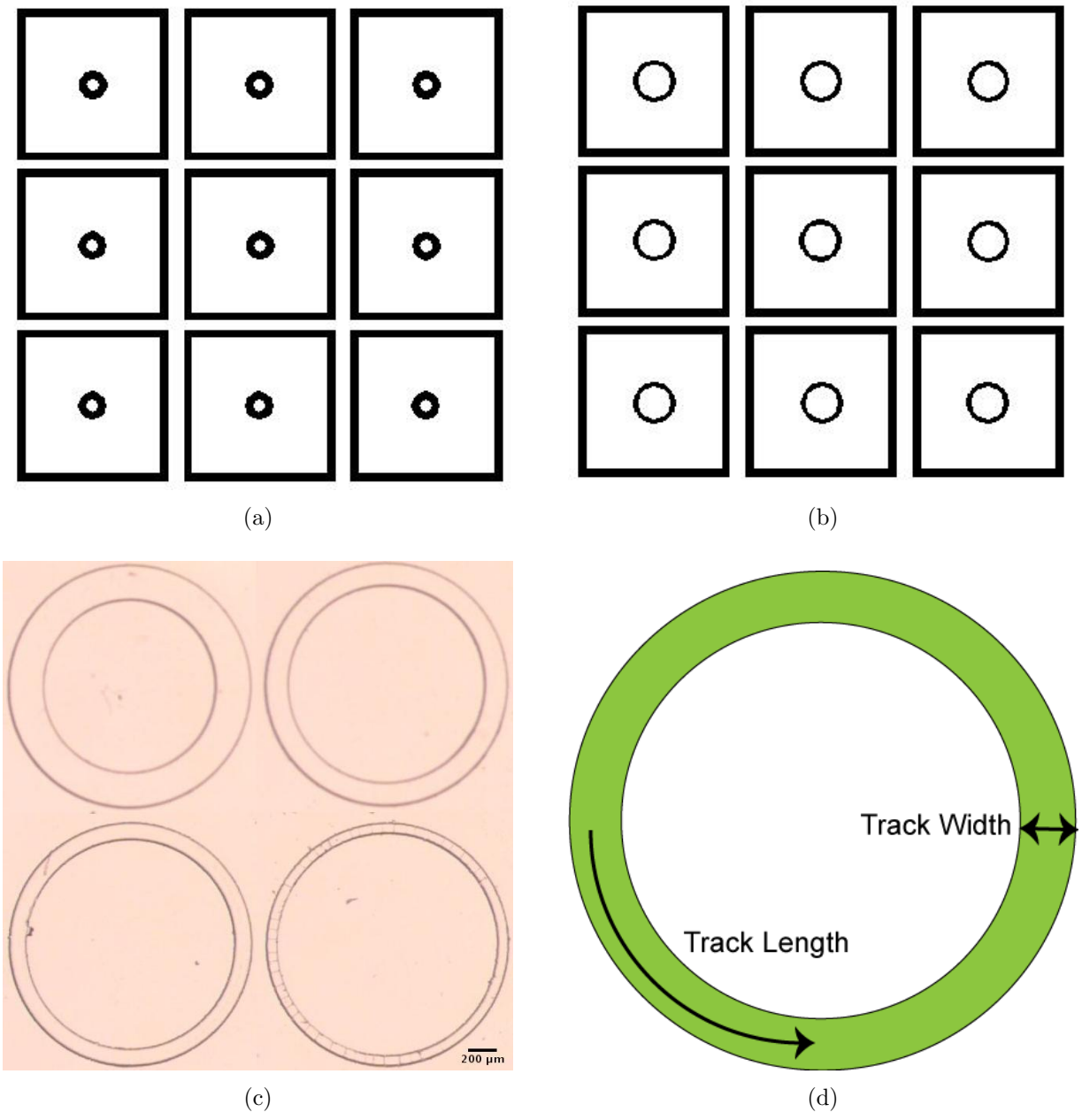

Figure 4: Microstamping process: from creation to stamping-part b

(a) Microstamps with outer radius 200μm surrounded by grid structure. (b) Microstamps with outer radius 300μm surrounded by grid structure. (c) Photomicrograph of a PDMS stamp with ring stamps of varying sizes. (d) Schematic of the loop design with parameters of interest

that the rings are mostly planar and differ on an average by $0.05 \pm 0.03\mu$m and there is no significant difference in the means (Ttest $p > 0.01$).

Next we proceeded to characterize the amount of protein transferred during the stamping process. In order to promote long-term maintenance of the protein on the surface of the substrate, we choose to encapsulate the protein along with poly-ethyleneglycol (PEG). PEG has been used in the past as a substrate for microcontact printing of adhesive proteins to maintain neuronal cultures, since it is know to be non-permissive for extended culture periods [63]. We compared between two groups, PEGulated and non-PEGulated cases of PLL conjugated to FITC (Figure 6).

Pegulation of the protein produced a sharp punctate type dispersion of the protein over the substrate. In comparison, no pegulation led to a much more homogeneous but lesser dispersion of the protein over the surface. For the purposes of this study it was decided to used the non-pegulated form of printing, since it led to a homogeneous transfer of the protein over the substrate. Secondly, culture periods extending for 15 days does not have any adverse effects on the stamped pattern, PEGulation of the protein is more desirable for culture periods lasting for 1 month as indicated in [63].

2.3.3 Culturing neurons on stamped substrates

Primary mice E17 neurons were cultured over the stamped substrates. In all cases the substrates were glass coverslips which were cleaned and autoclaved before stamping the neurons. The stamping process involved coating the PDMS stamps with PLL+FITC, allowing it to dry over the surface and briefly bringing the stamp and the substrate in contact for a few seconds before separating them. The stamped substrates were then briefly rinsed in DDW

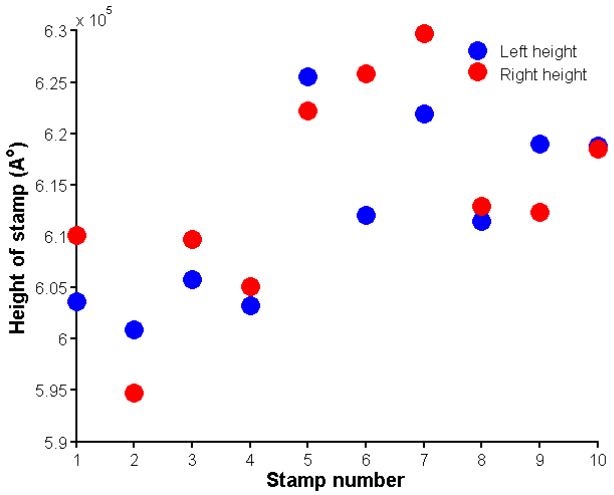

(a)

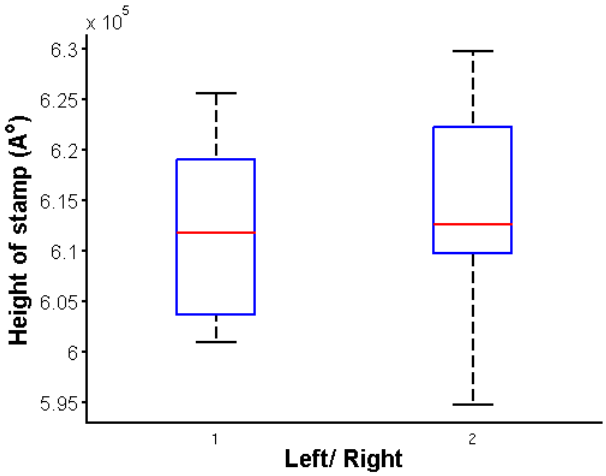

(b)

Figure 5: Stamp profilometer measurements

(a) Comparison of edge heights, left and right edge of a given stamp (b) Box-plot comparing the left and right edge heights, bold line inside the box is the sample median

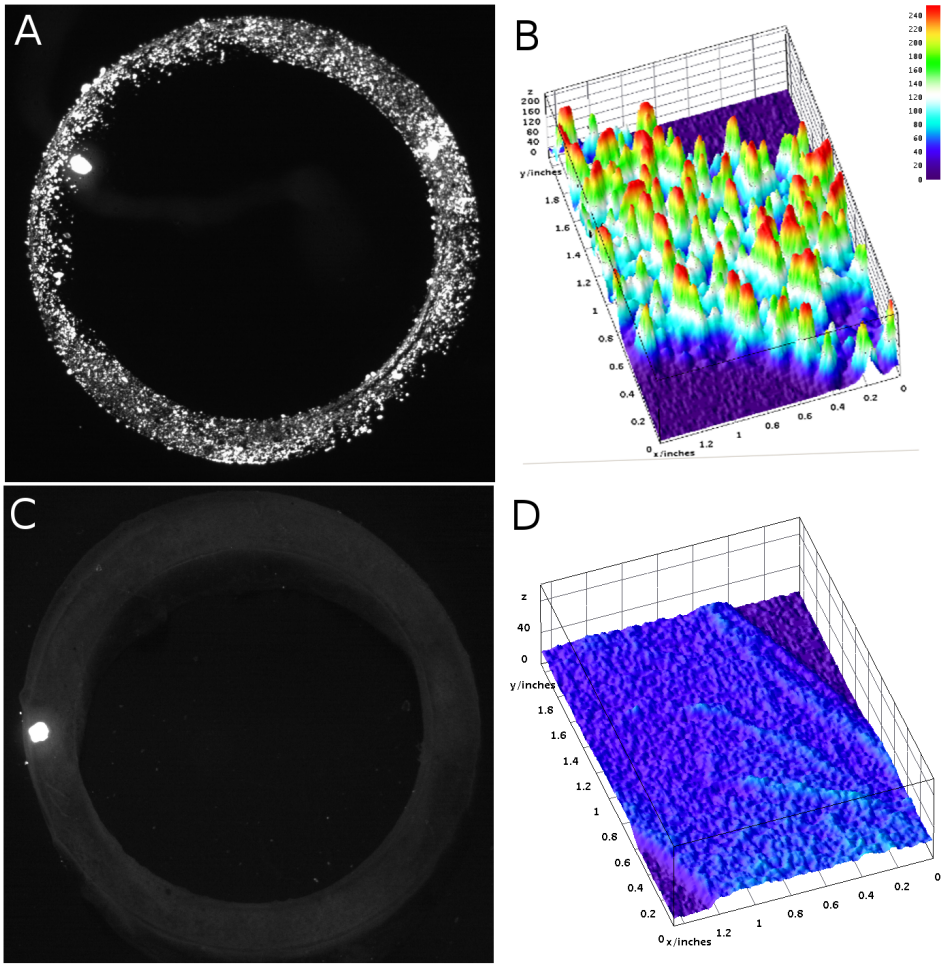

Figure 6: Protein transfer characterization

(a) Image of PLL+FITC encapuslated in PEG stamped over a glass substrate (b) Grayscale intensity of a small region of stamp (c) Image of PLL+FITC transferred over the substrate (d) Grayscale intensity of a small region of stamp

before plating neurons on them. Neurons plated on the stamped substrates formed networks that were restricted to the stamped regions. The cultures were maintained until 9 days in vitro (DIV) at which point they were fixed and probed using immunocytochemistry. The neuronal process were stained with axonal specific marker Tau-1 (red in Figure 7), the adhesive protein PLL was conjugated to FITC (green) and the nuclei was stained with nucleic dye Hoechst (blue). This experiment showcased (i) the amount of protein being transferred from the stamp to the ring was sufficient to maintain viable neuronal networks (ii) the PLL that was stamped on the substrate was attached to the surface at the time of fixing (DIV 9) (iii) Neurons plated by this method seemed to form clusters (large cell aggregates of 20 or more cells) at regular intervals, seen as huge circular masses in the images (arrowheads in Figure 7).

The number of clusters that appeared on each of these rings were counted and compared to the track width and the track lengths of the rings (Figure 8). Increase in track length forms clusters as compared to smaller track length there was a increase in the number of clusters till track length 1250μm following which the number of clusters seemed to plateau (Figure 8a). Similarly as the track widths increased, there was an increase in the number of clusters formed on the rings (Figure 8b). Within an individual track width, the number of clusters increased with an increase in track length as well (Figure 8c). Since fixed samples are extremely delicate, not many networks were intact at the end of the process and number of data points are not evenly matched.

Large cell aggregates of neurons disrupt pattern formation in the existing culture by deveating away from the patterned regions. Formation of such large clusters can be attributed partly to patterning of the substrate. Patterning the surface forms large areas which do

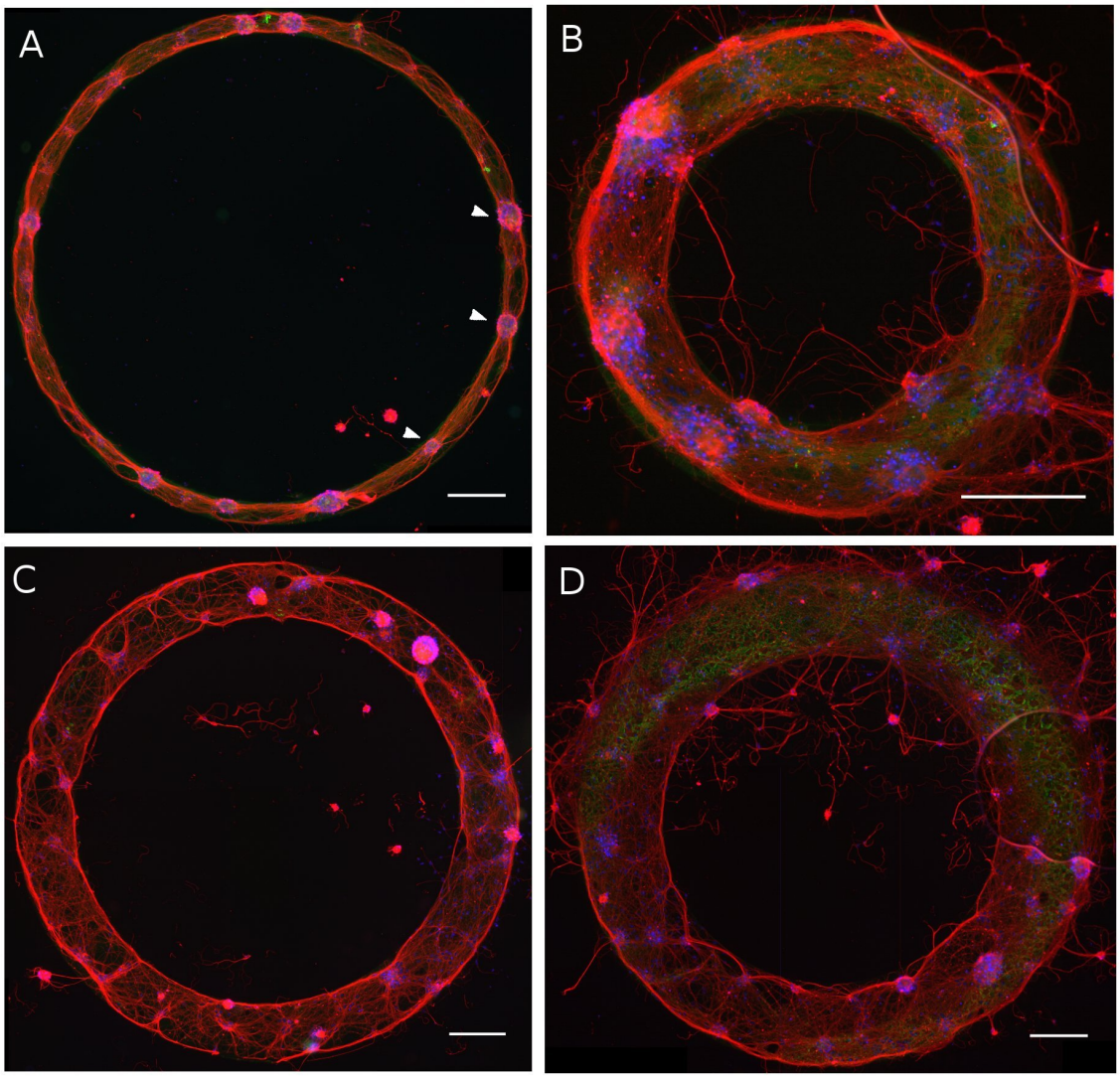

Figure 7: First generation of 'ring' shaped neuronal networks

(a) Outer diameter = 1800μm, track width = 75μm (b) Outer diameter = 800μm, track width = 150μm (c) Outer diameter = 1750μm, track width = 200μm (d) Outer diameter = 1750μm, track width = 300μm. Scale bar in all image corresponds to 200μm.

not support cell adhesion, larger the non-patterned area more number of cell aggregates are formed [64]. These cell aggregates have the ability to remain in these 'neurospheres' for a period of up to 24hrs before apoptosis sets in. During this time they can reattach themselves to patterned regions and integrate in the existing pattern [64]. In order to reduce the number of clusters, we decided to plate neurons in serum media as compared to non-serum media which does not promote the growth of glia. Glia acts as a surface over which neurons can adhere, most standard culturing techniques require the pre-plating of a glial monolayer before neurons are plated [65]. We hypothesized that the plating of neurons along with glia allows for a better support over patterned regions, preventing neurons to end up in 'neurospheres', thus allowing for lesser disruption in the patterns. In order to allow the growth of glia over the patterned substrate, we switched the primary cultures from E17 mice to E19 rat cultures in serum enriched medium.

2.3.4 Second generation of neurons cultured on stamped substrates

The next round of stamped substrates involved using E19 rat hippocampal neurons cultured in serum enriched media. We chose to use neurons from the hippocampus since the hippocampus is a homogeneous source of typical neurons found in the CNS [23].The patterned substrates were washed briefly before plating the cells. Cells were plated at different densities to determine the optimal density that would be required for future experiments, our aim was to achieve a cell density of 50-100 cells per ring. Cells were plated at $> 10^6, 10^5$ and 10^4cells/ml and the number of cells that ended up in each ring was counted by fixing the cells at DIV7. Figure 10 indicates the number of cells per ring in the second generation of ring networks, the cells were plated on rings with the same track width -100μm in all cases.

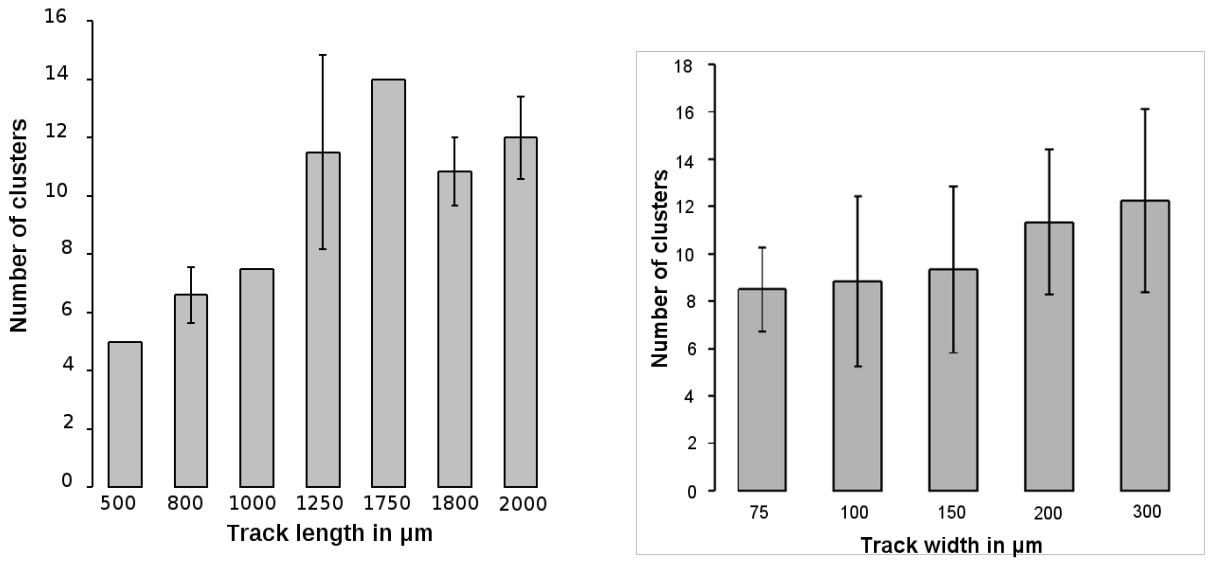

(a) (b)

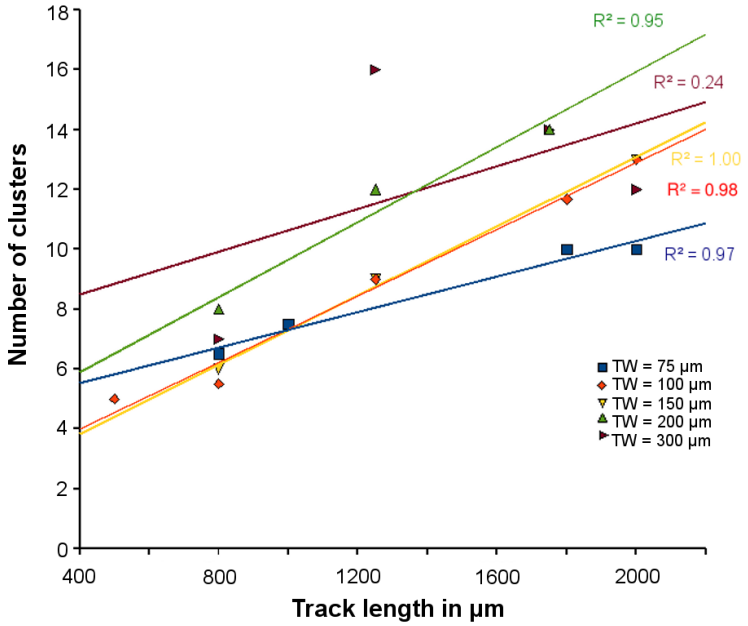

(c)

Figure 8: Analysis of cluster formation on varied ring parameters

(a) Number of clusters versus track length (b) Number of clusters versus track widths (c) Trends indicating the effect of track length at varying track lengths.

A density of 10^5cells/ml resulted in $40-70$ neurons per ring, whereas $> 10^6$cells/ml resulted in $\approx$ 200 neurons per ring which results in excessive crowding inside the ring. Similarly 10^4cells/ml resulted in too few cells in each ring and no proper completion of the ring networks. Table 2 is a summary of average number of cells per ring at various ring dimensions, these dimensions are based on Table 1.

Figure 9 is representative of ring networks of various dimensions, all plated at 10^5cells/ml. We confirmed presence of nerve cells using antibodies specific to neurons - Tau1 and nuclei with Hoechst. Immunocytochemistry revealed neurons that adhered largely to the adhesive protein PLL and extended process within the patterned region to form 'ring' shaped networks. Thus a cell density of 10^5 cells/ml was chosen for all the future experiments as it yielded $40-70$ cells per ring which was determined as the optimum number of cells per network [66].

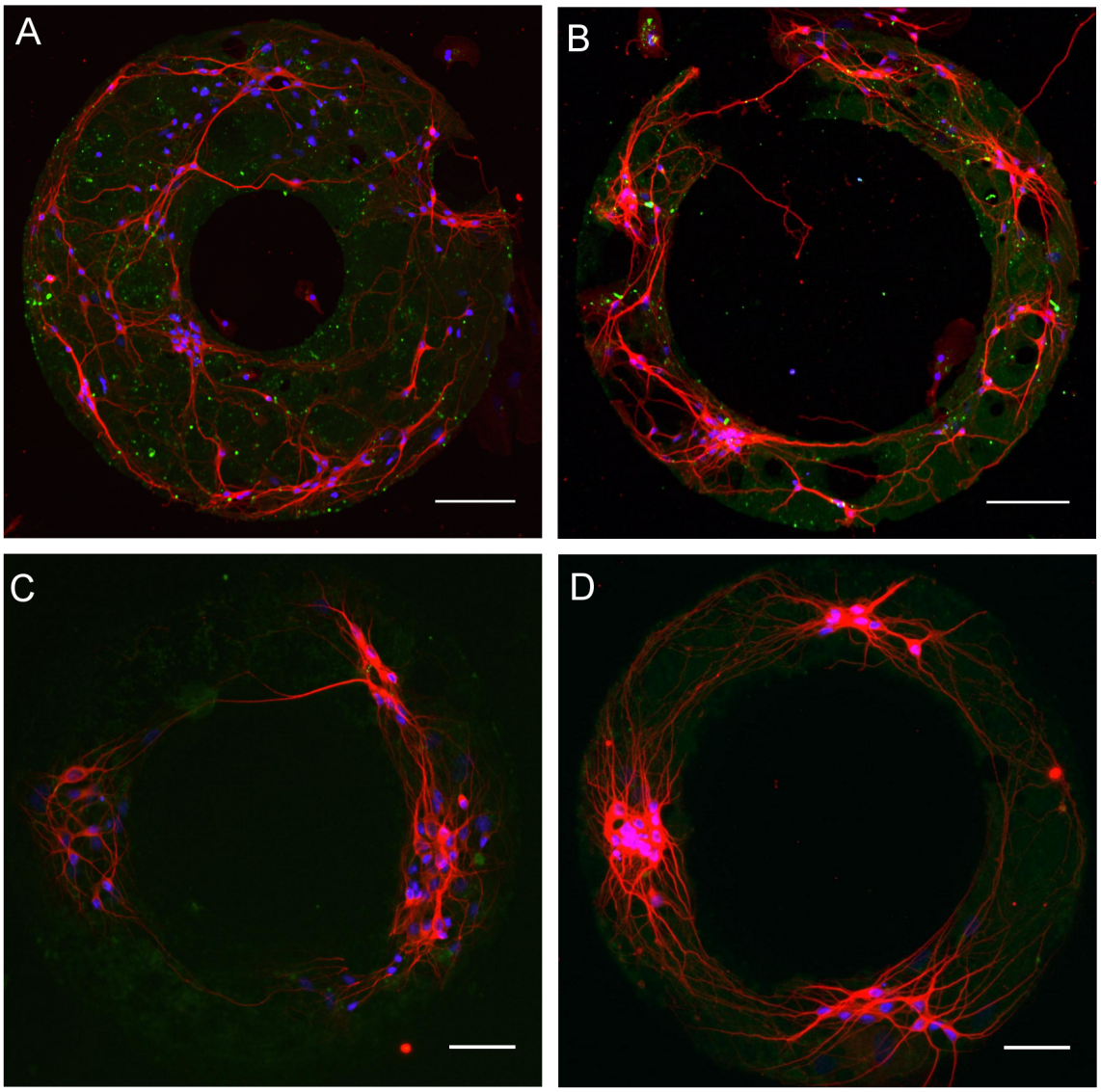

Figure 9: Second generation of 'ring' shaped neuronal networks

(a) Outer diameter = 300μm, track width = 200μm (b) Outer diameter = 300μm, track width = 100μm (c) Outer diameter = 200μm, track width = 75μm (d) Outer diameter = 200μm, track width = 100μm. Scale bar in all image corresponds to 100μm.

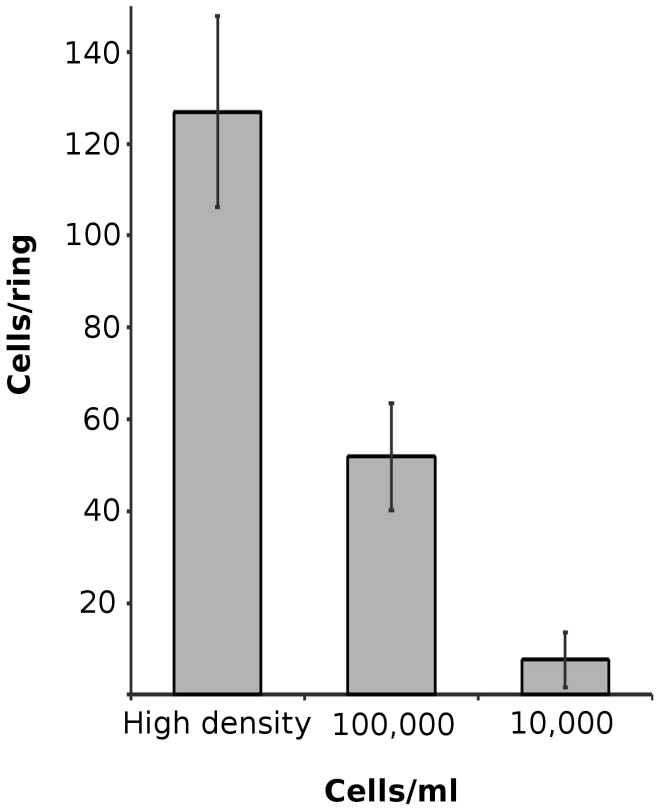

Figure 10: Number of cells per ring

Number of cells per ring for the second generation ring networks (high density- $>$ 10^6cells/ml). Reproduced by permission of The Royal Society of Chemistry [67]

Table 2: Average cells per ring for various ring dimensions

Density ($cells/ml$)	Cell/ring ($Average \pm sd$)	Track width (μm)	Outer Radius (μm)
$> 10^6$	198.80±45.53	200	300
	127.00±20.75	100	300
	51.60±16.91	125	200
10^5	44.33±11.37	50	200
	51.90±11.64	100	200
	92.50*	150	300
10^4	5.00±5.04	125	200
	7.61±6.02	100	200
	13.64±8.83	150	300

* Only one smample was collected

2.3.5 Ring cultures form synapses

We finally tested to see if these ring cultures formed synapses. In order to observe the synapses, we immunostained ring networks that were allowed to grow up to 12 DIV with the presynaptic marker Synapsin1. The synaptic marker was observed in a typical punctate manner (Figure 11). The immunostaining revealed extensive synapses formation spread over the network. It was observed that in general there was a clustering of synapses close to the cells bodies. However, synapses were also observed at distal regions, that had a high degree of neuronal processes. Previous studies have shown that patterning does not adversely affect synapses formation and that the number of synapses formed at cultures of similar densities remained similar in patterned and random networks [30].

2.4 CONCLUSION

In this chapter we showed that microcontact printing is a versatile tool that can be used to restrict neuronal networks to 'ring' shaped geometries. Microfabricated stamps of even height were obtained that facilitated homogeneous deposition of protein ink over the substrate. Since the protein ink was still visible after 15 days in culture, it was decided that pegulation of the protein ink was not necessary. The neurons reliably formed networks over regions printed with neural adhesive proteins. It was observed that when plated at high densities, the networks displayed clustering of neurons and that the number of clusters seemed to increase with increase in track length at all track widths. However, these clusters prevented the networks from maintaining defined geometries over extended periods of time.

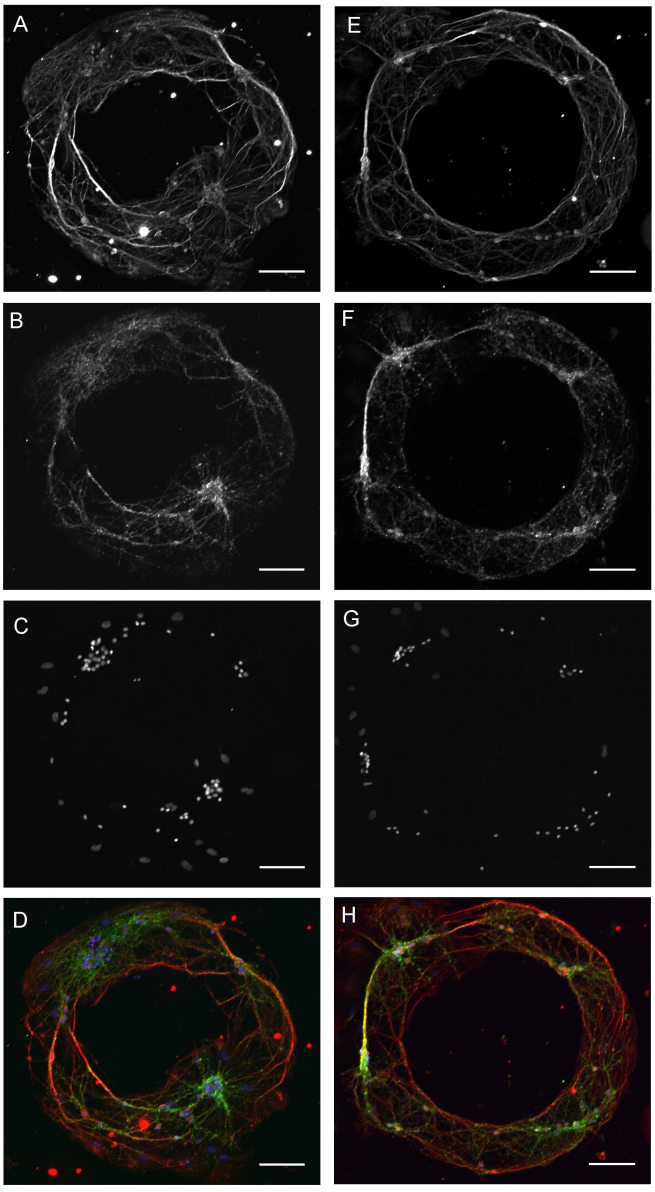

Figure 11: Ring networks form synapses

Ring netwroks of two different sizes Track width - 150μm (left panel) and 100μm (right panel) were immunostained for neuronal (red), synaptic (green) and nuclear (blue) markers. (A,E). Neuronal marker Tubulin-1 shows the spread of neuronal processes. (B,F). Pre-synaptic marker Synapsin1. (C,G). Nuclear marker Hoechst. (D,H). Merge shows the extent of co-localization and spread of synapses in the ring network. Scale bar = 100μm.

In order to reduce the clustering, we hypothesized that glial monolayers would reduce the clustering. We then switched the culture medium to a serum supplemented media. In this new media, it was observed that the clustering effect disappeared. It was also observed that a cell density of 10^5 cells/ml yielded $\sim 40 - 70$ neurons per ring. These cultures were successfully maintained for extended periods of time (3 weeks) without disruption of the ring geometry. Finally, we immunostained these networks to see if they formed synapses. We noticed that all the cultures that were stained were positive for presynaptic formations indicating the formation of synapses.

2.5 DISCUSSION

Microfabrication of stamps to obtain neuronal networks was carried out. Here we observed that when the cells were plated a optimal densities, it was possible to form ring shaped neuronal networks. The formation of these networks depended largely on the deposition of protein over the glass substrate. In many cases, it was observed that inhomogeneous deposition caused voids in the network. In this work we present only the ring shaped networks, and have avoided talking about the role of the grid surrounding the rings. Initial experiments involved patterning the ring without a supporting grid. Here it was observed that the cells were not viable for more than a few days and were mostly unhealthy. The role of the ring shaped geometry is to reduce the number of pathways available for activity signals to propagate. It is our belief, that by reducing the number of pathways available for propagation of activity, we can remove some of the confounding effects of the larger network from relevant network properties. We also checked for the formation of synapses around DIV 12. It is

well known that the height of synaptogenesis in *in vitro* cultures is around DIV 9-12. Thus by performing the staining this late into the culture we hoped to have crossed the critical period of synaptogenesis. Experiments performed in the future chapters also consider this into account. Although, in this body of work we created stamps of a few different size, we were able to perform experiments in the future chapters on two different sizes that differed in their track widths by 50μm.

3.0 CONSTRAINING INSIDE MICROFLUIDIC DEVICES

3.1 INTRODUCTION

The second technique to constrain neuronal networks is to restrict networks inside a microfluidic device. These devices have been popularized in the last decade by the Whitesides group[16, 68, 17, 69, 70]. It offers researchers precise spatiotemporal control over the microenvironment at a cellular scale, at low costs and with a high degree of repeatability.

During development, neurons extend their axons over long distances in response to some soluble gradient of an attractor or repulsor. Traditionally, such research was performed by generating passive gradients by placing a source of the soluble factor very close to the cells and allowing for diffusion to carry the factor. Such techniques do not have the ability to control the gradient over a period of time. These can be used to investigate the response in a very binary manner (yes or no).

Microfluidics offers researchers the ability to recreate such developmental gradients at a cellular scale. It also offers precise control over the formation of such gradients in a spatial and temporal manner. Most gradient generators consist of multiple micro-channels that break down soluble factors by serial dilution, then introduce them to a region containing cells [17, 20]. Another significant development of microfluidic application was developed

by the Jeon group [71, 72, 42] (Figure 12a). This device significantly improves over the Campenot chamber (figure 12b) developed previously to study the role of NGF [38]. The basic design of both devices calls for separation of neuronal cell bodies from their distal nerve terminals. The Campenot chamber however does not differentiate between the types of nerve terminals (axons and dendrites). In order to study local proteins in the axons only, Taylor and colleagues developed a microfluidic device [42] that is capable of separating the axons form the rest of the nerve terminals. This device is also capable of controlling the local micro-environments of the chamber containing the cell bodies and the opposing chamber containing the axons. At the heart of this device are very small micro-channels that connect the two chambers (axonal and somal chambers). These micro-channels allow the passage of small neuronal processes but not the entire cell body. The micro-channels also exert high resistance to the flow of fluids, thus making it hard for fluids to flow from one chamber to the other, ensuring fluidic isolation of the two chambers. In our study we use a microfluidic device similar to that developed by the Jeon group with a few minor modifications in the dimensions of the device. We successfully constructed two variants of the devices, one with two chambers that are capable of housing cells connected via microgrooves and the other with three chambers connected via microgrooves.

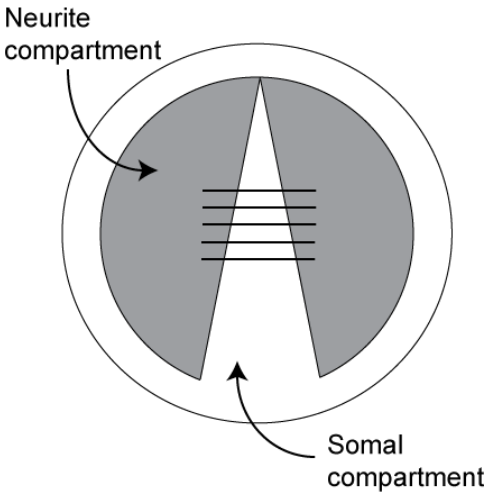

(a)

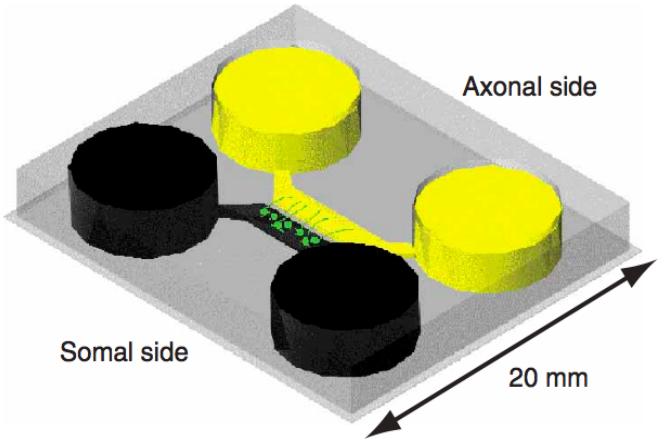

(b)

Figure 12: Microfluidic device to restrict neurons

(a) Schematic of Campenot chamber with somal compartment and neurite compartment. The cross-hatches represent grooves on the surface act as guides to axons extending from the somal chamber to the neurite chamber (b) Schematic of Microfluidic device with somal side and axonal side. Neurons (green) are seen extending their axons from the somal chamber to the axonal chamber (adapted from [42]).

3.2 MATERIALS AND METHODS

3.2.1 Microfabrication

The microfluidic device is fabricated by a two-step process. The main parts of the device are the micro-channels and the chambers. The micro-channels are approximately 3-5μm tall and 7-10μm wide. The fluidic chambers are approximately 60μm tall. In order to achieve these distinct height profiles, the device is fabricated in two steps. The first step lays down a layer 3-5μm tall, this layer is then exposed to a mask that contains the pattern of the micro-channels only. The specific protocol involves cleaning and dehydrating mechanical grade Si wafer (University wafers, MA) at 150°C, followed by spinning photoresist SU8-3025 (Microchem, Il) over the Si wafers at 400 rpm for 25 sec followed by 3000 rpm for 45 sec to form a layer 3-5μm in thickness. The coated wafer is then soft baked at 95°C for 2 min or until the resist has set. The wafer is then exposed to UV light for 17 sec followed immediately by hard baking at 95°C for 2 min or until the features are clearly embossed on the surface. The wafer is developed in SU8 developer until all features are clear, then hard baked at 150°C for 30 min.

The developed wafer from the first step is then coated with a new layer of photoresist that is approximately 60μm tall. The wafer is then soft baked at 95°C for 15-20 min or until the photoresist is deemed dry. This coated wafer is then aligned with a mask that contains the features for the second layer followed by exposure to UV light for 20 sec. The wafer is then baked for 5-8 min following exposure (care needs to be taken to prevent over-exposure) or until the feature of the second layer appears embossed over the photoresist. This is then developed until all features are clear and hard baked at 150°C for 30 min. PDMS is mixed

in a 1:10 ratio of hardener to elastomer, poured over the master and allowed to cure at 95°C for 120 min. Once cooled the PDMS is cut using a sharp scalpel and the media wells are removed using a 4″ biopsy punch. The PDMS molds are then cleaned under a stream of nitrogen gas and stored under DI water for up to 1 week or can be used immediately.

3.2.2 Cell culture

Cleaned device were air dried and placed in contact with 25mm glass-coverslips. The device adhere non-reversibly onto the glass substrate. In order to prevent formation of bubbles inside the device, the device are first washed with a low-surface tension fluid like 70% ethanol. This is them replace with culture washed (GIBCO, Invitrogen, Carlsbad, CA) and loaded with poly-l-lysine in borate buffer. The PLL was allowed to adhere onto the surface for 30 min and rinsed with more culture water. The device are then filled with culture media and placed inside the incubator for at least 2 hrs before cells are loaded.

Primary visual cortical neurons are harvested from embryonic day 17-18 mice. Briefly, the lower 1/3 of the cortex was removed and treated with trypsin and DNAase for 10 min at 37° followed by gentle washing in HBSS. The cortices are then titurated mechanically using three grades of fire polished glass pipettes in culture medium until all the chunks were broken. The dissociated cells were plated in microfluidic devices at native concentration (usually between $2-3$ million cells/ml. Approximately 10μL of cell suspended media was loaded into each of the fluidic reservoirs and the cells were allowed to flow into the device and adhere onto the glass surface. The culture medium consisted of Neurobasal medium (GIBCO, Invitrogen, Carlsbad, CA) supplemented with 2% B-27 (GIBCO, Invitrogen, Carlsbad, CA), 0.25% Glutamax (GIBCO) and 50 units/ml of penicillin/streptomycin (Sigma, St. Louis,

MO). The culture medium was changed every 24hr by replacing one-third of the media with fresh media.

Primary hippocampal neurons were harvested from embryonic day 18-19 rats. Hippocampi were removed from rats and treated with trypsin for 15 min at 37° followed by gentle washing in HBSS. The hippocampi were then titurated mechanically using a fire polished pipette in culture medium until all the chunks were broken down. The dissociated cells were plated in microfluidic devices at native concentration (usually between $2-3$ million cells/ml. The culture medium consisted DMEM (GIBCO, Invitrogen, Carlsbad, CA) supplemented with 10% heat-inactivated bovine calf serum (HyClone), 10% Ham's F-12 with glutamine (Bio-Whittaker), 50 units/ml penicillin/streptomycin (Sigma. St. Louis, MO, St. Louis, MO), and 1X B-27 supplement (GIBCO, Invitrogen, Carlsbad, CA). Twenty-four hours after plating, one-third of the culture medium was replaced with the same medium supplemented with 20 mM KCl. Cytosine arabinoside (AraC) (Sigma. St. Louis, MO, St. Louis, MO) was added to the culture dish (final concentration, 5 μM) around 7-10 days in vitro (div) to prevent overgrowth of glial cells.

3.2.3 Morphology analysis

For the analysis of morphological parameters we use ImageJ (Wayne Rasbald, NIH) loaded with the NeuronJ plugin [73]. Briefly, the images of neurons were loaded and the neurites were traced and classified as neurites. Similarly the cell circumference was traced and classified as soma. Once the images were traced, a summary of the morphological parameters was outputted by the program. These output parameters were then saved for further analysis.

3.2.4 Calcium imaging and electrophysiology

Stock solution of Calcium sensitive dye Fluo4-AM (Invitrogen) at 1.5mM was prepared in dimethyl-sulphoxide (DMSO). The above solution was diluted in Hanks buffer solution (HBS - containing $150mM$ NaCl, $3mM$ KCl, $3mM$ $CaCl_2$, $2mM$ $MgCl_2$, $10mM$ Hepes, and $5mM$ glucose (pH 7.4)) to give a final concentration of 2.5μM. Cells were typically incubated for 45 min-1hr at room temperature in the dark before the commencement of the experiment. All images were taken on a LeicaDMB microscope and acquired by a CCD camera-Roper Scientific 512B on RSimage. The images were analyzed offline using a custom written Matlab software (Mathworks). Changes in fluorescence were reported as

$$\frac{\Delta F}{F} = \frac{(F_0 - B_0) - (F_1 - B_1)}{F_0 - B_0} \tag{3.1}$$

where,

F_0, B_0 = intensities of the somas, background at first frame

F_1, B_1 = intensities of the somas, background vary with time [74].

All devices were stimulated with a Grass SD-9 stimulator. The electrodes were placed in the media reservoirs , one at each end such that the field produced would encompass one chamber. The stimulator was controlled by a Master-8 (AMPI systems) controller unit, used to synchronize the stimulator and the camera used for imaging. In most cases, a train of stimuli was used to observe stimulation in the cells.

3.3 RESULTS

The objective of this body of work was to constrain neurons inside a microfluidic device in order to create an electrophysiological platform to investigate the role of patterned growth. Here we developed different types of microfluidic devices that are each capable of housing a population of neurons for extended periods of time. These device have the ability to maintain one or more populations of neurons each capable forming a network. These devices also have the ability of maintain isolated fluidic mixtures that could be used to maintain each of the above populations under different conditions.

3.3.1 Neurons mature faster in microenvironments

We began by looking at the behavior of neurons inside microfluidic devices. The aim of the project was the see if there were any significant differences in the maturation of neurons in microenvironments as compared to traditional *in vitro* methods. In order to do this, we plated neurons under two different culture conditions. One involved plating the neurons inside a microfluidic device and the other involved plating the same number of neurons under similar conditions, but in a regular open culture (similar to a Petri dish). Once the cells were plated, images of single cells were acquired at five different time points and basic morphological parameters were compared. We compared, the number of neurites the originated from each cells, the average length of these neurites, the circumference of the soma and the average length of all neurites from single isolated cells. It was observed that there were fewer number of neurites that originated from each cells inside a microfluidic device. The circumference of the somas under each condition remained the same (Figure 13).

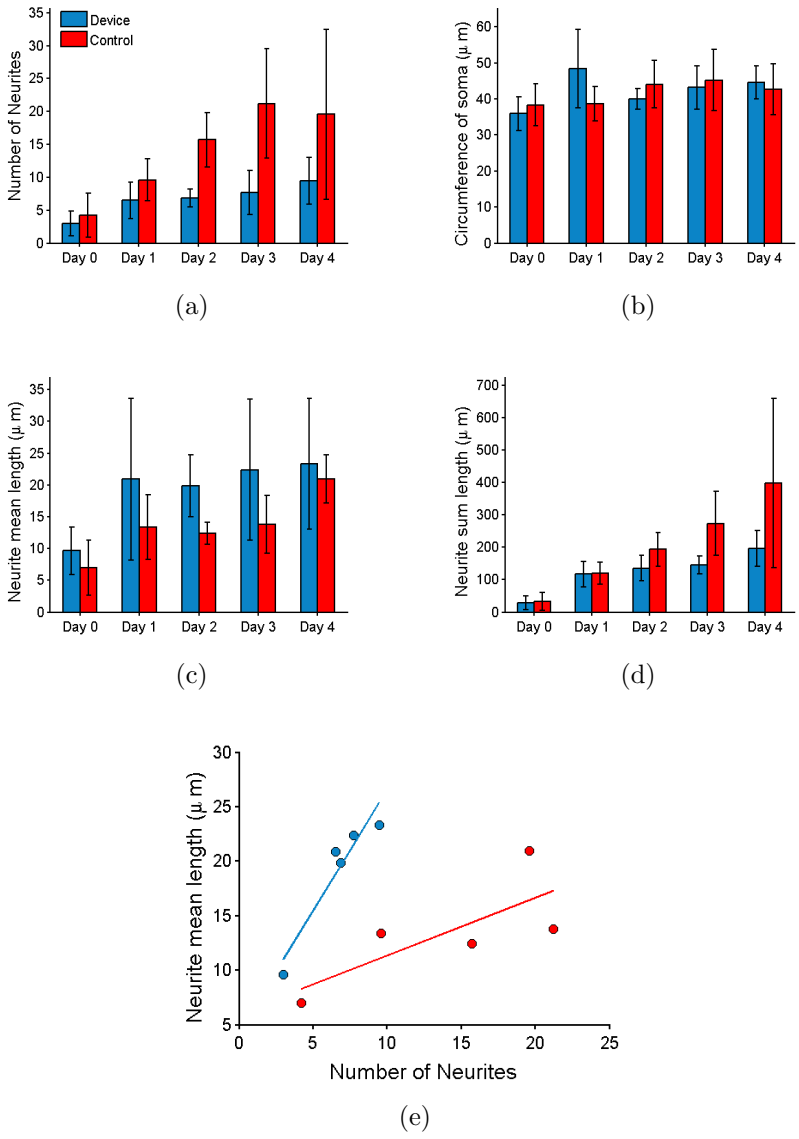

Figure 13: Summary of Neuronal morphology in microfluidic devices

(A). Number of neurites on each cell inside microfluidic chamber and control device (B). Mean circumference of somas (C). Mean length of a single neurite (D). Mean of sum length of neurites (E). Scatter plot of number of neurites vs. average length of neurites for cell in traditional *in vitro* culture (red) and cells in microfluidic device (blue). Cells have fewer longer neurites inside microenvironments.

Interestingly, we noticed that cells in a microfluidic environment produced fewer but longer neurites as compared to cells in a traditional *in vitro* culture (Figure 13). At each of the time points measured, the cells in a microfluidic device had fewer but longer neurites as compared to cells in the controls. The results though interesting are expected. In microenvironments, cells receive important signals much sooner as a result of diffusion inside these devices, as a result they tend to mature and develop sooner.

3.3.2 Two and three chambered microfluidic device

Microfluidic device was constructed based on the design by Rhee et.al. [75] . The design was modified to make the chambers smaller and have fewer grooves to facilitate easy imaging under a microscope. The device itself consists of two chambers $5cm$ long connected to each other by 120 microgrooves of three different lengths. The microgrooves themselves are $7\mu m$ wide and $3-4\mu m$ tall. The microgrooves serve two purposes, 1) to allow the growth of neuronal processes from either chamber to the other side and 2) to fluidically isolate the micro-environments of the two chambers by creating high resistance. We fabricated microfluidic devices in three different sizes $200, 450$ and 1000μm respectively (Figure 14).

We also tested to see whether neurites that were growing inside 1000μm length microgrooves were axonal in nature as was reported previously [42]. In Figure 14b we immunostained neurons that were allowed to grow for a period of 1 week from a single chamber. It was noticed that after 1 week many neurites were able to extend across the 1000μm

barrier and that most of these processes stained positive for anti-tau1 an axonal marker and not as much for anti-MAP2 a dendritic marker. It was observed that when the length of the microgrooves was 1000μm there were very few dendrites that crossed the barrier at the 2 week point of fixation.

Finally we also created a device that had three chambers capable of maintaining cells for extended periods of time. The purpose of creating this device was to use the central chamber as a 'testing' chamber that can be loaded with agents to exclusively affect neural processes and not the cells bodies in the opposing chambers. Figure 15 shows an immunostained network of cortical neurons that was maintained inside the three chambered device. The somas are restricted to the two outer chambers while the neural processes were allowed to grow toward the central chamber.

3.3.3 Electrical stimulation of neurons

Using the microfluidic devices described in the previous section, we tested to determine whether the neurons inside the device could be activated via field stimulation. The neurons were plated inside microfluidic devices and allowed to grow for 12 days. The neurons were then loaded with calcium indicator Fluo4-AM for 1hr before commencement of experiment. In order to electrically stimulate the neurons, we inserted two silver electrodes into the reservoir section of the device (Figure 16A, schematic) such that the subsequent electrical field encompassed a single chamber. The silver electrodes we connected to an external stimulator unit (Grass SD-9). The stimulus was a train of pulses at 10Hz at 80V.

It was observed upon stimulation cells responded robustly to the electrical stimulation. Not only did the cells on the same side as the electrode respond, but the cells in the opposing

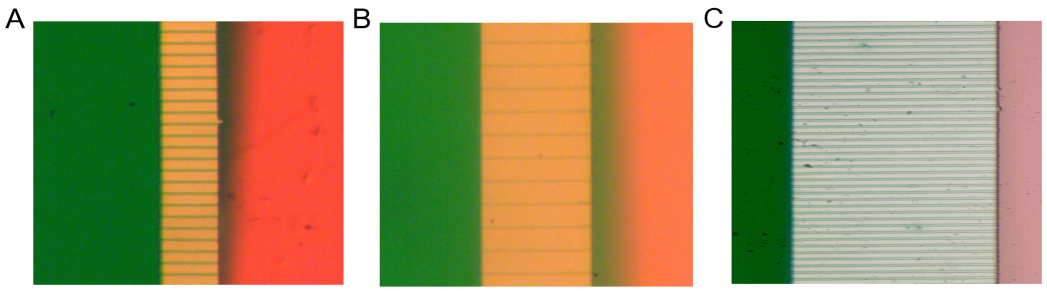

(a)

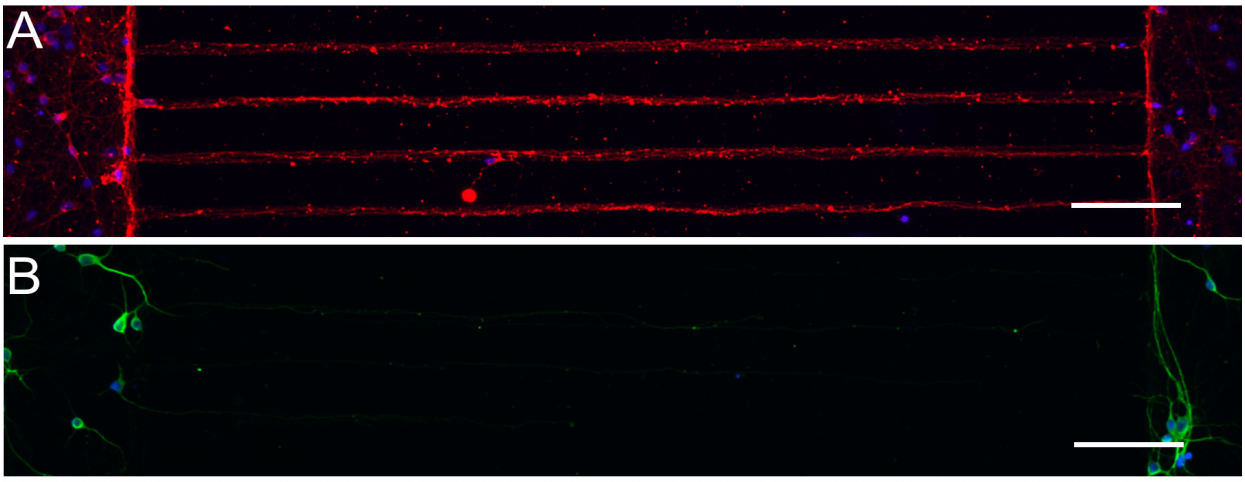

(b)

Figure 14: Microfluidic device with microgrooves

(aA) Microfluidic device with two chambers(green and red).The chambers are connected via microgrooves (green lines) that are 200μm in length. (aB) Length of Microgrooves = 450μm. (aC) Lenght of microgrooves = 1000μm. (bA) Neurons (blue) cultured in microfluidic device with microgrooves of length = 1000μm immunostained for axonal marker Tau1 (red). (bB) Similarly neurons (blue) cultured within a microfluidic device with microgrooves of lenght = 1000μm immunostained for dendritic marker MAP2 (green). Scale bar 100μm.

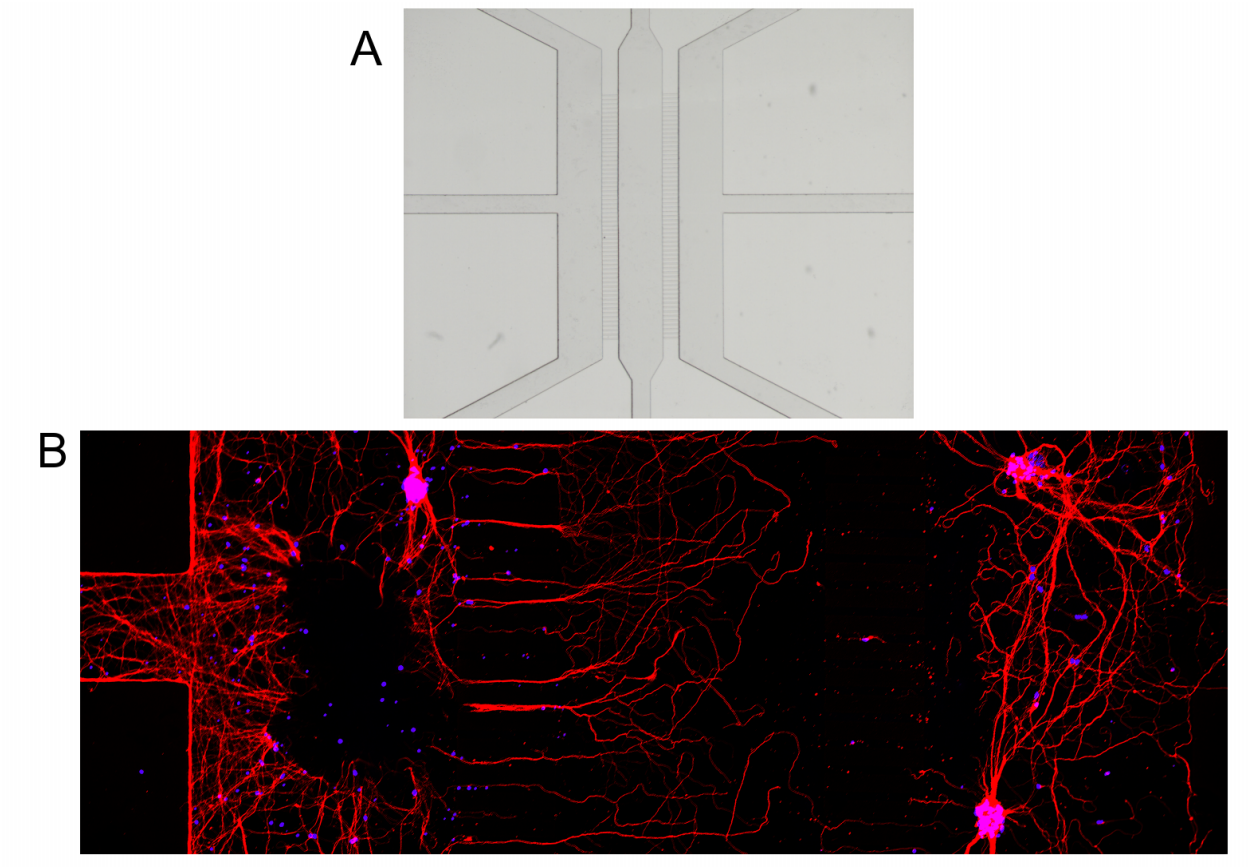

Figure 15: Three Chambered microfluidic device

(A). Photomicrograph of microfluidic device with three chambers. Left and right chambers are loaded with cells from side ports. (B). Immunostaining of cells grown inside microfluidic device and stained against axonal marker Tau1 (red) and nuclear marker Hoechst 33342 (blue).

chamber also responded to the stimulus. Finally, upon introducing a solution with high [K^+] (know to globally activate cells) all the cells responded to the stimulus. The electrode was moved to the opposing chamber and stimulated, here again it was observed that the cells responded reliably to the electrical stimulation.

3.3.4 High-throughput study of Heterologous synapses

Synapses are specialized structures that are formed by a complex of cell adhesion molecules that involves both the pre- as well as the post-synapse. Synaptogenesis is the precisely co-ordinated act of a presynaptic axon establishing contact with a postsynaptic dendrite. CNS neurons have been shown, *in vitro* to synapse onto non-neuronal cells expressing synaptic proteins, forming 'heterologous synapses' [76]. This system allow for a "bottom-up" approach to studying the genetic and molecular requirements for synaptogenesis. However, the non-neuronal cells proliferation typically renders these co-culture setups unusable after 48 hrs. Similarly, the pharmacological techniques to prevent non-neuronal cell growth are detrimental to the neurons.

Here we demonstrate a modified-Campenot Chamber technique to maintain heterologous synapses up to a period of 1 week. By extending the co-culture period, we are able to expand the capabilities of in vitro testing of synaptic molecules and their dependence on synaptic initiation and modulation. This extended period will also allow us to explore the timing requirements of key proteins using the heterologous synapse approach.

We use standard soft lithography to fluidically isolate two microchambers while allowing axonal connectivity between them. This allows the two cell populations to be maintained in separate culture conditions, yet able to connect cellularly. This platform allows for extended

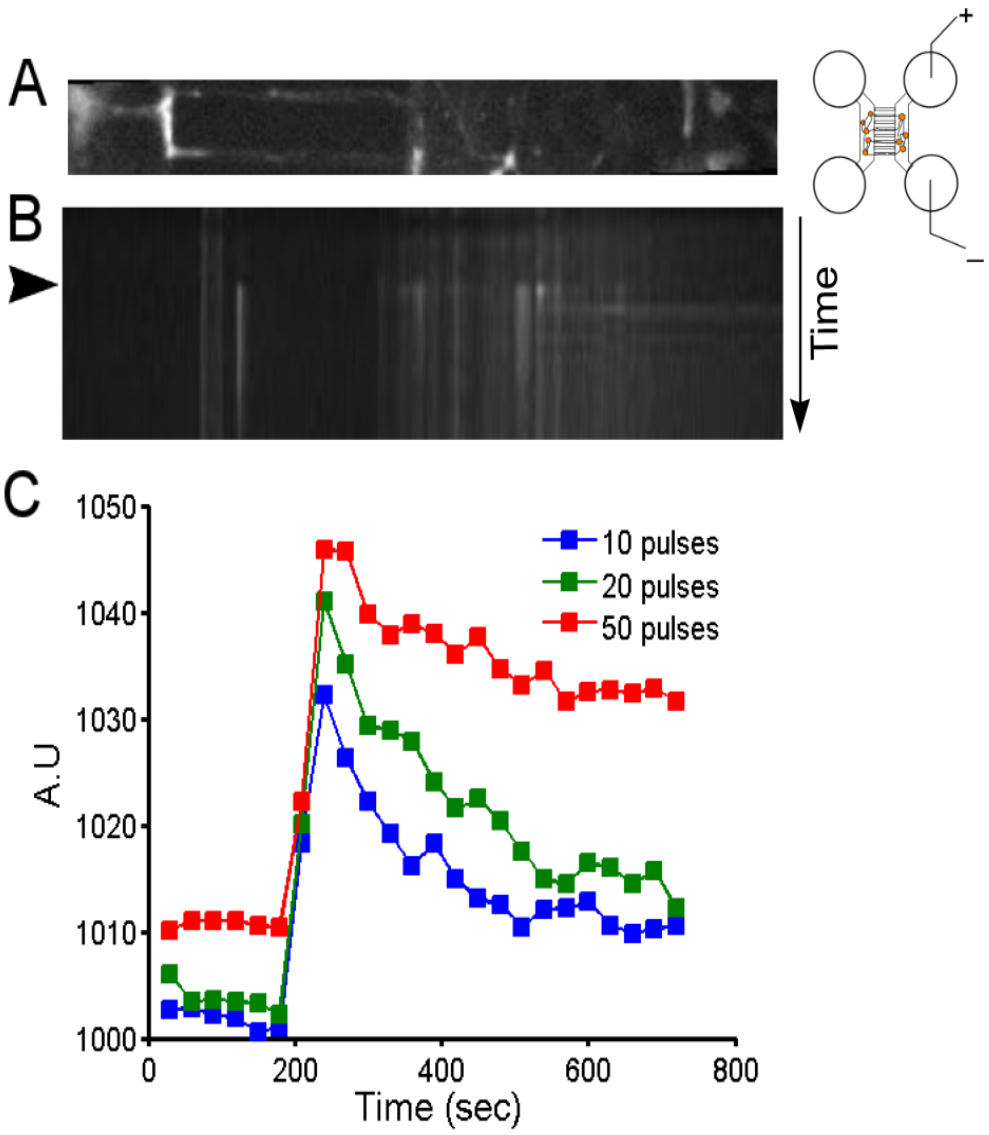

Figure 16: Field stimulation of neurons inside microfluidic device

(A). Fluorescence image of neurons inside a microfluidic device loaded with calcium indicator Fluo4-Am. The electrode was placed in the left chamber, neurites can be seen crossing the microgrooves (schematic). (B). Line scan across the device stimulated at 180 sec (arrowhead) shows an increase in the calcium on either side of the microgroove barrier. (C). Fluorescence intensity across ROI for three $10, 20$ and 50 pulses delivered at $10Hz$.

testing of candidate synaptic molecules and their role in creating functional synapses. In this experiment we test the hypothesis whether co-expressing Syncam2 (SC2) and Neuroligin1 (NL1) have any symbiotic effect on the formation of synapses. For this we co-culture neurons with HEK293 cells expressing either SC2, NL1 or both molecules together. Both these molecules have been shown to induce synapse formation in HEK293 cells [76, 77] We use standard soft lithography to construct the microfluidic chambers developed by Jeon and colleagues [75]. This method allows for fluidic isolation of the two micro-chambers while allowing axonal connectivity between them. This allows the two cell populations to be maintained in separate culture conditions, yet able to connect cellularly. This platform allows for extended testing of candidate synaptic molecules and their role in creating functional synapses.

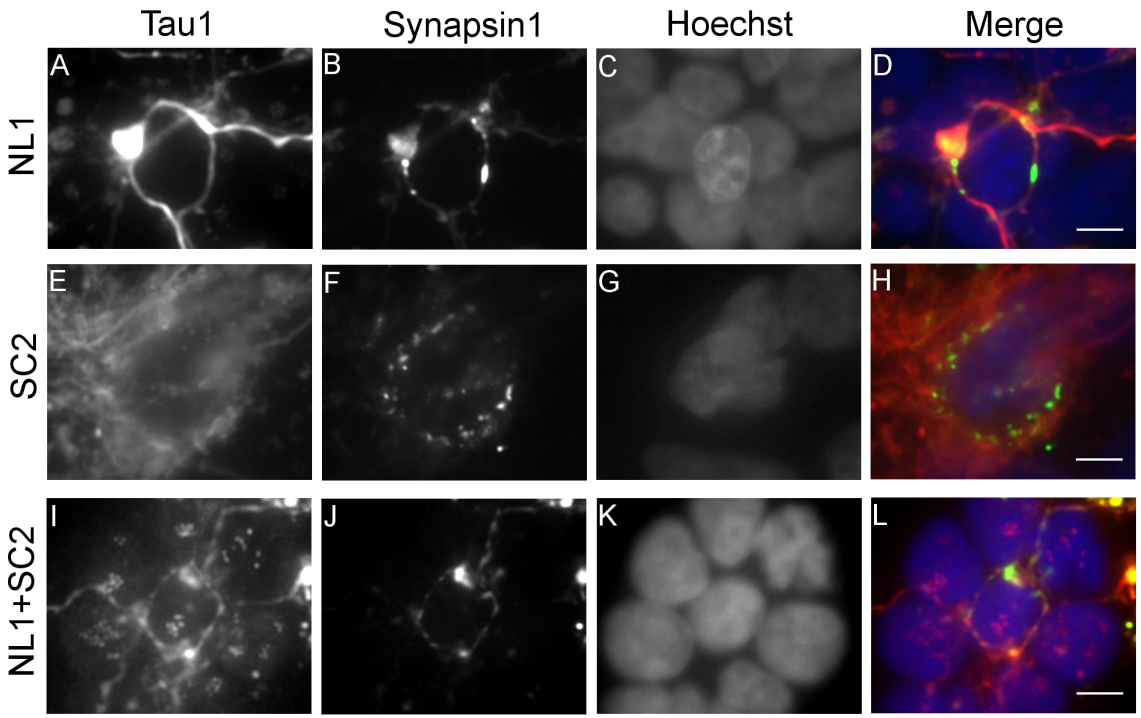

Figure 17: High-throughput heterologous synapse in a microfluidic device

Three groups of HEK293 cells transfected with Neuroligin1 (NL1), Syncam2 (SC2) and both NL1 and SC2 were studied. (A,E,I) Neuronal processes stained with Tau1. (B,F,J) Pre-synaptic marker synapsin1 indicating pre-synaptic sites along the neuronal process. (C,G,K) HEK293 nucleus stained with hoechst33342. (D,H,L) Merge of all three channels indicating the formation of presynaptic terminals along the neuronal processes along HEK293 cells. Scale bar = 25μm.

To test the hypothesis of any symbiotic relationship between synaptic adhesion molecules, HEK293 cells expressing either NL1, SC2 or both were co-transfected with GFP. These cells were introduced inside a microfluidic device that contained neurons in one chamber extending their processes towards the opposing chamber. After one week of culturing, both the neurons and the HEK cells were found to be healthy, immunostaining of these devices revealed the formation of synapses between neurons and HEK cells (figure 17). All possible synaptic contact points were counted, we found on a average neurons formed 7.5 ± 2.8 synapses onto HEK cells expressing NL1 alone. Neurons formed 6.8 ± 4.2 synapses onto HEK cells expressing SC2 only and 8.0 ± 4.6 synapses onto HEK cells expressing both NL1 and SC2 together. We however did not find any statistical significance supporting evidence of a symbiotic effect such as increased synapse formation of expressing both NL1 and SC2. Other parameters such as area of co-localization can be used as a metric for size of the synapse. We however restricted the analysis to number of synapses.

3.4 CONCLUSION

Here we have created a platform in which two networks of neurons are physically constrained inside microfluidic chambers and are connected to each other via small microgroove that permit the grow of neurites. These microfluidic devices are capable of fluidically isolating each population. We observed that only axons traversed thought microgrooves that were 1000μm, however both axons and dendrites traversed through the shorter microgrooves [72]. We demonstrated two unique applications by culturing neurons in microfluidic devices (i) this device can be used to culture two separate populations of neurons that are connected

to each other in a specific manner (ii) culturing cells on one side and non-neuronal cells on the other side allows for the assaying of potential synaptogenic molecules.

We showed the formation of heterologous synapses between neurons and HEK293 cells inside a microfluidic device. We were capable in extending the period of co-culture from the standard 2 days to 1 week by maintaining each cell population in a fluidically isolated manner. Though we successfully observed the formation of heterologous synapses in all three groups (NL1, SC2 and NL1+SC2), we however did not notice any symbiotic effect of expressing both proteins with respect to number of synapses formed. Thus, the proposed microfluidic device can be used as a platform to assay potential synaptogenic molecules in a combinatorial manner.

We also finally show here the integration of this microfluidic device to an electrophysiological setup. It was possible to stimulate the cells inside the device in one chamber and notice activity in the opposing chamber. Such a platform can be used to maintain gradient of trophic factors in order to create a network that is predominantly uni-directional in nature. This aim however, was not fully materialized and we ended up with bi-directional networks in all cases.

3.5 DISCUSSION

Early culture systems like the Campenot chambers were some of the first methods described to look at isolated axonal populations. The applications of this culture system to neuroscience has been beneficial in a lot of the early studies involving growth factors and their roles. However, Campenot chambers were not efficient and required a lot of 'home-remedies'

(such as additon of excessive grease to prevent leaking) to work successfully. The advent of microtechnologies makes it possible to make microfluidic devices that are capable of maintaining neuronal populations for extended periods of time. Here we describe a method to maintain two neuronal populations in a microfluidic device for extended periods of time based on the designs of Taylor et.al[42]. The microfluidic device has two chambers that are connected via a series of microgrooves that allow neurites to extend across the populations. The length of the microgrooves alone was sufficient to allow for selective growth of axons, as compared to a mixture of axons and dendrites.

Here we have demonstrated a technique to study potential synaptogenic molecules and to investigate potential symbiotic effects between molecules using these microfluidic devices. We have shown that HEK293 cells expressing known synaptogenic molecules are able to form synapses with neurons, cultures inside microfluidic compartments. By restricting the neuronal cell bodies to one compartment, it is possible to maintain the two cell populations in different mediums. It is also possible to use drugs on one population without affecting the opposing population. Here we notice no change in number of synapses when the HEK293 cells are expressing both NL1 and SC2. Further studies could look at different time points of expression of the synaptogenic molecule, to tease out the precise timing of such events.

We then integrated the existing microfluidic device to an electrophysiological setup in order to stimulate cells inside the device. Using calcium imaging we noticed a sharp increase in the calcium intensity of the cells immediately following stimulation. Thus we have created a platform that can be used to monitor as well as stimulate cells inside a microfluidic device where each population can be fluidically isolated from the other.

4.0 REVERBERATORY ACTIVITY IN 'RING' NETWORKS [1]

4.1 INTRODUCTION

The ability of the brain to hold information online is a remarkable feat. Working memory involves holding traces of memory for short periods of time. It is believed that persistent activity in recurrently connected networks of the cortex is responsible for retaining such information over short periods of time [78, 79]. Persistent activity from single unit recordings [80] (Figure 18) as well as fMRI imaging in working memory tasks [81] show increased levels of activity sustained for short periods of time ranging from milliseconds to seconds after the cessation of the initial stimulus. This ability of local brain circuits to maintain activity after cessation of the initiating input has been observed in various brain regions including the prefrontal cortex and the thalamus [82, 83, 84, 85]. It has been proposed that reverberating activity in recurrent neuronal networks underlies such observed persistent activity [86, 87]. Small *in vitro* neuronal networks cultured in defined geometries have been used to study persistent activity [66] and information transfer [88].

It is believed that persistent activity in the cortex is responsible for holding such information for short periods of time[78] [79]. Persistent activity from single unit recordings[80]

[1] Reproduced by permission of The Royal Society of Chemistry [67]

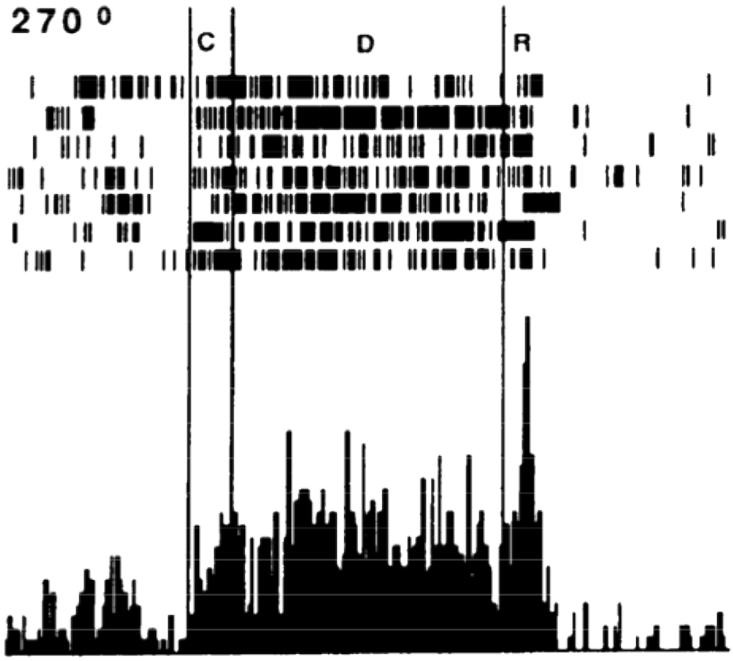

Figure 18: Persistent activity during delayed-response tasks

Persistent activity displayed at single unit recordings in the dorsolater prefrontal cortex of a non-human primate[89]. The monkey observes is shown a cue for a short duration of time, following which it is expected to wait untill a response cue is displayed. After the response cue is displayed, the monkey reaches out to the cue. C- Onset of Cue, D- delay, R- Response.

as well as fMRI imaging in working memory tasks[81] show increased levels of activity sustained for short periods of time ranging from milliseconds to seconds. This ability of local circuits to maintain activity after cessation of the initial input has be observed in various brain regions [82][83][84][85]. It has been proposed that reverberating activity in recurrent neuronal networks underlies such observed persistent activity [86][87]

In this chapter we use the ring networks that were described in the previous chapters as a platform to study reverberatory activity *in vitro*. Here we show that the ring networks were capable of generating stimulus evoked reverberatory activity. This reverberatory activity was enhanced when network inhibition was inhibited pharmacologically. The nature of the persistence of this reverberatory activity was shown to be due to asynchronous neurotransmitter release.

4.2 RECURRENT NETWORK ACTIVITY

Recurrent network activity is thought to be responsible for persistent activity in the cortex [90, 66]. Multiple brain areas including the prefrontal cortex, the hippocampus and the mediotemporal cortex are connected in a recurrent manner. Recurrent networks are capable of generating rhythmic oscillatory activity. This oscillatory activity arises due to the positive feedback nature of the recurrent connections. Small *in vitro* networks of recurrently connected hippocampal neurons display a similar form of activity upon a single suprathreshold stimulation termed, 'reverberations' [66]. These small networks were cultured

over 1mm spots of poly-L-Lysine over a glial mono-layer into small island cultures. It was shown that the often neglected asynchronous neurotransmitter release was responsible for the reverberations.

However it was also noted, not all small networks displayed reverberating activity. Reverberation properties (duration and occurrence) displayed a great degree of variability. A blockade of phasic synaptic inhibition via gamma-Amminobutyric acid ($GABA_A$) receptor antagonist bicucculine methiodide (BMI) greatly improved these characteristics and helped overcome some of the inherent inhomogeneity of these randomly formed networks. However, if the role of inhibition in such small networks are to be studied in more detail, usage of BMI may not be the best option. Any improvement over the inhomogeneity of the networks will be beneficial. Here we describe a method to improve upon the inhomogeneity of the random circular network by restricting the neurons to grow in a 'loop' like geometry, we hope to introduce a degree of control over the homogeneity of the network.

4.3 NEURAL ADHESIVE MOLECULES IN DEFINED GEOMETRIES

During development cells are constantly migrating, responding to various extracellular molecules. These extracellular molecules are presented to cells often in the form of a gradient. *In vitro* these conditions are recreated by bead assays, stripe assays etc., and are well suited for studying guidance molecules. Adhesion molecules are typically presented in the form of static gradients [26]. Typically cells are grown on glass substrates or tissue culture polystyrene. To obtain optimum cell adhesion, these surfaces are treated with adhesive proteins and by changing the surface chemistry. By changing the surface chemistry, the areas over which

adhesive proteins reside can be controlled. The application of lithographic techniques to microtechnology fabrication has allowed the control of such proteins up to a micron range, which coincides with that of a single cell. To pattern adhesive proteins using lithography, we create a micron scale stamp with an elastomer, the stamp is brought in contact with the substrate to transfer adhesive protein in a defined geometric pattern.

Microcontact printing (μCP) has been used to restrict neuronal networks to specified geometries [3, 28, 63] and also to investigate the role of axonal guidance molecules [91]. Early demonstration of *in vitro* control over neuronal polarity at a single neuron level was demonstrated by Stenger and colleagues [92] where they used microlithography to pattern growth permissive surfaces to control neuronal polarity. μCP techniques have since been applied to restrict dissociated neurons to defined geometrical patterns for various applications such as patterning of surface gradients as well for axonal guidance studies [31, 93, 26]. Specific designs also restrict the locations of soma. By restricting soma to locations near electrodes on micro electrode arrays, improvements in recording quality have been shown [3, 2, 30, 22]. Microcontact printing is a powerful technique for restricting and defining the allowable geometry of a developing *in vitro* neuronal network. We utilize this technique to control the geometries used for the present work.

4.4 PERSISTENT ACTIVITY AND INFORMATION TRANSFER

Recurrent networks are capable of generating rhythmic oscillations as the network activity continually propagates around and is fed back into the network. Small circular islands of neuronal networks, containing 50-100 neurons, have been used to allow the formation of

small recurrent networks without confounding effects of a larger external network. These small networks of recurrently connected hippocampal neurons display a form of persistent activity upon stimulation with a single suprathreshold pulse termed 'reverberation' [66]. The reverberation within the network allows for a persistent activity lasting long after ($>$ 2sec) cessation of the input stimulus. These networks allow the realization of persistent activity similar to that associated with early *in vitro* memory formation with easy access to external experimental variables, but are limited in their ability to know the activity pathway taken by the reverberations.

4.5 MATERIALS AND METHODS

4.5.1 Microfabrication

Cleaned silicon wafers were coated with a layer of negative photoresist SU8-3025 (Microchem) at $60 - 70\mu$m thickness and baked for 20 min. Stamps were created by exposing a high-resolution mask to UV light for 20 sec. The wafer was then developed until all features were well defined, washed in IPA and hard baked at 150°C for 30 min. The masters were then washed to remove any un-crosslinked photoresist and other organic solvents in 5% TritonX-100 for 20 min, followed by two washes in DDW. PDMS (DOW Corning) was throughly mixed in a 1:10 ratio of hardener to resin and degassed. The degassed mixture was then poured over the master and allowed to bake at 95°C for 2 hrs followed by cooling. The height of the 'ring' structures in PDMS stamps were approximately $60 - 65\mu$m.

To verify the resolution of the stamps, scanning electron micrography (SEM) images of the stamps were acquired. Briefly, the stamps were sputter coated with a layer of palladium and loaded in the chamber at a 60° angle. Images of the PDMS stamps were also acquired on a stereoscope and dimensions of the track widths were compared to the CAD dimensions. To verify the resolution of the actual stamped proteins and the stamp, fluorescently labeled proteins were stamped on cleaned glass slides. Images of these stamps were then compared to the PDMS stamps. Image analysis was performed on ImageJ (Wayne Rasbald, NIH)

Stamping of proteins was performed as follows, PDMS stamps were cleaned by sonicating in DDW for 20 min then dried under a stream of nitrogen. The stamps were then charged in an oxygen plasma machine for 20 sec and protein was immediately pipetted over the surface of the stamp. The protein was then incubated with the PDMS stamp for a know duration of time in the dark. The PDMS stamps were dried under a stream of nitrogen. Immediately following drying the protein was stamped on an oxygen plasma charged glass coverslip ($22x22$ mm). A know weight was placed on top of the stamp for homogeneous distribution of protein on the glass coverslip. The PDMS stamps were removed carefully from the coverslip after 5 min.

4.5.2 Cell culture

Medium-density cultures of dissociated embryonic rat hippocampal neurons were prepared according to a previously described protocol with minor modifications, as approved by University of Pittsburgh IACUC. Hippocampi were removed from E19 embryonic rats and treated with trypsin for 15 min at 37°C, followed by washing and gentle trituration. The dissociated cells were plated on poly-L-lysine-coated glass coverslips in 35-mm petri dishes with

100,000 cells/ml per dish. The culture medium was Dulbecco's minimum essential medium (DMEM; BioWhittaker) supplemented with 10% heat-inactivated bovine calf serum (Hyclone), 10% Ham's F12 with glutamine (BioWhittaker), 50 U/ml penicillin-streptomycin (Sigma) and 1x B-27 (Invitrogen/Gibco). Twenty-four hours after plating, 1/3 of the culture medium was replaced with the same medium supplemented with 20 mM KCl. Cytosine arabinoside (AraC, Sigma) was added to the culture dish (final concentration, $5\mu M$) around 7-10 DIV (days in vitro) to prevent overgrowth of glial cells. The optimal period for these cultures to be used for the experiments was 10-14 DIV. Hippocampal neurons were plated on glass coverslips stamped with PLL+FITC formed ring structures. The resulting networks were observed taking shape of the ring structure as well as the grid structure. The ring structures in themselves were isolated from the rest of the grid. In some cases it was observed that the neurons in the ring grow over the central part of the ring, these rings were not used for any of the analysis. It was also observed that when glia were allowed to grow uncontrollably, the neurons were not able to maintain the ring structure for a period longer that 7-10 DIV. In order to prevent this from happening an anti-mitotic agent Cytosine Arabinocide was added to the cultures at a final concentration of 5μm between DIV 5-7. The neuronal networks were later identified using immunostaining methods. Neuronal processes and cell bodies were identified using either MAP2 or Tau1 antibody which is specific to dendrites and axons respectively. The original stamped rings structure was visible since it was stamped with PLL conjugated with FITC. All cell bodies were stained with Hoechst-33342. These results show that microcontact printing can be used to create recurrent neuronal networks in a precise manner. The glass coverslips are fixed in 4% paraformaldehyde with sucrose, permeabilized

with 5% Triton X-100 and washed three times respectively with PBS. They are then blocked in 5% BSA for 1 hr, following which they are probed with primary antibody at 1:100 for 1 hr, Secondary antibodies at 1:1000, washed, 1:1000 of Hoechst (Molecular probes) , washed and mounted in fluormount G (Southern biotech).

4.5.3 Calcium imaging and electrophysiology

Field stimulation of all ring structures was performed using a bipolar theta glass capillary electrode (Warner instruments). The electrode was placed $< 50\mu$ from the cell that was being stimulated. The cells were maintained in Hepes buffered-saline (HBS) containing $150mM$ NaCl, $3mM$ KCl, $3mM$ $CaCl_2$, $2mM$ $MgCl_2$, $10mM$ Hepes, and $5mM$ glucose (pH 7.4). In all cases control stimuli refers to a single pulse $2ms$ long. Paired pulse stimuli (PPS) are two or three pulses $200ms$ apart and $2ms$ long at $80V$ applied using a external unit (Grass, SD-9). Stock solutions of bicuculline methiodide (BMI) and EGTA-AM (Sigma Research Bio- chemicals) were first prepared in water or DMSO and diluted $(1 : 1,000)$ in HBS before being used. Throughout the experiment the cells were perfused with fresh bath solution at a constant rate of $\sim$ 1ml/min.

Stock solution of Calcium sensitive dye Fluo4-AM (Invitrogen) at 1.5 mM was prepared in DMSO. The above solution was diluted in HBS to give a final concentration of 2.5μM. Cells were usually incubated for 45 min-1hr at room temperature in the dark before the commencement of the experiment. All images were taken on a LeicaDMB microscope, were acquired by a CCD camera-Roper Scientific 512B on RSimage.

$$\frac{\Delta F}{F} = \frac{(F_0 - B_0) - (F_1 - B_1)}{F_0 - B_0} \tag{4.1}$$

where,

F_0, B_0 = intensities of the somas, background at first frame

F_1, B_1 = intensities of the somas, background vary with time [74].

4.5.4 Analysis and statistics

All analysis of calcium movies were performed offline using custom Matlab (Mathworks) scripts. Movies were initially loaded in ImageJ (NIH image, Wayne Rasbald) and ROIs were selected from bright-field images bases on the health of cells, healthy cells tend to look 'plump' in phase-contrast images. Once the ROIs were selected, the ROIs were superimposed over the calcium movies frames and the average intensity of each ROI at each frame was saved in a single *.text file. Typically a single movie contained $15 - 20$ ROIs, for each ring culture a given condition was repeated five times (control, BMI, EGTA etc.). The *.text file was used as the input for the Matlab script which sorted the ROIs based on frame number and trial number. The output of the Matlab files were $\Delta F/F$ plots ad text files with parameters such as $\Delta(F/F)_{max}$, half-width times for each ROI for each trial.All statistics were performed within Matlab. Comparison of means for all parameters was performed by a Wilcoxon rank-sum method unless otherwise mentioned. All values are reported as mean±SEM unless mentioned otherwise.

4.6 RESULTS

4.6.1 Extracellular field stimulation

Extracellular field stimulation with a theta-glass electrode filled with external bath solution, placed very close to the cells in a ring network was capable of eliciting activity in the neighboring cells. Theta glass electrodes were chosen as the method of stimulation over wide-field stimulation in order to localize the area over which cells are stimulated. This method of stimulation was highly sensitive to location of cells with respect to pipette (figure 19), as the pipette was moved away from the cells we observed a lack of stimulation of the cells. The average mean -$\Delta F/F$ over all the ROIs of the ring culture was significant at positions 1 and 2 respectively (figure 19d Means±Sd = 0.88±0.57, 0.92±0.56, 0.14±0.02 at position 1,2,3 respectively). A common problem that is encountered in *in vitro* neural cell cultures is the occurrence of spontaneous burst activity. Typically spontaneous activity occurs in neural network with high density. However, in our case we did not observe any spontaneous activity in ring cultures with calcium imaging, possibly due to the number of cells per ring $\sim$ 40-70 cells resulting from low-density cultures.

4.6.2 Extracellular stimulation yields repeatable activation

In order to infer workings of biological systems, it is imperative to conduct experiments in a reliable, consistent and repeatable manner. Typically experiments dealing with Calcium imaging require multiple trials per experiment due to the highly variable nature of the observed signal. Therefore it is important to check for the degree of repeatability of activity observed upon extracellular stimulation.

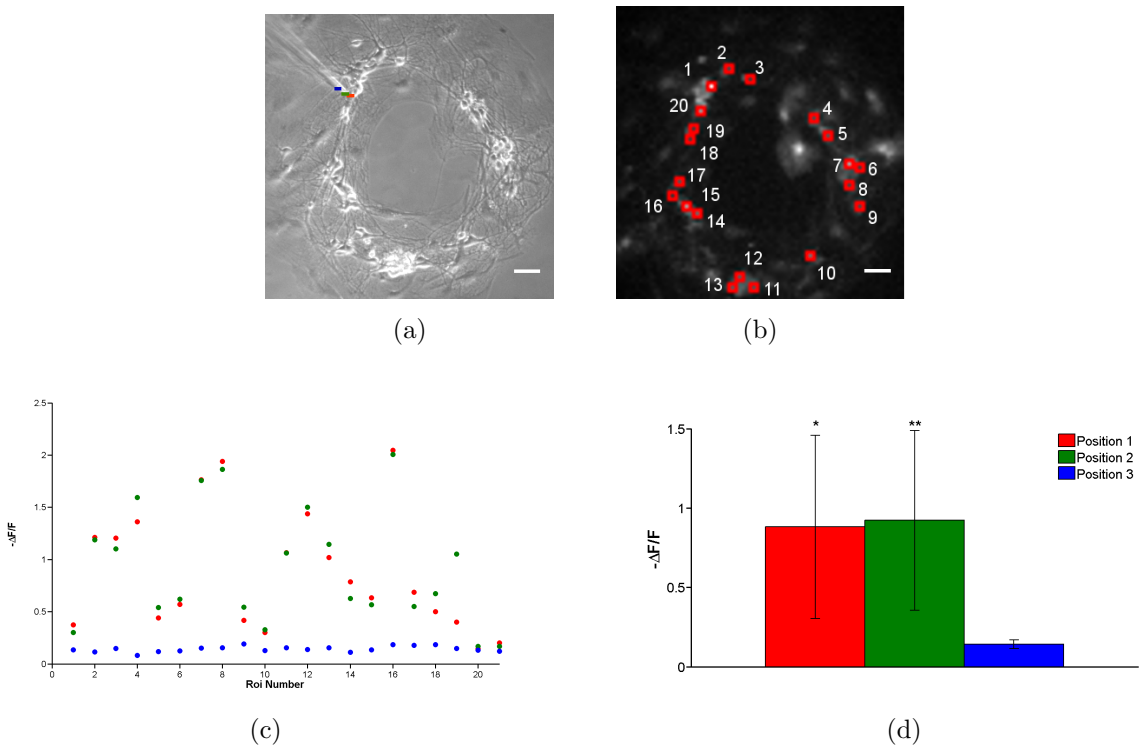

Figure 19: Scatter plot at different stimulator positions

Ring networks incubated in Fluo4-AM were stimulated using a bipolar pipette (pipette in bright field image). The pipette was positioned at three different positions (color bars). a.) Map with the different pipette stimulator positions b.) Map of the ring culture showing all the ROIs. c.) Scatter plot of various ROIs from the above ring culture at different position of the extracellular stimulator d.) Averaged mean -$\Delta F/F$ over all ROIs is significant at position 1,2 respectively. Red- position1, Green - position 2, Blue - position 3. scale bar = 100μm.

We tested the ability of the ring networks to propagate an action potential along the ring network. We used the calcium-sensitive Fluo4 AM indicator dye to examine the onset of electrical activity in neurons within our network. External bipolar electrode was placed near the ring culture and minimal field potentials were used to excite the nearest neurons in the network. An emCCD camera was used for high-speed capture of fluorescent images of the network.

Prior to data analysis, circular regions of interest (ROIs) were chosen from bright-field images of the network at regions appearing to correspond to neuronal soma. Changes in fluorescence observed for those locations were used to assess activity within the network. The magnitude of all of the scales was maintained at the same height to show the range in fluorescence response. Since these ROIs were chosen without knowledge of their fluorescence baselines and responses, a wide variation in observed response magnitudes is expected . Though magnitudes differed, temporal response of ROIs were similar. These responses were characterized by a quick rise in fluorescence (typically 2 frames of the movie, or approx. 60ms) followed by a slow exponential decay (typically 2-4 sec). There were no spontaneous responses observed above baseline. We further ensured the response was due to our stimulus by using multiple stimulus pulses. Figure 20b show the responses of those ROIs to two and three stimulating pulses, respectively. There is response in each ROI to each stimulus. Even the ROI that only shows a slight response in the single stimulation case (Figure 20bB, bottom trace) shows a substantial response to two and three stimuli (Figures 20bC,D, bottom traces, respectively). Note that magnitude scale is held constant for traces from a single stimulus, but the magnitude scale is different for each stimuli. In figure 20a five

successive trials from a single region of interest are plotted along with the mean of all trials (dark red trace) along with the first standard deviation bounds(light red filling), 22% of all recorded data points were outside the first standard deviation bounds. We next tested to see how reliably the network of cells responded to multiple stimuli. The network was stimulated with 1, 2 and 3 pulses that were 200 ms apart (figure 20b), in each case the ROIs in the network reliably followed the stimuli. Each trace is a mean over five successive trials (red trace) bound by the standard deviations (light red filling), below each trace is the mean baseline of the same ROI from five successive trials of null stimulus recorded before the stimuli trials. The average age of the culture used was 12.9±1.2 days, typically the height of synpatogenesis is between 10-12 days, we wanted to stimulated the networks after most of the synapses were formed.

4.6.3 Reverberation in ring cultures

Ring shaped neuronal networks displayed a form of network activity analogous to persistent activity - reverberations (figure 21). A single extracellular stimulation to the network resulted in reverberations that lasted up to a few seconds. These reverberations happened in an all-or-none manner. Reverberations in these networks resulted in a significant increase in the mean fluorescence levels of the ROIs.

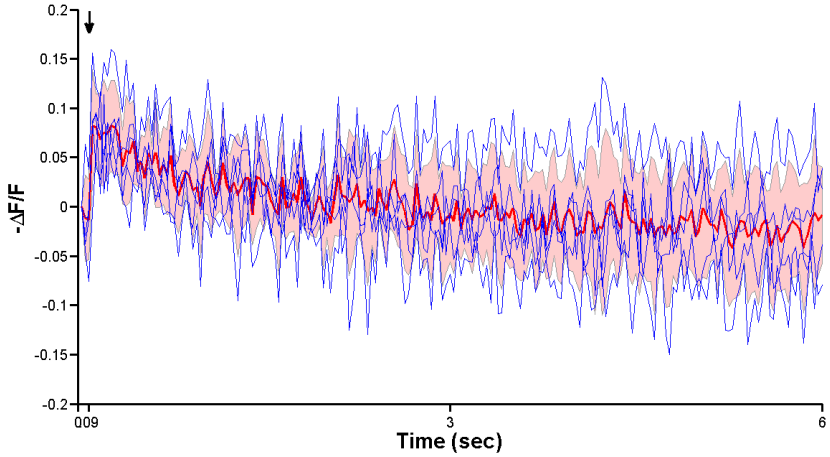

(a)

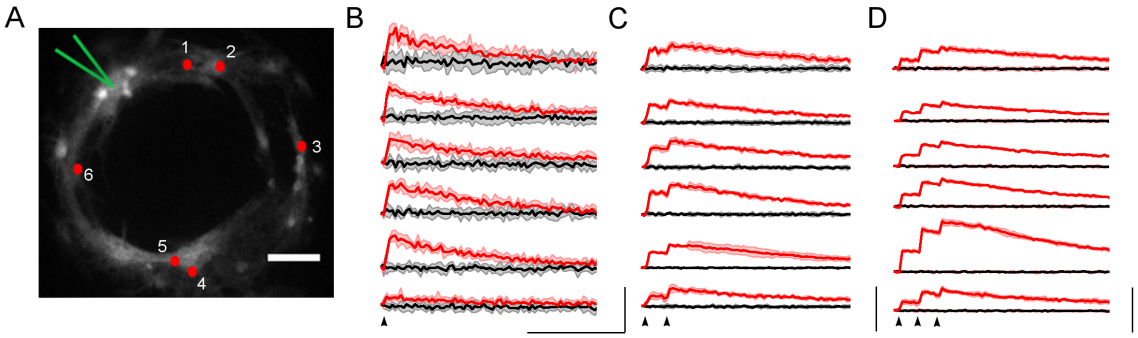

(b)

Figure 20: Network response to multiple stimuli

a.) Five successive trials from a single ROI (blue traces) plotted along with mean trace (bright red) and bound by the first standard deviation (light red filling) b.) A. Map of the ring culture showing all the ROIs (red dots) with pipette position indicated (green). All analyzed ROIs respond to one, two and three stimuli respectively. The pulses were 2ms long, seperated by 200ms indicated by arrowheads. The responses are the average of five trials indicated by dark red trace and bound by the standard deveation (pale red filling). Black trace is response of same ROI during no stimulaton. Scale bar for fluorescent image = 100μm, Scale bar for plots 1.6 sec , 0.5, 1, 2.5 -$\Delta F/F$ respectively. Arrowheads indicate time of stimuli.

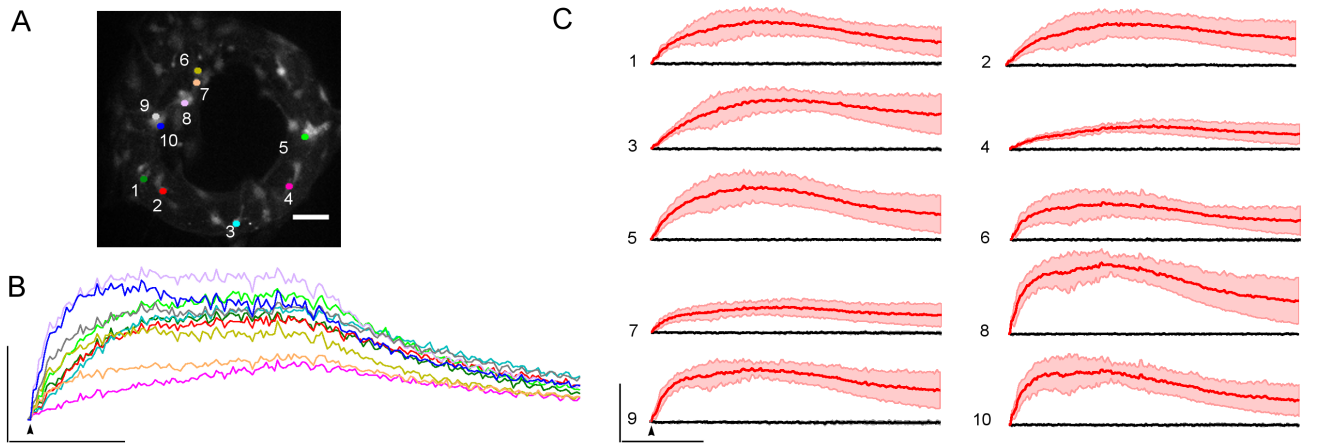

Figure 21: Reverberations in ring networks

Reverberation in ring networks were noticed upon stimulation with single pulse. A.) Map of ring network with color coded ROIs B.) Typical response to stimulation from one trial showing reverberations after the initial stimuli. Colored traces indicated the respective ROI in A. C.) Average response from all 10 ROIs from five trials. Black traces are the baseline responses of the same ROI for no stimulation. Scale bar for fluorescence image = 100μm. Scale bar for plots 2.0 sec, -2 $\Delta F/F$ for B and 2.5 sec, -2 $\Delta F/F$ for C. Arrowheads indicate time of stimuli.

It was also observed that these reverberations lasted a couple of seconds while non-reverberation cases lasted up to a few milliseconds. We measured three parameters of each Calcium signal, the maximum change in fluorescence intensity, the time to maximum and the time width at half the maximum. The change in fluorescence intensity gives an estimate of the amount of calcium entering the cell, subsequently the intracellular concentration of calcium $[Ca^{+2}]_i$. The average change in fluorescence intensity for non-reverberating cases is $(0.23 \pm 0.16\text{A.U})$ while the average change in fluorescence intensity for reverberation cases is $(1.41 \pm 1.43\text{A.U})$. The time taken to reach the maximum is a crude estimate of the number of inputs to the system, longer the time to reach maximum, more number of incoming signals. The average time taken to reach the maximum in non-reverberation cases is $(0.36 \pm 0.09\text{sec})$, while the average time take in reverberation cases is $(0.83 \pm 0.73\text{sec})$. Lastly, the time width at half the maximum is an estimate of the length of the reverberation episode .The average half-times for non-reverberating cases is $(0.43 \pm 0.29$ sec) and the half-times for the reverberating cases is $(1.35 \pm 1.2$ sec).

However it was also observed that not all networks that were stimulated displayed this form of reverberations. Indeed only about 13.3% of the networks that were stimulated displayed this form of reverberations (table 3). In the rest of the cultures, the networks typically responded to the initial stimuli and die out , i.e. the signal does not persist.

Table 3: Reverberations in ring cultures

Label	Control	BMI	Track width (μm)
04/21/10 - exp2	Y	n/a	100
05/18/10 - exp1	N	Y	100
05/19/10 - exp2	N	N	100
06/01/10 - exp2	N	N	150
06/01/10 - exp4	n/a	Y	150
06/02/10 - exp1	N	n/a	150
06/02/10 - exp2	N	Y	150
06/02/10 - exp3	n/a	Y	150
06/02/10 - exp4	N	Y	150
06/21/10 - exp1	N	Y	100
06/21/10 - exp2	N	Y	100
06/21/10 - exp3	Y	n/a	100
06/28/10 - exp2	n/a	N	100
06/28/10 - exp3	n/a	Y	150
06/29/10 - exp1	N	Y	150
07/27/10 - exp1	N	N	200
07/27/10 - exp2	n/a	Y	150
08/03/10 - exp1	N	Y	150
08/03/10 - exp2	N	Y	150
08/09/10 - exp1	N	Y	200

Y- Reverberations were observed; N- Reverberations were not observed

4.6.4 Blocking inhibition enhances reverberations

A majority of the networks that were stimulated did not display any reverberations, but responded only to the initial stimuli (figure 20b). This led us to question the balance of inhibitory to excitatory cells in the networks. Since *in vitro* cultures produce an inhomogeneous mixture of cells, it is possible that networks do end up with a random number of inhibitory cells. Stimulation of these networks leads to a feedback of inhibitory cells which prevents the network from displaying any form of reverberations. To test this idea, we made use of the pharmacological $GABA_A$ blocker - bicuculline methiodide (BMI). Thus we hypothesize an increase in the number of synapses recruited with a blockade of $GABA_A$ receptors

Our goal was to completely block all forms of inhibition, but at the same time we also wanted to ensure there were no dose dependent effects of BMI on the reverberation parameters. We performed a dose-dependence experiment and varied the concentration of BMI ranging from $0 - 10\mu M$. We noticed an immediate effect of BMI on the three reverberation characteristics, $\Delta F/F$, Time to $\Delta F/F_{Max}$ and Half-width time.

Networks that did not display any form of reverberations were incubated with the GABA blocker BMI. Addition to BMI to these networks induced reverberations in previously non-reverberating networks (table 3). It was observed that in 75% of non-reverberating networks BMI was capable of inducing reverberations. The reverberations that were induced by addition of BMI were similar to the reverberations that were observed during some of the control cases. We also checked to see if there were any dose dependent effects of BMI to reverberations characteristics. It was observed that at BMI concentrations of $\leq 2.5\mu M$ reverberations induced were significantly shorter as compared to the reverberations induced at greater concentrations.

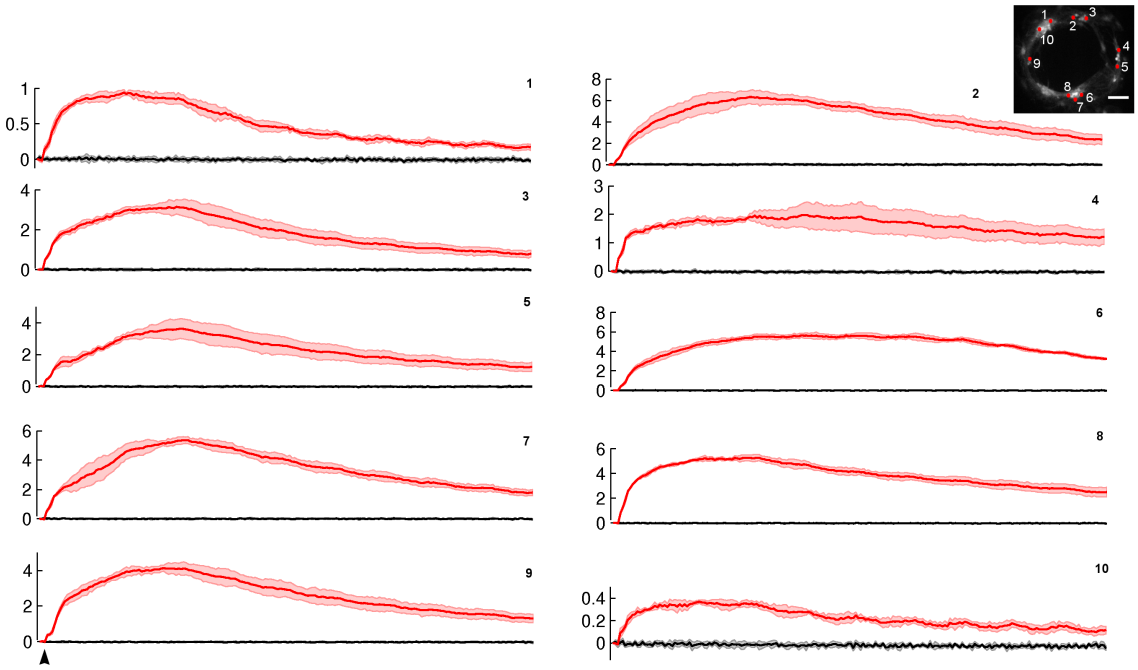

Figure 22: Blocking inhibition enhances reverberations

Typical response of ROIs when network was incubated in $10\mu M$BMI. Each ROI shows a persistence of the initial stimulus indicated by the arrowhead. Each trace is the mean response (dark red trace) over five trials bound by the sd, black trace is the baseline response of the same ROIs over five trials. Inset: Ring networks with the analyzed ROIs. Scale bar 100μm, all traces are 6.6sec long.

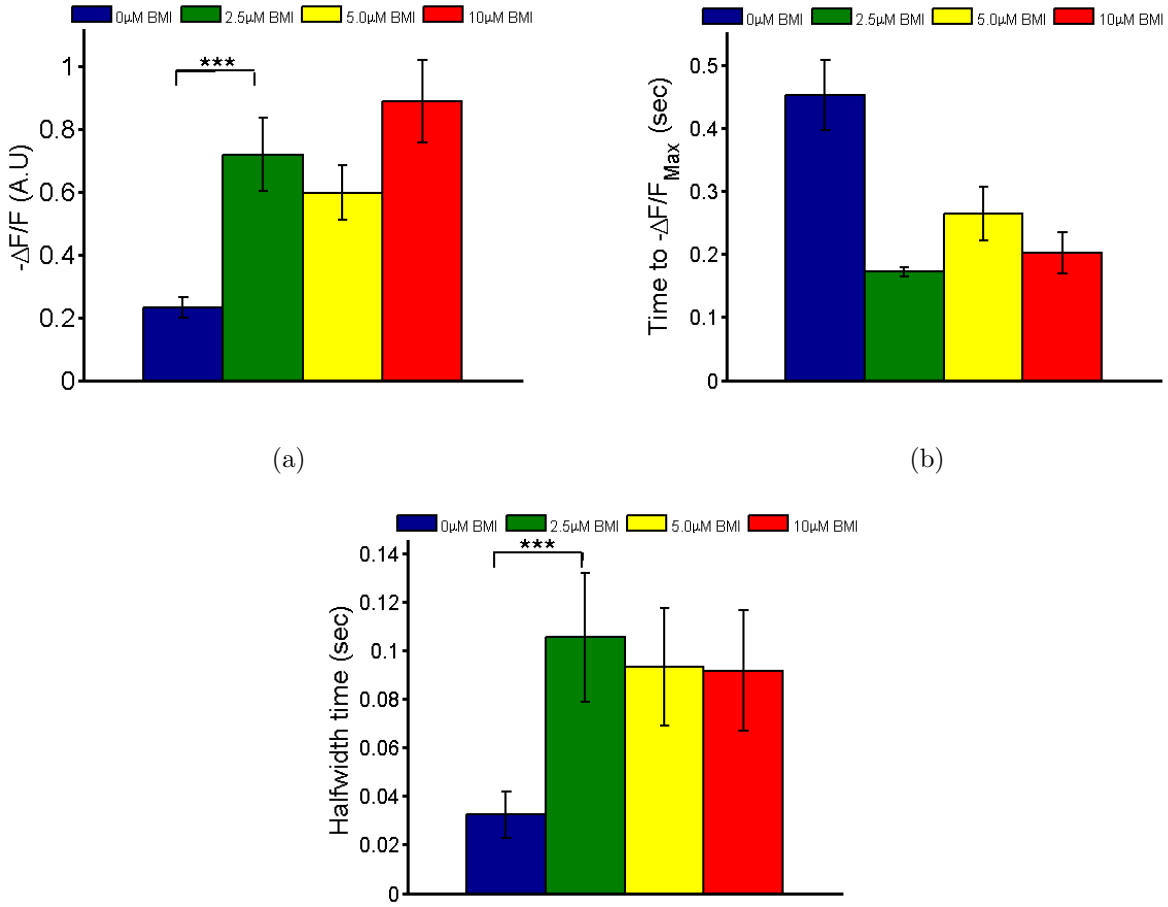

Figure 23: Dose dependent effects of BMI on reverberation characteristics

Dose dependent effects of BMI on reverberations characteristics. Ring networks was incubated in different concentrations of BMI followed by stimulations. a.) Effect of varying doses of BMI on mean $\Delta F/F$. b.) Effect of BMI on time to $\Delta F/F_{Max}$. c.) Effect of BMI on half-width times.

4.6.5 Role of asynchronous synaptic transmission

Asynchronous neurotransmitter release is a phenomena which occurs at physiological conditions. Often times due to a build-up of neurotransmitter vesicles at the pre-synapse, there is a high probability of fusion of these vesicle to release their payload of neurotransmitter, following an action potential due to elevated levels of pre-synaptic calcium. This condition is called asynchronous neurotransmitter release. Reverberations in ring networks is often reported as multiple events following the initial stimulus. It was hypothesized by [66] that asynchronous transmission between each event kept the system in a reverberating state. To test this idea, we use the slow calcium chelator EGTA-AM, after incubating the networks with $100\mu M$ EGTA-Am for $10min$ reverberations were completely abolished. However, the synchronous phase of transmission at the time of stimulus application was still evident. EGTA-AM abolished reverberations in 100% of all analyzed networks ($n = 5$).

Figure 24 shows ROIs from a network (previously reverberating) incubated with EGTA-AM for $10min$. Stimulation of this network shows activation immediately after the stimulus, but no subsequent reverberations.

4.6.6 Summary

In summary we have shown that ring networks are capable of evoking reverberatory activity. These reverberations are characterized by multiple events following the stimulus and can last up to a few seconds. The average half-width times for reverberations is 1.35 ± 1.2sec. Not all networks displayed this form of reverberatory activity, in fact only 13.3% of the networks displayed them. Reverberations are enhanced by blocking network inhibition and 75% of networks in which inhibition was blocked displayed reverberations. Reverberations

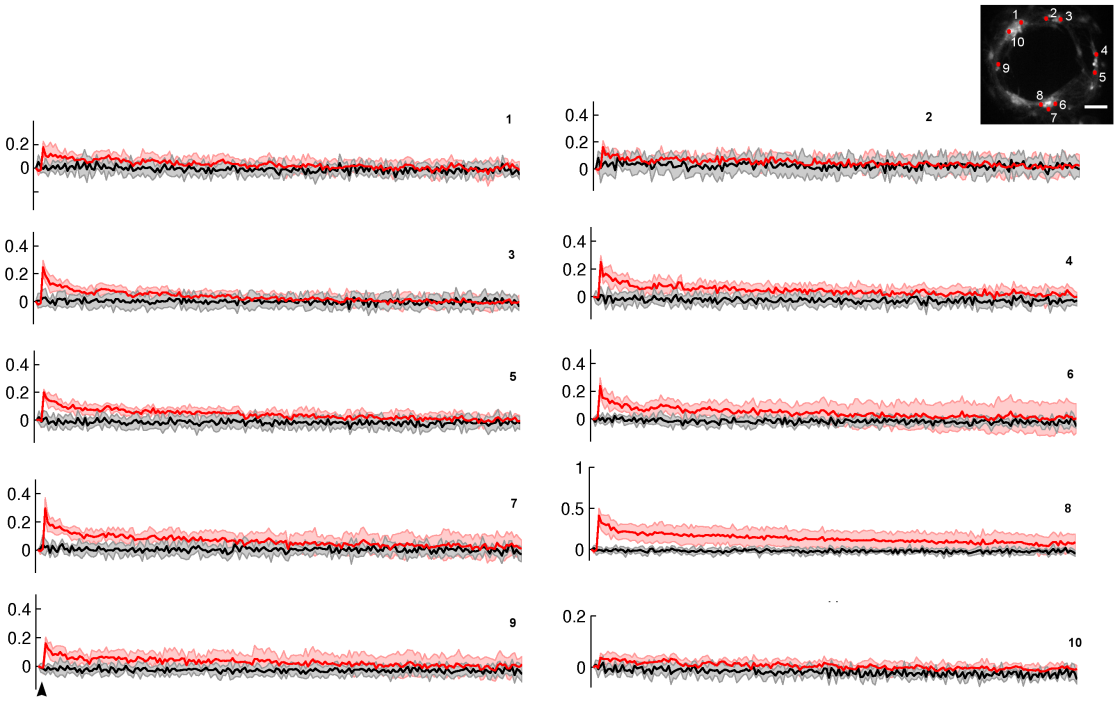

Figure 24: Asynchronous transmitter release is required for reverberations

Typical response of ROIs when network was incubated in EGTA-AM. Each Roi shows just the synchronous phase of transmission following the initial stimuli denoted by the arrowhead. Each trace is the mean response (dark red trace) over five trials bound by the sd, black trace is the baseline response of the same ROIs over five trials. Inset: Ring networks with the analyzed ROIs. Scale bar 100μm, all traces are 6.6sec long.

are maintained by asynchronous neurotransmitter release. Blocking asynchronous neurotransmitter release completely abolished network reverberations. The average half-width time of reverberations with EGTA-AM fell from 1.35 ± 1.2sec to 0.27 ± 0.24sec.

Another observation which was made was the maintenance of network architecture despite the blockade of inhibition. In other words, we ranked the order of firing of cells based in the intensity of change in fluorescence. Cells that underwent reverberation typically had greater change in fluorescence as compared to cell that didn't. We noticed that cells which responded with higher changes in fluorescence during control trials were the same cells that responded after the addition of BMI. Figure 26 is a plot of normalized $-\Delta F/F$ for control and BMI cases the colors of each point is the baseline fluorescence of the ROI. We notice a strong linear trend in the order of cell responses. This could mean that cells that responded during control cases were the same cells that responded after application of BMI i.e. the architecture of the network is preserved. Blocking of inhibition does not change the architecture of the network.

Finally we looked to see if there were any changes in the reverberation characteristics among rings of different sizes. It can be hypothesized that changes in the size of the ring network might change certain features of network connections. This in turn may change the behavior of reverberations in these rings. To look at these effects, we looked at two sizes of rings that varied by $50\mu m$ in track width thickness ($100\mu m$ and $150\mu m$). Table 4 summarizes the reverberation characteristics for ring networks of two different sizes.

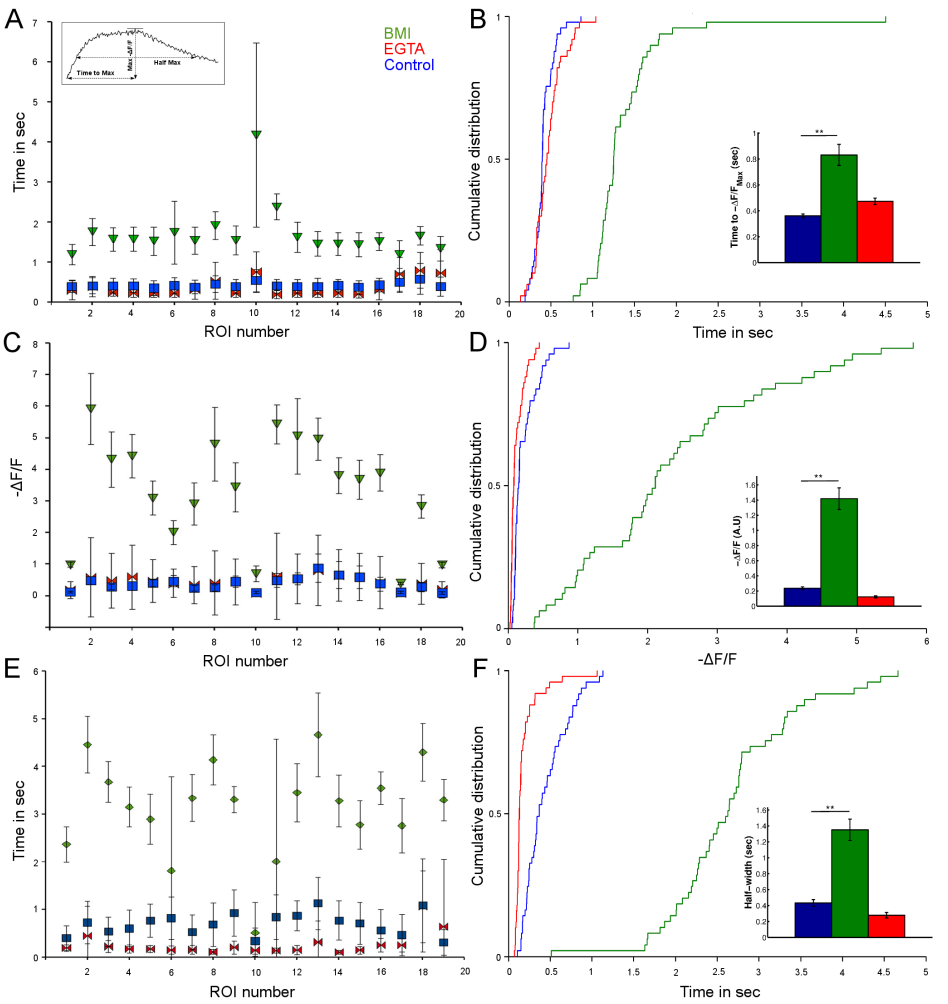

Figure 25: Summary of reverberations in ring networks

A.) Scatter plot of time to max from consecutive trials for control, BMI and EGTA cases B.) Cumulative distribution of all analyzed ROIs (inset: Mean time to max over all ROIs, $p < 0.05$) C.) Scatter plot of $\Delta F/F$ D.) Cumulative distribution of all analyzed ROIs (inset: Mean change in fluorescence over all ROIs, $p < 0.05$) E.)Scatter plot of half width time F.)Cumulative distribution of all analyzed ROIs (inset: Mean half-width over all ROIs, $p < 0.05$). $n = 68, 99, 50$ROIs for control, BMI and EGTA cases. p values are for Wilcoxon rank-sum test.

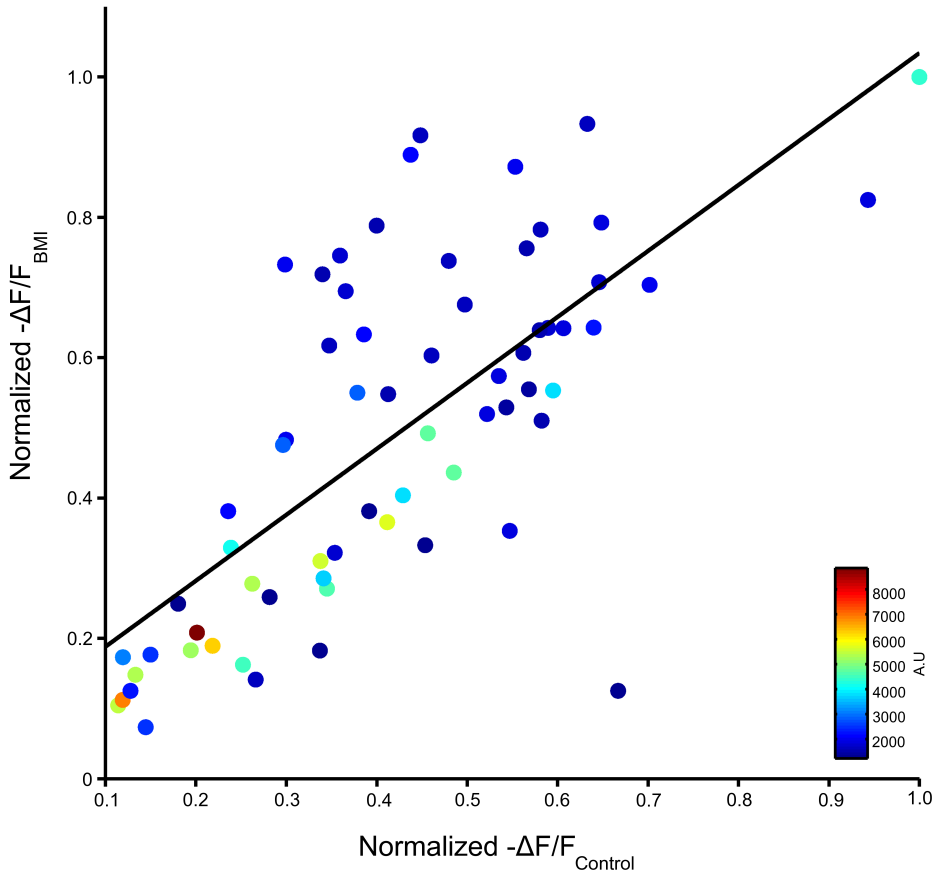

Figure 26: Network architecture is preserved

Scatter plot of normalized change in fluorescence of BMI and control cases. Linear regression line fitted to data with $R^2 = 0.5$ for $(n = 4)$ cultures. Overlaid on each point is the baseline fluorescence of the ROI prior to stimulations.

Table 4: Summary of reverberations characteristics for varying ring sizes

	Track width $150\mu m$		Track width $100\mu m$	
	Control	BMI	Control	BMI
Max $-\Delta F/F(A.U)$	0.23 ± 0.01	1.41 ± 0.14	0.28 ± 0.05	1.25 ± 0.11
Time to $-\Delta F/F_{Max}(sec)$	0.36 ± 0.01	0.83 ± 0.08	0.47 ± 0.02	0.94 ± 0.04
Half-width (sec)	0.43 ± 0.04	1.35 ± 0.13	0.28 ± 0.02	1.52 ± 0.12

4.7 CONCLUSION

We have developed a method to culture sparse neuronal networks of a defined geometry that allows for the repeatable observation of persistent activity. The current geometry allows formation of recurrently-connected ring-shaped neuronal networks. The ring network defined through this geometry limits both the upper extent of the network as-well-as the lower extent. We use these limitations to not only better-define the range of possible path-lengths, but also limit the likelihood of destructive interference by decreasing the possible connection pathways within the network. This ring-geometry was used to form the experimental networks used throughout this experiment.

We have demonstrated neuronal cultures in a ring-shaped geometry through microstamping adhesive proteins onto the substrate surface. Dissociated neurons plated onto the substrate will grow almost exclusively on the protein coating. Likewise, neuronal processes will comply with the geometry of the protein stamp through 2 weeks of growth and development (later time-points were not assessed in this study). One of the crucial factors to the quality of the network geometry is the quality of the protein stamp. Since the stamped protein promotes neuronal adhesion and growth, areas with more protein will be more likely to promote neuronal adhesion and growth (data not shown). The neurons were plated at a density of $100,000$ cells/ml. This density created networks containing similar numbers of cells as those used in previous studies [66] (Figure 10). Extended neuronal growth and recurrent network morphology were verified through immunocytochemistry to ensure suitable experimental networks (Figure 9).

The ring-shaped networks created here were functionally connected in a recurrent fashion. We assessed this by stimulating networks at a single location along their circumference and observing activity changes around the entire network. Functional connectivity was verified through use of single, double and triple pulse stimuli (Figure 20B). The monitored ROIs were seen to increase their fluorescence immediately following each stimulus. This behavior is consistent with the actions of a functionally connected network. We further immunostained these ring networks for synaptic markers and verified for the formation of synapse throughout the network (Figure 11).

Although formation of a small, defined, functional neuronal network is useful, of particular interest is the establishment of a neuronal network capable of reliable production of persistent activities, similar to those seen *in vivo* during working- memory processes. A limited number of networks exhibited a drastically different response from that described earlier. This response was characterized by a large slow increase in fluorescence with a much longer raised fluorescence. Though this response occurred in a limited fashion under control conditions, we could induce this response regularly when the inhibitory inputs in the network were blocked by addition of BMI. Characterization of the differences between these responses demonstrate a persistent activity achieved in these cultures under uninhibited conditions. These characteristics demonstrate a clear difference between responses to single pulses and persistent activity, similar to those seen previously [66].

These differences were quantified through measures of the maximal activity signal. An additional observation was that there was a consistent relationship of activity strength among neuronal groups in a single network, regardless of activity strength. Although one might expect that the signal arising from a short-duration signal might vary among different ROIs,

one might also suspect that the strong persistent phase might cause a saturation of the signal in all regions. We found that the relative strength seen between ROIs during a short-duration signal was maintained for persistent phases also (Figure 26). The figures shows a linear trend when we plot the relative strength at a node not displaying persistence of signal vs. the strength of the same node during persistent phases (i.e. the stronger ROIs at control conditions are the stronger ROIs under BMI condition). This result is consistent with previous studies that found signal strength is maintained throughout a network pathway [88]. Also, through this study we used two slightly different network geometries, $300\mu m$ outer radius with track width of either 150 or $100\mu m$. The slight differences in measures seen between these two track widths showed no significance (Table 4), but suggest those geometry parameters might effect activity.

Two other parameters not explicitly explored in this study is the onset and termination of the persistent phase of activity. The onset of this persistent phase of activity, while initiated by the external electrical stimulus, can be enabled by changing the balance of inhibitory and excitatory connections. We ensure that imbalance here through the use of BMI. Of similar interest is the termination of the persistent phase of activity. Lau *et al.* showed asynchronous release of neurotransmitter from pre-synaptic terminals is important for maintenance of reverberatory activity [66]. Activity-dependent increase in pre-synaptic residual calcium enhances asynchronous neurotransmitter release and such reverberations are terminated by a slow timescale synaptic depression [94, 95]. Suppression of this activity specifically abrogates the persistent phase without affecting the initial propagation around the network. Our EGTA-AM experiments show that the persistent activity observed here is of the same form demonstrated in earlier work [66].

Some of the possible reasons for the termination of the persistent phase of activity:

1. In one dimensional networks it was concluded that the main obstacle for information transport was the physical thinning of the network in certain areas. This thinning prevents a build-up of presynaptic activity in order for it to be transmitted [88]. 2. Asynchronous release of neurotransmitter from pre-synaptic terminals is important for reverberatory activity [66]. Activity- dependent increase in pre-synaptic residual calcium enhances asynchronous neurotransmitter release and such reverberations are terminated by a slow timescale synaptic depression [94]. 3. It is thus possible that termination of these persistent phases of activity in one-dimensional networks is a combination of reduced synaptic connectivity in thin areas of the network which in-turn leads to a reduced levels of asynchronous neurotransmitter release at pre-synaptic sites.

It was also observed that there was no significant difference in the reverberations characteristics between the two sizes of rings that were compared in this study Table 4. One possible reason for this observation is that the track width was varied by 50μm which was not large enough to notice a difference. The other possible reason for such an observation is due to reorganization of the synapses [35]. Networks of neurons that scale in size display an inverse relation of synaptic strength to size of the network. That is, in order to maintain activity in the network, as the size of the network increases and more synapses are formed, the strength of these synapses however is weaker. Large networks have many weak synapses and small network have few strong synapses. This scaling of synapses is a possible mechanism by which networks prevent runway positive feedback. Thus, it is possible that such scaling at synapses is responsible for maintaining the reverberation characteristics of ring networks.

5.0 CONCLUSIONS AND FUTURE WORK

In this thesis we have described two methods by which networks of neurons can be constrained. The purpose of these constraining techniques is to better understand network phenomena that are otherwise confounded by effects of large random networks. The work was broadly divided into two sections, one dealing with constraining inside microfluidic devices and the other, constraining over selective regions of patterned protein.

5.1 CONSTRAINING INSIDE MICROFLUIDIC DEVICE

Microfluidic devices are steadily gaining a strong foot-hold in neurosciences. Here we have demonstrated, the use of these devices to maintain groups of neurons for extended periods of time. Using microfabrication tools, we created microfluidic devices that were capable of maintaining cells for extended periods of time. One of the important considerations for long-term maintenance of cells is the replenishment of nutrient media at frequent intervals. Since the volumes of nutrient media that are housed in these device is in the order of a few nano liters, the effective nutrients in the media are consumed much faster as compared to larger volumes of nutrient media. The advantage of using microfluidic devices is in availability of

trophic factors. The small scale of the device allows for much faster diffusion of important trophic factors through the devices.

The development of the nervous system is a precisely orchestrated event that entails the creation of diffusable gradients of trophic factors. Microfluidic devices offer researchers the ability to create precise gradients of similar trophic factors. The micro-scale of these devices allows for the spread of these diffusable factors in a more effective manner and in higher concentrations as compared to traditional cell culture techniques. Here we demonstrate the versatility of these devices by culturing nerve cells. Neurons are one of the more metabolically active cells in the body requiring large amounts of nutrients. Culturing neurons inside such microfluidic devices is a challenging task, since this requires frequent changes of nutrient media in order to keep up with the metabolic needs of the cells.

We compared the development of neurons inside a microfluidic device as compared to their development on a traditional platform. By imaging the neurons at periodic intervals, we compared the growth profiles of neurons in each of the above platforms. Interestingly, we found that neurons inside microfluidic devices had fewer and longer processes as compared to their counterparts in a cell culture plates with the same area. Neurons on the other platform had larger number of short processes. From the results that were obtained it seems that neurons develop and extend processes much faster than in traditional systems.

We next made a series of microfluidic devices that were capable of maintaining more than one population of neurons for extended periods of time. We created these devices based on the devices of the Jeon group [42, 71] with slight modifications. These microfluidic devices are capable of maintaining two populations of neurons in a fluidically isolated manner. By adjusting the hydrostatic gradients of nutrient median in each of these populations, it is

possible to maintain a fluidic isolation between the two chambers. The other unique aspect of these devices is a set of microgrooves that connect the two populations. These microgrooves are on the order of a few microns and allow for the growth of neuronal processes thorough them.

5.2 CONSTRAINING USING MICROCONTACT PRINTING

Microcontact printing is a versatile tool that has been used for a variety of studies in neuroscience. We have demonstrated the use of μCP to selectively restrict neuronal networks to ring shaped geometries. Using microfabrication tools, we crated polymer reliefs of ring geometries of varying sizes that can be used to print adhesive proteins over glass substrates. The methods we used lead to the creation of stamps that were planar, promoting even deposition of protein over the substrate. Early experiments that were not very successful in homogeneous protein deposition yielded networks that seemed to be restricted over the substrate in an un-even manner. It was also observed that when a high density of neurons were plated over these stamped substrates, they seemed to display a clustering of cell bodies in a random manner. This clustering was very detrimental to the actual ring geometry since it prevented networks from extending over the geometry in an even manner, it also makes it difficult to perform any kind of data analysis from individual cell bodies.

In order to reduce the clustering, we hypothesized that a glial monolayer would reduce the clustering by providing a preferred substrate for the neurons to grow on. In order to promote the growth of glial cells, we switched the culture medium to a serum supplemented media. Serum supplemented media promoted the growth of glial cells. In this new media, it was

observed that the clustering effect disappeared. The cells were distributed over the network in an even manner as was observed upon immunostaining with neuronal and dendritic markers. It was also observed that a cell density of 10^5 cells/ml yielded $\sim 40 - 70$ neurons per ring, densities lower than that were not successful in promoting the ring geometry. These cultures were successfully maintained for extended periods of time (3 weeks) without disruption of the ring geometry.

Next these cultures were immunostained to see if they formed synapses. We used the pre-synaptic marker Synapsin1 to check for synapses. Synapsin1 typically displays synapses in a punctate manner that is spread over the surface of a neuron. We noticed that all the cultures that were probed were positive for pre-synaptic formations. Thus, in the first part of this work we have shown successfully that neurons can be restricted to a ring shaped geometry and that these ring shapes can be precisely controlled by the stamps used to print the protein. We also went on to show that these ring networks can be maintained for extended periods of time and that they form synapses.

We have developed a method to culture sparse neuronal networks of a defined geometry that allows for the repeatable observation of persistent activity. The current geometry allows formation of recurrently-connected ring-shaped neuronal networks. The ring network defined through this geometry limits both the upper extent of the network as-well-as the lower extent. We use these limitations to not only better-define the range of possible path-lengths, but also limit the likelihood of destructive interference by decreasing the possible connection pathways within the network. This ring-geometry was used to form the experimental networks used throughout this experiment.

The ring-shaped networks created here were functionally connected in a recurrent fashion. We assessed this by stimulating networks at a single location along their circumference and observing activity changes around the entire network. Functional connectivity was verified through use of single, double and triple pulse stimuli. The monitored ROIs were seen to increase their fluorescence immediately following each stimulus. This behavior is consistent with the actions of a functionally connected network.

Although formation of a small, defined, functional neuronal network is useful, of particular interest is the establishment of a neuronal network capable of reliable production of persistent activities, similar to those seen *in vivo* during working-memory processes. A limited number of networks exhibited a drastically different response from that described earlier. This response was characterized by a large slow increase in fluorescence with a much longer raised fluorescence. Though this response occurred in a limited fashion under control conditions, we could induce this response regularly when the inhibitory inputs in the network were blocked by addition of BMI. Characterization of the differences between these responses demonstrate a persistent activity achieved in these cultures under uninhibited conditions. These characteristics demonstrate a clear difference between responses to single pulses and persistent activity, similar to those seen previously [66].

These differences were quantified through measures of the maximal activity signal. An additional observation was that there was a consistent relationship of activity strength among neuronal groups in a single network, regardless of activity strength. Although one might expect that the signal arising from a short-duration signal might vary among different ROIs, one might also suspect that the strong persistent phase might cause a saturation of the signal in all regions. We found that the relative strength seen between ROIs during a short-duration

signal was maintained for persistent phases also. The figures shows a linear trend when we plot the relative strength at a node not displaying persistence of signal vs. the strength of the same node during persistent phases (i.e. the stronger ROIs at control conditions are the stronger ROIs under BMI condition). This result is consistent with previous studies that found signal strength is maintained throughout a network pathway. Also, through this study we used two slightly different network geometries, $300\mu m$ outer radius with track width of either 150 or $100\mu m$. The slight differences in measures seen between these two track widths showed no significance, but suggest those geometry parameters might effect activity.

Two other parameters not explicitly explored in this study is the onset and termination of the persistent phase of activity. The onset of this persistent phase of activity, while initiated by the external electrical stimulus, can be enabled by changing the balance of inhibitory and excitatory connections. We ensure that imbalance here through the use of BMI. Of similar interest is the termination of the persistent phase of activity. Lau *et al.* showed asynchronous release of neurotransmitter from pre-synaptic terminals is important for maintenance of reverberatory activity [66]. Activity-dependent increase in pre-synaptic residual calcium enhances asynchronous neurotransmitter release and such reverberations are terminated by a slow timescale synaptic depression [94][95]. Suppression of this activity specifically abrogates the persistent phase without affecting the initial propagation around the network. Our EGTA-AM experiments show that the persistent activity observed here is of the same form demonstrated in earlier work [66].

We have shown that ring networks are capable of producing persistent activity upon a single stimulation. This persistent activity is monitored via the calcium signal produced at each cell. In this body of work all the imaging that was performed towards the analysis

of persistent activity was performed at $30Hz$. This imaging resolution is not adequate to reveal events that happen at shorter time scales. One of the interesting studies that can be performed in the future with higher temporal resolution is to look for repeated patterns of activation among the cells. It is possible that among the ROIs analyzed, there exists a sequence of activation (i.e ROI1 activated before ROI2 etc.). If such a sequence exists, does the same sequence of events repeat in successive trials? Each such sequence can be termed an activity pattern, and if so how many such activity patterns exists in a single culture. It is believed that events relating to memory storage and consolidation are relayed in certain brain areas in select patterns. For example, the sight of a red Robin may create a pattern of activity in the brain, the same pattern when replayed is then associated with a red Robin. The persistent activity patterns observed in these ring cultures can be though as analogous to activity patterns in the brain, if so how many such patterns can co-exist in culture.

Another interesting question that can be asked is regarding the role of plasticity. Are such networks plastic? Do they respond differently upon repeated activation? What causes the difference in response, if any? Such question can be asked with the current setup.

More broader questions pertaining to mental health can be asked using the current setup. How is this form of persistent activity affected in diseased states. Mutations of ion channels have been implicated in certain disease conditions. Expressing these mutated transgenes in such networks and looking at the patterns of activity that emerge can be useful in understanding the disease states.

APPENDIX A

FIELD STIMULATION VOLATAGE

Extracellular field stimulatation at $50, 80$ and $100V$ was carried out to determine the minimum stimuli required to evoke activity in cells. We performed an experiment and stimulated a ring network at the above mentioned voltages followed by incubation in $10\mu M$ BMI and repeated the order of stimulation. We observed that at $50V$ both the control as well as the BMI cases did not differ significantly. However at $80, 100V$ both the $\Delta F/F$ and the half-width time were significantly more that that at control. At $80V$, control - $0.06 \pm 0.008(A.U)$ BMI - $0.2 \pm 0.02(sec)$, $p < 0.005$ (Student's t-test) and at $100V$, control $= 0.09 \pm 0.01(A.U)$. BMI $= 039 \pm 0.06(sec)$ $p < 0.005$ (Student's t-test).

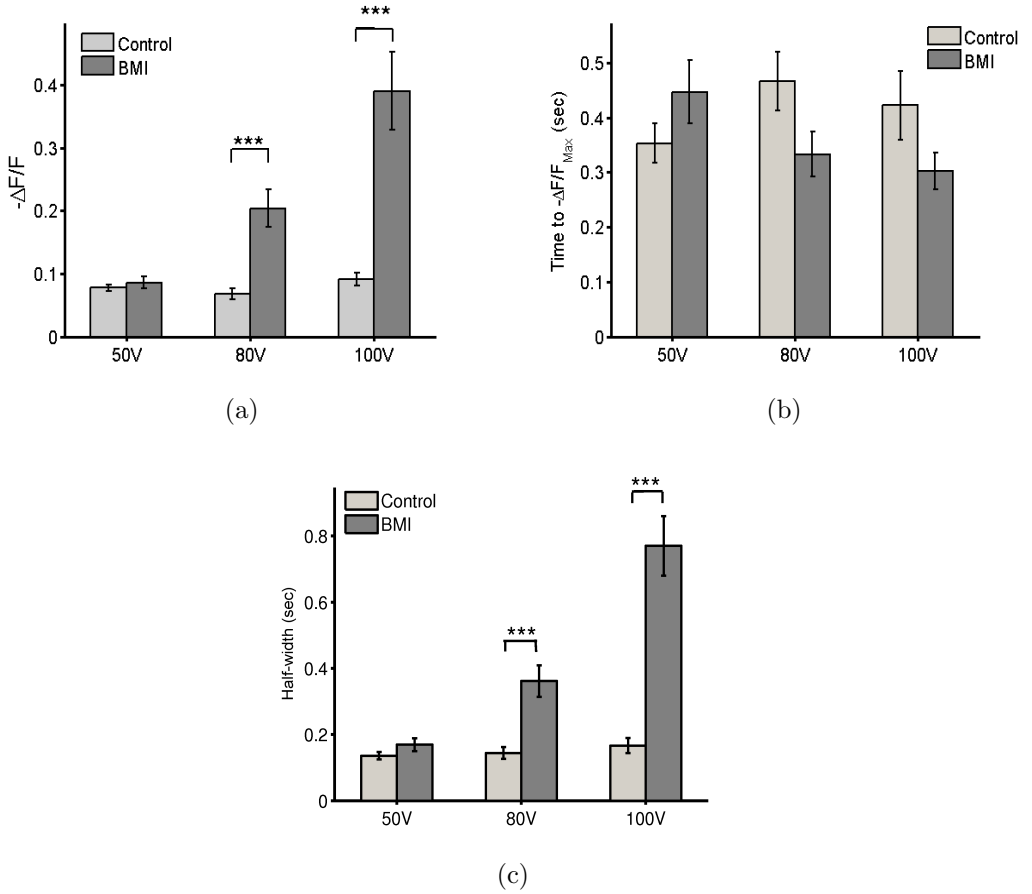

Figure 27: Voltage dependence effects on reverberation characteristics

a.) Effect of varying stimulation voltage on mean $\Delta F/F(A.U)$. b.) Effect of stimulating voltage on time to $\Delta F/F_{Max}(sec)$. c.) Effect of stimulating voltage on half-width times.

APPENDIX B

MATLAB CODES

```
% Version 5.0 of the Ca image analysis. This file is to generate plots of
% Ca intensities of stimulation movies. The file takes inputs from baseline
% movies as well as stim movies. The baseline movies are used to calculate
% the threshold. All plots are linearized by differentiating the time series.
Created 5/26/10 by AV


clc;
clear all;
%% Input parameters


x = input('Enter the number of ROIs '); % specify number of Rois including one
for background (make sure the background roi is the last roi in the set)
stim = input('Enter the stimulation Voltage ') ; % specify the stimulation voltage
```

```
Acq = input('Enter the Acquisition rate ' ); % Acquition rate in seconds

frame = input('Enter the number of frames ');

y_baseline = input('Enter the number of baseline trials ');

% Specify the number of baseline trials, all files in trial_bl_* format

y_stim = input('Enter the number of control stimulus trials ') ;

% specify the number of trials conducted save all files in trial_stim_* format

Frames = (1) : (frame); % Number of frames in the movies

%Acq_time =


%% Baseline trials


for B=6:y_baseline % Read Baseline trials



    [Slno_bl, Area_bl, Mean_bl, Min_bl, Max_bl, int_dens_bl] =

    textread(['trial_bl' int2str(B) '.txt'], '%f %f %f %f %f %f'); % loading data



    % Sorting data, specify the plotting parameter, Max, int_dens etc.


    for i=0:(frame-1)


        Roi_int_dens_bl(1:x,i+1) = int_dens_bl ( (x*i)+1 : x * (i+1) );
```

```
        Roi_min_bl(1:x,i+1) = Min_bl ( (x*i)+1 : x * (i+1) );

        Roi_max_bl(1:x,i+1) = Max_bl ( (x*i)+1 : x * (i+1) );

        Roi_mean_bl(1:x,i+1) = Mean_bl ( (x*i)+1 : x * (i+1) );


    end


    %%
    % Calculation delaF/F, deltaf/f = [(fo-b0) - (f1-b1)]/(f0-b0)
    %where f0,b0 =  intensity of first frame and f1,b1 are time dependent


    clear  ('deltaf_int_dens_bl', 'Norm_mean_bl');



    for j = 1:(x)
        for k = 1:frame



 % deltaf_int_dens_bl(j,k) = -[(Roi_int_dens_bl(j,1) - Roi_int_dens_bl(x,1))
    - (Roi_int_dens_bl(j,k) - Roi_int_dens_bl(x,k))]/ (Roi_int_dens_bl(j,1)
    - Roi_int_dens_bl(x,1));


% deltaf_mean_bl(j,k) = -[(Roi_mean_bl(j,1) - Roi_mean_bl(x,1))
- (Roi_mean_bl(j,k) - Roi_mean_bl(x,k))] / (Roi_mean_bl(j,1)
```

```
- Roi_mean_bl(x,1));


  deltaf_int_dens_bl(j,k) = -[(Roi_int_dens_bl(j,1) - Roi_int_dens_bl(x,1))
  - (Roi_int_dens_bl(j,k) - Roi_int_dens_bl(x,k))]/ (Roi_int_dens_bl(j,1)
  - Roi_int_dens_bl(x,1));


  deltaf_mean_bl(j,k) = -[(Roi_mean_bl(j,2) - Roi_mean_bl(x,2))
  - (Roi_mean_bl(j,k) - Roi_mean_bl(x,k))] / (Roi_mean_bl(j,2)
  - Roi_mean_bl(x,2));



      end
   end

   % saving each paramater in a file

   % raw data
   trial_set_bl.Slno(:,:,B) = Slno_bl;
   trial_set_bl.Area(:,:,B) = Area_bl;
   trial_set_bl.Mean(:,:,B) = Mean_bl;
   trial_set_bl.Min(:,:,B) = Min_bl;
   trial_set_bl.Max(:,:,B) = Max_bl;
   trial_set_bl.int_dens(:,:,B) = int_dens_bl;
```

```
    % sorted data
    trial_set_bl.Roi_int_dens(:,:,B) = Roi_int_dens_bl;
    trial_set_bl.Roi_min(:,:,B) = Roi_min_bl;
    trial_set_bl.Roi_max(:,:,B) = Roi_max_bl;
    trial_set_bl.Roi_mean(:,:,B) = Roi_mean_bl;
    %
    % % deltaf/f data
    trial_set_bl.deltaf_mean(:,:,B) = deltaf_mean_bl;
    trial_set_bl.deltaf_int_dens(:,:,B) = deltaf_int_dens_bl;
    %

end
%% Control trials
for S=6:y_stim % Read control stimulus trials

    [Slno, Area, Mean, Min, Max, int_dens] =
    textread(['trial_stim' int2str(S) '.txt'], '%f %f %f %f %f %f');
    % loading stimulation movies

    % % Sorting data, specify the plotting parameter, Max, int_dens etc.

    for i=0:(frame-1)
```

```
    Roi_int_dens(1:x,i+1) = int_dens ( (x*i)+1 : x * (i+1) );
    Roi_min(1:x,i+1) = Min ( (x*i)+1 : x * (i+1) );
    Roi_max(1:x,i+1) = Max ( (x*i)+1 : x * (i+1) );
    Roi_mean(1:x,i+1) = Mean ( (x*i)+1 : x * (i+1) );



end
% Calculation delaF/F, deltaf/f = [(f0-b0) - (f1-b1)]/(f0-b0)
% where f0,b0 =  intensity of first frame and f1,b1 are time dependent

clear  ('deltaf_int_dens', 'Norm_mean');
clear ('i', 'j', 'k');



for j = 1:(x)
    for k = 1:frame

        %deltaf_int_dens(j,k) = -[(Roi_int_dens(j,1) - Roi_int_dens(x,1))
        - (Roi_int_dens(j,k) - Roi_int_dens(x,k))]/ (Roi_int_dens(j,1)
        - Roi_int_dens(x,1));

        %deltaf_mean(j,k) = -[(Roi_mean(j,1) - Roi_mean(x,1))
```

```
        - (Roi_mean(j,k) - Roi_mean(x,k))] / (Roi_mean(j,1)
        - Roi_mean(x,1));

        deltaf_int_dens(j,k) = -[(Roi_int_dens(j,2) - Roi_int_dens(x,2))
        - (Roi_int_dens(j,k) - Roi_int_dens(x,k))]/ (Roi_int_dens(j,2)
        - Roi_int_dens(x,2));

        deltaf_mean(j,k) = -[(Roi_mean(j,2) - Roi_mean(x,2))
        - (Roi_mean(j,k) - Roi_mean(x,k))] / (Roi_mean(j,2)
        - Roi_mean(x,2));

         %deltaf_mean(j,k) = [ Roi_mean(j,k) - Roi_mean(x,k)];

    end
end


% saving each paramater in a file

% Raw data
trial_set.Slno(:,:,S) = Slno;
trial_set.Area(:,:,S) = Area;
trial_set.Mean(:,:,S) = Mean;
```

```
    trial_set.Min(:,:,S) = Min;
    trial_set.Max(:,:,S) = Max;
    trial_set.int_dens(:,:,S) = int_dens;

    % Sorted data
    trial_set.Roi_int_dens(:,:,S) = Roi_int_dens;
    trial_set.Roi_min(:,:,S) = Roi_min;
    trial_set.Roi_max (:,:,S)= Roi_max;
    trial_set.Roi_mean(:,:,S) = Roi_mean;

    % DeltaF/f data

    trial_set.deltaf_mean(:,:,S) = deltaf_mean;
    trial_set.deltaf_int_dens(:,:,S) = deltaf_int_dens;



end
%% Calculating the mean per ROI for baseline

%temp_rois_bl(:,:,:) = zeros;

for l = 1:x-1
    for t = 1:y_baseline
```

```
        temp_rois_bl(t,:,l) = trial_set_bl.deltaf_mean(l,:,t);
    end
end


% Plotting Baseline movies each Roi per trial, each subplot contains the behavior of a
%  single ROI (x, rois) for as many number of trials (y, trials)

figure(1); % each ROI for baseline movies and the means
clear ('i', 'j', 'k');

for j = 1:x-1 % plotting the mean of the baseline

    if mod(x,2) == 0

        Framesinv = Frames(end:-1:1);
        mbase=mean(temp_rois_bl(:,:,j));
        sbase=std(temp_rois_bl(:,:,j));
        subplot(x/2,2,j), plot(mbase, 'LineWidth', 1.2 , 'color', 'black')
        set(gca, 'ylim', [-0.5 0.5]);
        hold on;
        hbase = fill([Frames Framesinv] , [mbase-sbase mbase(Framesinv)
        +sbase(Framesinv)], 0.8*ones(1,3));
```

```
        set(hbase,'edgecolor', 0.6*ones(1,3))
        uistack(hbase, 'down');



    else

        Framesinv = Frames(end:-1:1);
        mbase=mean(temp_rois_bl(:,:,j));
        sbase=std(temp_rois_bl(:,:,j));
        subplot(x/2,2,j), plot(mbase, 'LineWidth', 1.2 , 'color', 'black')
        set(gca, 'ylim', [-0.5 0.5]);
        hold on;
        hbase = fill([Frames Framesinv] ,
        [mbase-sbase mbase(Framesinv)+sbase(Framesinv)], 0.8*ones(1,3));
        set(hbase,'edgecolor', 0.6*ones(1,3))
        uistack(hbase, 'down');


    end


end
hold off
% set(gcf, 'color', 'none');
% se (gca, 'color', 'none');
```

```
%exportfig(gcf, 'Rois_baseline_v5.0.eps', 'width', 8, 'height', 15,
'fontmode','fixed', 'fontsize', 8, 'Color', 'cmyk', );



%% Calculation mean per ROI for stimulus conditon

clear('l', 't');



for l = 1:x-1
    for t = 1:y_stim
        temp_rois_stim(t,:,l) = trial_set.deltaf_mean(l,:,t);
    end
end



figure(2) % Plots of each ROI per trial for the stimulus conditon
clear ('i', 'j', 'k');



for i = 1: y_stim
```

```
for j = 1:x-1 % plotting the mean for the stimulus condition


    if mod(x,2) == 0
        Framesinv = Frames(end:-1:1);
        sumstim=sum(temp_rois_stim(:,:,j));
       % mstim=mean(temp_rois_stim(:,:,j));
        mstim = sumstim/5;
       % sstim=std(temp_rois_stim(:,:,j));
       sstim = sqrt(var(temp_rois_stim(1:y_stim,:,j),0));



        subplot(x/2,2,j),plot(mstim, 'LineWidth', 1.2, 'color', 'red' );
       % set(gca, 'ylim', [-0.2 6.5]);
        hold on;
        hstim = fill([Frames Framesinv] , [mstim-sstim mstim(Framesinv)
        +sstim(Framesinv)],[1, 0.8, 0.8]);
        set(hstim,'edgecolor', [1, 0.6, 0.6])
        uistack(hstim, 'down');
    else
        Framesinv = Frames(end:-1:1);
```

```
            sumstim=sum(temp_rois_stim(:,:,j));
            mstim = sumstim/5;
            sstim = sqrt(var(temp_rois_stim(1:y_stim,:,j),0));
            subplot(x/2,2,j),plot(mstim, 'LineWidth', 1.2, 'color', 'red' );
            %set(gca, 'ylim', [-0.5 5]);
            hold on;
            hstim = fill([Frames Framesinv] , [mstim-sstim mstim(Framesinv)
            +sstim(Framesinv)],[1, 0.8, 0.8]);
            set(hstim,'edgecolor',[1, 0.6, 0.6] )
            uistack(hstim, 'down');

        end

    end
%end

hold off

%exportfig(gcf, 'Rois_stims_v5.0.eps', 'width', 6, 'height', 15,
 'fontmode','fixed', 'fontsize', 8, 'Color', 'cmyk');
%% plotting both stimulus condition and baseline condition in one plot

figure(3)
```

```
clear ('i', 'j', 'k');
clear ('mbase', 'sbase', 'mmstim', 'sstim', 'sumstim');

for j = 1:x-1 % plotting the mean for the stimulus condition

    if mod(x,2) == 0

        Framesinv = Frames(end:-1:1);

        mbase=mean(temp_rois_bl(:,:,j));
        sbase=std(temp_rois_bl(:,:,j));
        sumstim=sum(temp_rois_stim(:,:,j));
        mstim = sumstim/5;
        sstim = sqrt(var(temp_rois_stim(1:y_stim,:,j),0));

        subplot(x/2,2,j),plot(mbase, 'LineWidth', 1, 'color', 'black' );
       % set(gca, 'ylim', [-0.5 2.5]);
        hold on;
        hbase = fill([Frames Framesinv] , [mbase-sbase mbase(Framesinv)
        +sbase(Framesinv)], 0.8*ones(1,3));
        set(hbase,'edgecolor', 0.6*ones(1,3))
        uistack(hbase, 'down');
```

```
    subplot(x/2,2,j),plot(mstim, 'LineWidth', 1, 'color', 'red' );
    hstim = fill([Frames Framesinv] , [mstim-sstim mstim(Framesinv)
    +sstim(Framesinv)], [1, 0.8, 0.8]);
    set(hstim,'edgecolor',[1, 0.6, 0.6] )
    uistack(hstim, 'bottom');

else

    Framesinv = Frames(end:-1:1);

    mbase=mean(temp_rois_bl(:,:,j));
    sbase=std(temp_rois_bl(:,:,j));
    sumstim=sum(temp_rois_stim(:,:,j));
    mstim = sumstim/5;
    sstim = sqrt(var(temp_rois_stim(1:y_stim,:,j),0));
    %           mstim=mean(temp_rois_stim(:,:,j));
    %            sstim=std(temp_rois_stim(:,:,j));
    subplot(x/2,2,j),plot(mbase, 'LineWidth', 1, 'color', 'black' );
    %set(gca, 'ylim', [-0.5 3.5]);
    hold on;
    hbase = fill([Frames Framesinv] , [mbase-sbase mbase(Framesinv)
```

```
        +sbase(Framesinv)], 0.8*ones(1,3));
        set(hbase,'edgecolor', 0.6*ones(1,3))
        uistack(hbase, 'down');



        subplot(x/2,2,j),plot(mstim, 'LineWidth', 1, 'color', 'red' );
        hstim = fill([Frames Framesinv] , [mstim-sstim mstim(Framesinv)
        +sstim(Framesinv)], [1, 0.8, 0.8]);
        set(hstim,'edgecolor',[1, 0.6, 0.6] )
        box off;
        %axis off;
        uistack(hstim, 'bottom');
       % title('trial j');


    end

end

hold off

%exportfig(gcf, 'Trials_stim_composite_v5.0.eps', 'width', 6, 'height', 10,
'fontmode','fixed', 'fontsize', 8, 'Color', 'cmyk');
```

```
%% Plot of each trial

figure(4);

clear ('i', 'j', 'k');

for i = 1:x-1
    for j = 1:y_stim

        hold all;

        if mod(y_stim,2) == 0

            subplot(y_stim/2,2,j),plot(trial_set.deltaf_mean(i,:,j)) %'Color' , 'red');
             %set(gca, 'ylim', [-0.5 5]);
            % subplot(y/2,2,j),plot(Acq_time,trial_set(j).deltaf_mean(i,:),
            'LineWidth', 1) %'Color' , 'red');
        else
            subplot((y_stim/2)+0.5,2,j),plot(trial_set.deltaf_mean(i,:,j)) % 'Color' , '
            % set(gca, 'ylim', [-0.5 5]);
            % subplot((y/2)+0.5,2,j),plot(Acq_time,trial_set(j).deltaf_mean(i,:),
            'LineWidth', 1) % 'Color' , 'red')
```

```
        end

        %         title ('Mean');
        %         xlabel('Time (sec)');
        %         ylabel('-DeltaF/F');

    end
    title(pwd);
end

%exportfig(gcf, 'Trials_stim_fivetrials_v5.0.eps',
'width', 8, 'height', 15,
'fontmode','fixed', 'fontsize', 8, 'Color', 'cmyk');

%%
```

BIBLIOGRAPHY

[1] G. W. Gross, B. K. Rhoades, H. M. Azzazy, and M. C. Wu, "The use of neuronal networks on multielectrode arrays as biosensors," *Biosensors & bioelectronics*, vol. 10, pp. 553–67, Jan 1995.

[2] J. C. Chang, G. J. Brewer, and B. C. Wheeler, "Modulation of neural network activity by patterning," *Biosensors & bioelectronics*, vol. 16, pp. 527–33, Sep 2001.

[3] Y. Nam, J. Chang, D. Khatami, G. Brewer, and B. Wheeler, "Patterning to enhance activity of cultured neuronal networks," *Nanobiotechnology*, Jan 2004.

[4] A. Kumar and G. Whitesides, "Features of gold having micrometer to centimeter dimensions can be formed through a combination of stamping with an elastomeric stamp and an alkanethiol "ink"followed by chemical etching," *Applied Physics Letters*, vol. 63, p. 2002, 1993.

[5] Y. Xia, E. Kim, X. Zhao, J. Rogers, M. Prentiss, and G. Whitesides, "Complex optical surfaces formed by replica molding against elastomeric masters," *Science*, vol. 273, pp. 347–9, Jul 1996.

[6] X. Zhao, Y. Xia, and G. Whitesides, "Fabrication of three-dimensional micro-structures: Microtransfer molding," *Advanced Materials*, vol. 8, pp. 837–&, Jan 1996.

[7] E. Kim, Y. Xia, and G. Whitesides, "Polymer microstructures formed by moulding in capillaries," 1995.

[8] E. Kim, Y. Xia, X. Zhao, and G. Whitesides, "Solvent-assisted microcontact molding: A convenient method for fabricating three-dimensional structures on surfaces of polymers," *Advanced Materials*, vol. 9, pp. 651–654, Jan 1997.

[9] Y. Xia and G. M. Whitesides, "Soft lithography," *Angwante Chemie*, vol. 37, pp. 550–575, Mar 1998.

[10] R. Wadhwa, C. F. Lagenaur, and X. T. Cui, "Electrochemically controlled release of dexamethasone from conducting polymer polypyrrole coated electrode," *J Control Release*, vol. 110, pp. 531–41, Feb 2006.

[11] M. V. Kopanitsa, N. O. Afinowi, and S. G. N. Grant, "Recording long-term potentiation of synaptic transmission by three-dimensional multi-electrode arrays," *BMC neuroscience*, vol. 7, p. 61, Aug 2006.

[12] D. B. Weibel, P. Garstecki, and G. M. Whitesides, "Combining microscience and neurobiology," *Curr Opin Neurobiol*, vol. 15, pp. 560–7, Oct 2005.

[13] T. M. Pearce and J. C. Williams, "Microtechnology: meet neurobiology," *Lab on a chip*, vol. 7, pp. 30–40, Jan 2007.

[14] G. M. Whitesides, "The origins and the future of microfluidics," *Nature*, vol. 442, pp. 368–73, Jul 2006.

[15] D. J. Beebe, G. A. Mensing, and G. M. Walker, "Physics and applications of microfluidics in biology," *Annual review of biomedical engineering*, vol. 4, pp. 261–86, Jan 2002.

[16] S. Takayama, J. C. McDonald, E. Ostuni, M. N. Liang, P. J. Kenis, R. F. Ismagilov, and G. M. Whitesides, "Patterning cells and their environments using multiple laminar fluid flows in capillary networks," *Proc Natl Acad Sci USA*, vol. 96, pp. 5545–8, May 1999.

[17] S. K. W. Dertinger, X. Jiang, Z. Li, V. N. Murthy, and G. M. Whitesides, "Gradients of substrate-bound laminin orient axonal specification of neurons," *Proc Natl Acad Sci USA*, vol. 99, pp. 12542–7, Oct 2002.

[18] S. Lang, A. C. von Philipsborn, A. Bernard, F. Bonhoeffer, and M. Bastmeyer, "Growth cone response to ephrin gradients produced by microfluidic networks," *Analytical and bioanalytical chemistry*, vol. 390, pp. 809–16, Feb 2008.

[19] A. C. von Philipsborn, S. Lang, J. Loeschinger, A. Bernard, C. David, D. Lehnert, F. Bonhoeffer, and M. Bastmeyer, "Growth cone navigation in substrate-bound ephrin gradients," *Development*, vol. 133, pp. 2487–95, Jul 2006.

[20] C. J. Wang, X. Li, B. Lin, S. Shim, G.-L. Ming, and A. Levchenko, "A microfluidics-based turning assay reveals complex growth cone responses to integrated gradients of substrate-bound ecm molecules and diffusible guidance cues," *Lab on a chip*, vol. 8, pp. 227–37, Feb 2008.

[21] G. M. Walker, H. C. Zeringue, and D. J. Beebe, "Microenvironment design considerations for cellular scale studies," *Lab on a chip*, vol. 4, pp. 91–7, Apr 2004.

[22] C. D. James, R. Davis, M. Meyer, A. Turner, S. Turner, G. Withers, L. Kam, G. Banker, H. Craighead, M. Isaacson, J. Turner, and W. Shain, "Aligned microcontact printing of micrometer-scale poly-l-lysine structures for controlled growth of cultured neurons on planar microelectrode arrays," *IEEE Trans Biomed Eng*, vol. 47, pp. 17–21, Jan 2000.

[23] G. Banker and K. Goslin, "Culturing nerve cells," p. 666, Jan 1998.

[24] G. L. Ming, H. J. Song, B. Berninger, C. E. Holt, M. Tessier-Lavigne, and M. M. Poo, "camp-dependent growth cone guidance by netrin-1," *Neuron*, vol. 19, pp. 1225–35, Dec 1997.

[25] H. J. Song, G. L. Ming, and M. M. Poo, "camp-induced switching in turning direction of nerve growth cones," *Nature*, vol. 388, pp. 275–9, Jul 1997.

[26] A. C. V. Philipsborn, S. Lang, A. Bernard, J. Loeschinger, C. David, D. Lehnert, M. Bastmeyer, and F. Bonhoeffer, "Microcontact printing of axon guidance molecules for generation of graded patterns," *Nature protocols*, vol. 1, pp. 1322–1328, Oct 2006.

[27] D. Kleinfeld, K. H. Kahler, and P. E. Hockberger, "Controlled outgrowth of dissociated neurons on patterned substrates," *J Neurosci*, vol. 8, pp. 4098–120, Nov 1988.

[28] D. W. Branch, J. M. Corey, J. A. Weyhenmeyer, G. J. Brewer, and B. C. Wheeler, "Microstamp patterns of biomolecules for high-resolution neuronal networks," *Medical & biological engineering & computing*, vol. 36, pp. 135–41, Jan 1998.

[29] S. B. Jun, M. R. Hynd, N. Dowell-Mesfin, K. L. Smith, J. N. Turner, W. Shain, and S. J. Kim, "Low-density neuronal networks cultured using patterned poly-l-lysine on microelectrode arrays," *J Neurosci Methods*, vol. 160, pp. 317–26, Mar 2007.

[30] M. Jungblut, W. Knoll, C. Thielemann, and M. Pottek, "Triangular neuronal networks on microelectrode arrays: an approach to improve the properties of low-density networks for extracellular recording," *Biomed Microdevices*, vol. 11, pp. 1269–78, Dec 2009.

[31] T. Cornish, D. W. Branch, B. C. Wheeler, and J. T. Campanelli, "Microcontact printing: a versatile technique for the study of synaptogenic molecules," *Mol Cell Neurosci*, vol. 20, pp. 140–53, May 2002.

[32] A. P. Quist, E. Pavlovic, and S. Oscarsson, "Recent advances in microcontact printing," *Anal Bioanal Chem*, vol. 381, pp. 591–600, Feb 2005.

[33] A. Tourovskaia, X. Figueroa-Masot, and A. Folch, "Differentiation-on-a-chip: a microfluidic platform for long-term cell culture studies," *Lab on a chip*, vol. 5, pp. 14–9, Jan 2005.

[34] R. Segev, M. Benveniste, E. Hulata, N. Cohen, A. Palevski, E. Kapon, Y. Shapira, and E. Ben-Jacob, "Long term behavior of lithographically prepared in vitro neuronal networks," *Phys Rev Lett*, vol. 88, p. 118102, Mar 2002.

[35] N. R. Wilson, M. T. Ty, D. E. Ingber, M. Sur, and G. Liu, "Synaptic reorganization in scaled networks of controlled size," *J Neurosci*, vol. 27, pp. 13581–9, Dec 2007.

[36] M. M. Segal, "Epileptiform activity in microcultures containing one excitatory hippocampal neuron," *Journal of Neurophysiology*, vol. 65, pp. 761–70, Apr 1991.

[37] M. M. Segal and E. J. Furshpan, "Epileptiform activity in microcultures containing small numbers of hippocampal neurons," *Journal of Neurophysiology*, vol. 64, pp. 1390–9, Nov 1990.

[38] R. B. Campenot, "Local control of neurite development by nerve growth factor," *Proc Natl Acad Sci USA*, vol. 74, pp. 4516–9, Oct 1977.

[39] S. Klostermann and F. Bonhoeffer, "Investigations of signaling pathways in axon growth and guidance," *Perspectives on developmental neurobiology*, vol. 4, pp. 237–52, Jan 1996.

[40] C. D. Deppmann, S. Mihalas, N. Sharma, B. E. Lonze, E. Niebur, and D. D. Ginty, "A model for neuronal competition during development," *Science*, vol. 320, pp. 369–73, Apr 2008.

[41] L. J. Cox, U. Hengst, N. G. Gurskaya, K. A. Lukyanov, and S. R. Jaffrey, "Intra-axonal translation and retrograde trafficking of creb promotes neuronal survival," *Nature*, vol. 10, pp. 149–59, Feb 2008.

[42] A. M. Taylor, M. Blurton-Jones, S. W. Rhee, D. H. Cribbs, C. W. Cotman, and N. L. Jeon, "A microfluidic culture platform for cns axonal injury, regeneration and transport," *Nat Methods*, vol. 2, pp. 599–605, Aug 2005.

[43] P. Tabeling, "Introduction to microfluidics," p. 301, Jan 2005.

[44] A. Taylor, S. Rhee, C. Tu, and D. Cribbs, "Microfluidic multicompartment device for neuroscience research," *Langmuir*, Jan 2003.

[45] L. N. Cornelisse, R. A. J. van Elburg, R. M. Meredith, R. Yuste, and H. D. Mansvelder, "High speed two-photon imaging of calcium dynamics in dendritic spines: consequences for spine calcium kinetics and buffer capacity," *PLoS ONE*, vol. 2, p. e1073, Jan 2007.

[46] G. Lynch, J. Larson, S. Kelso, G. Barrionuevo, and F. Schottler, "Intracellular injections of egta block induction of hippocampal long-term potentiation," *Nature*, vol. 305, pp. 719–21, Jan 1983.

[47] R. M. Mulkey and R. C. Malenka, "Mechanisms underlying induction of homosynaptic long-term depression in area ca1 of the hippocampus," *Neuron*, vol. 9, pp. 967–75, Nov 1992.

[48] J. E. Lisman and C. C. McIntyre, "Synaptic plasticity: a molecular memory switch," *Curr Biol*, vol. 11, pp. R788–91, Oct 2001.

[49] R. C. Malenka and M. F. Bear, "Ltp and ltd: an embarrassment of riches," *Neuron*, vol. 44, pp. 5–21, Sep 2004.

[50] A. Miyawaki, J. Llopis, R. Heim, J. M. McCaffery, J. A. Adams, M. Ikura, and R. Y. Tsien, "Fluorescent indicators for ca2+ based on green fluorescent proteins and calmodulin," *Nature*, vol. 388, pp. 882–7, Aug 1997.

[51] A. Miyawaki, O. Griesbeck, R. Heim, and R. Y. Tsien, "Dynamic and quantitative ca2+ measurements using improved cameleons," *Proc Natl Acad Sci USA*, vol. 96, pp. 2135–40, Mar 1999.

[52] A. E. Palmer and R. Y. Tsien, "Measuring calcium signaling using genetically targetable fluorescent indicators," *Nat Protoc*, vol. 1, pp. 1057–65, Jan 2006.

[53] R. M. Paredes, J. C. Etzler, L. T. Watts, W. Zheng, and J. D. Lechleiter, "Chemical calcium indicators," *Methods*, vol. 46, pp. 143–51, Nov 2008.

[54] R. Yuste and W. Denk, "Dendritic spines as basic functional units of neuronal integration," *Nature*, vol. 375, pp. 682–4, Jun 1995.

[55] R. Cossart, D. Aronov, and R. Yuste, "Attractor dynamics of network up states in the neocortex," *Nature*, vol. 423, pp. 283–8, May 2003.

[56] L. Tian, S. A. Hires, T. Mao, D. Huber, M. E. Chiappe, S. H. Chalasani, L. Petreanu, J. Akerboom, S. A. McKinney, E. R. Schreiter, C. I. Bargmann, V. Jayaraman, K. Svoboda, and L. L. Looger, "Imaging neural activity in worms, flies and mice with improved gcamp calcium indicators," *Nat Methods*, vol. 6, pp. 875–881, Dec 2009.

[57] B. Sakmann and E. Neher, "Single-channel recording," p. 700, Jan 2009.

[58] T. G. Ruardij, M. H. Goedbloed, and W. L. Rutten, "Adhesion and patterning of cortical neurons on polyethylenimine- and fluorocarbon-coated surfaces," *IEEE transactions on bio-medical engineering*, vol. 47, pp. 1593–9, Dec 2000.

[59] G. S. Withers, C. D. James, C. E. Kingman, H. G. Craighead, and G. A. Banker, "Effects of substrate geometry on growth cone behavior and axon branching," *J Neurobiol*, vol. 66, pp. 1183–94, Sep 2006.

[60] M. Song and K. E. Uhrich, "Optimal micropattern dimensions enhance neurite outgrowth rates, lengths, and orientations," *Annals of biomedical engineering*, vol. 35, pp. 1812–20, Oct 2007.

[61] Y. Nam and B. C. Wheeler, "Multichannel recording and stimulation of neuronal cultures grown on microstamped poly-d-lysine," *Conference proceedings : Annual International Conference of the IEEE Engineering in Medicine and Biology Society IEEE Engineering in Medicine and Biology Society Conference*, vol. 6, pp. 4049–52, Jan 2004.

[62] Y. Nam, K. Musick, and B. C. Wheeler, "Application of a pdms microstencil as a replaceable insulator toward a single-use planar microelectrode array," *Biomedical microdevices*, vol. 8, pp. 375–81, Dec 2006.

[63] D. W. Branch, B. C. Wheeler, G. J. Brewer, and D. E. Leckband, "Long-term maintenance of patterns of hippocampal pyramidal cells on substrates of polyethylene glycol and microstamped polylysine," *IEEE transactions on bio-medical engineering*, vol. 47, pp. 290–300, Mar 2000.

[64] H.-C. Zeng, Y.-C. Ho, S.-T. Chen, H.-I. Wu, H.-W. Tung, W.-L. Fang, and Y.-C. Chang, "Studying the formation of large cell aggregates in patterned neuronal cultures," *Journal of Neuroscience Methods*, vol. 165, pp. 72–82, Sep 2007.

[65] S. Kaech and G. Banker, "Culturing hippocampal neurons," *Nature protocols*, vol. 1, pp. 2406–15, Jan 2006.

[66] P.-M. Lau and G.-Q. Bi, "Synaptic mechanisms of persistent reverberatory activity in neuronal networks," *Proc Natl Acad Sci USA*, vol. 102, pp. 10333–8, Jul 2005.

[67] A. Vishwanathan, G.-Q. Bi, and H. C. Zeringue, "Ring-shaped neuronal networks: a platform to study persistent activity," *Lab on a chip*, Feb 2011.

[68] J. M. K. Ng, I. Gitlin, A. D. Stroock, and G. M. Whitesides, "Components for integrated poly(dimethylsiloxane) microfluidic systems," *Electrophoresis*, vol. 23, pp. 3461–73, Oct 2002.

[69] S. Takayama, E. Ostuni, P. LeDuc, K. Naruse, D. E. Ingber, and G. M. Whitesides, "Selective chemical treatment of cellular microdomains using multiple laminar streams," *Chem Biol*, vol. 10, pp. 123–30, Feb 2003.

[70] J. C. McDonald and G. M. Whitesides, "Poly(dimethylsiloxane) as a material for fabricating microfluidic devices," *Acc Chem Res*, vol. 35, pp. 491–9, Jul 2002.

[71] J. W. Park, B. Vahidi, A. M. Taylor, S. W. Rhee, and N. L. Jeon, "Microfluidic culture platform for neuroscience research," *Nature protocols*, vol. 1, pp. 2128–36, Jan 2006.

[72] A. Taylor, S. Rhee, and N. Jeon, "Microfluidic chambers for cell migration and neuroscience research," *Methods Mol. Biol*, Jan 2006.

[73] E. Meijering, M. Jacob, J.-C. F. Sarria, P. Steiner, H. Hirling, and M. Unser, "Design and validation of a tool for neurite tracing and analysis in fluorescence microscopy images," *Cytometry A*, vol. 58, pp. 167–76, Apr 2004.

[74] Z. A. Peterlin, J. Kozloski, B. Q. Mao, A. Tsiola, and R. Yuste, "Optical probing of neuronal circuits with calcium indicators," *Proc Natl Acad Sci USA*, vol. 97, pp. 3619–24, Mar 2000.

[75] S. W. Rhee, A. M. Taylor, C. H. Tu, D. H. Cribbs, C. W. Cotman, and N. L. Jeon, "Patterned cell culture inside microfluidic devices," *Lab on a chip*, vol. 5, pp. 102–7, Jan 2005.

[76] P. Scheiffele, J. Fan, J. Choih, R. Fetter, and T. Serafini, "Neuroligin expressed in nonneuronal cells triggers presynaptic development in contacting axons," *Cell*, vol. 101, pp. 657–69, Jun 2000.

[77] T. Biederer, Y. Sara, M. Mozhayeva, D. Atasoy, X. Liu, E. T. Kavalali, and T. C. Südhof, "Syncam, a synaptic adhesion molecule that drives synapse assembly," *Science*, vol. 297, pp. 1525–31, Aug 2002.

[78] P. S. Goldman-Rakic, "Cellular basis of working memory," *Neuron*, vol. 14, pp. 477–85, Mar 1995.

[79] J. M. Fuster, "Network memory," *Trends Neurosci*, vol. 20, pp. 451–9, Oct 1997.

[80] S. Funahashi, M. V. Chafee, and P. S. Goldman-Rakic, "Prefrontal neuronal activity in rhesus monkeys performing a delayed anti-saccade task," *Nature*, vol. 365, pp. 753–6, Oct 1993.

[81] R. Srimal and C. E. Curtis, "Persistent neural activity during the maintenance of spatial position in working memory," *Neuroimage*, vol. 39, pp. 455–68, Jan 2008.

[82] J. M. Fuster and G. E. Alexander, "Neuron activity related to short-term memory," *Science*, vol. 173, pp. 652–4, Aug 1971.

[83] O. Hikosaka and R. H. Wurtz, "Visual and oculomotor functions of monkey substantia nigra pars reticulata. iii. memory-contingent visual and saccade responses," *Journal of Neurophysiology*, vol. 49, pp. 1268–84, May 1983.

[84] O. Hikosaka, M. Sakamoto, and S. Usui, "Functional properties of monkey caudate neurons. iii. activities related to expectation of target and reward," *Journal of Neurophysiology*, vol. 61, pp. 814–32, Apr 1989.

[85] E. K. Miller, C. A. Erickson, and R. Desimone, "Neural mechanisms of visual working memory in prefrontal cortex of the macaque," *J Neurosci*, vol. 16, pp. 5154–67, Aug 1996.

[86] R. D. No, "Vestibulo-ocular reflex arc," *Arch Neurol Psychiatry*, vol. 30, pp. 245–291, Aug 1933. 10.1001/archneurpsyc.1933.02240140009001.

[87] D. Hebb, "The organization of behavior: A neuropsychological theory," *John Wiley & Sons Inc.*, Jan 1949.

[88] O. Feinerman and E. Moses, "Transport of information along unidimensional layered networks of dissociated hippocampal neurons and implications for rate coding," *Journal of Neuroscience*, vol. 26, p. 4526, Apr 2006.

[89] S. Funahashi, C. J. Bruce, and P. S. Goldman-Rakic, "Mnemonic coding of visual space in the monkey's dorsolateral prefrontal cortex," *Journal of Neurophysiology*, vol. 61, pp. 331–49, Feb 1989.

[90] X. J. Wang, "Synaptic reverberation underlying mnemonic persistent activity," *Trends Neurosci*, vol. 24, pp. 455–63, Aug 2001.

[91] A. A. Oliva, C. D. James, C. E. Kingman, H. G. Craighead, and G. A. Banker, "Patterning axonal guidance molecules using a novel strategy for microcontact printing," *Neurochem Res*, vol. 28, pp. 1639–48, Nov 2003.

[92] D. A. Stenger, J. J. Hickman, K. E. Bateman, M. S. Ravenscroft, W. Ma, J. J. Pancrazio, K. Shaffer, A. E. Schaffner, D. H. Cribbs, and C. W. Cotman, "Microlithographic determination of axonal/dendritic polarity in cultured hippocampal neurons," *Journal of Neuroscience Methods*, vol. 82, pp. 167–73, Aug 1998.

[93] J. M. Corey, B. C. Wheeler, and G. J. Brewer, "Micrometer resolution silane-based patterning of hippocampal neurons: critical variables in photoresist and laser ablation processes for substrate fabrication," *IEEE transactions on bio-medical engineering*, vol. 43, pp. 944–55, Sep 1996.

[94] V. Volman, R. C. Gerkin, P.-M. Lau, E. Ben-Jacob, and G.-Q. Bi, "Calcium and synaptic dynamics underlying reverberatory activity in neuronal networks," *Phys. Biol.*, vol. 4, pp. 91–103, Jun 2007.

[95] P. Lau and G. Bi, "Reverberatory activity in neuronal networks in vitro," *Chin. Sci. Bull.*, vol. 54, pp. 1828–1835, Jun 2009.